# Electrochemical Society

UNIV. OF MICHIGAN
MAY 1 2 1954
EAST ENGINEERING
LIBRARY

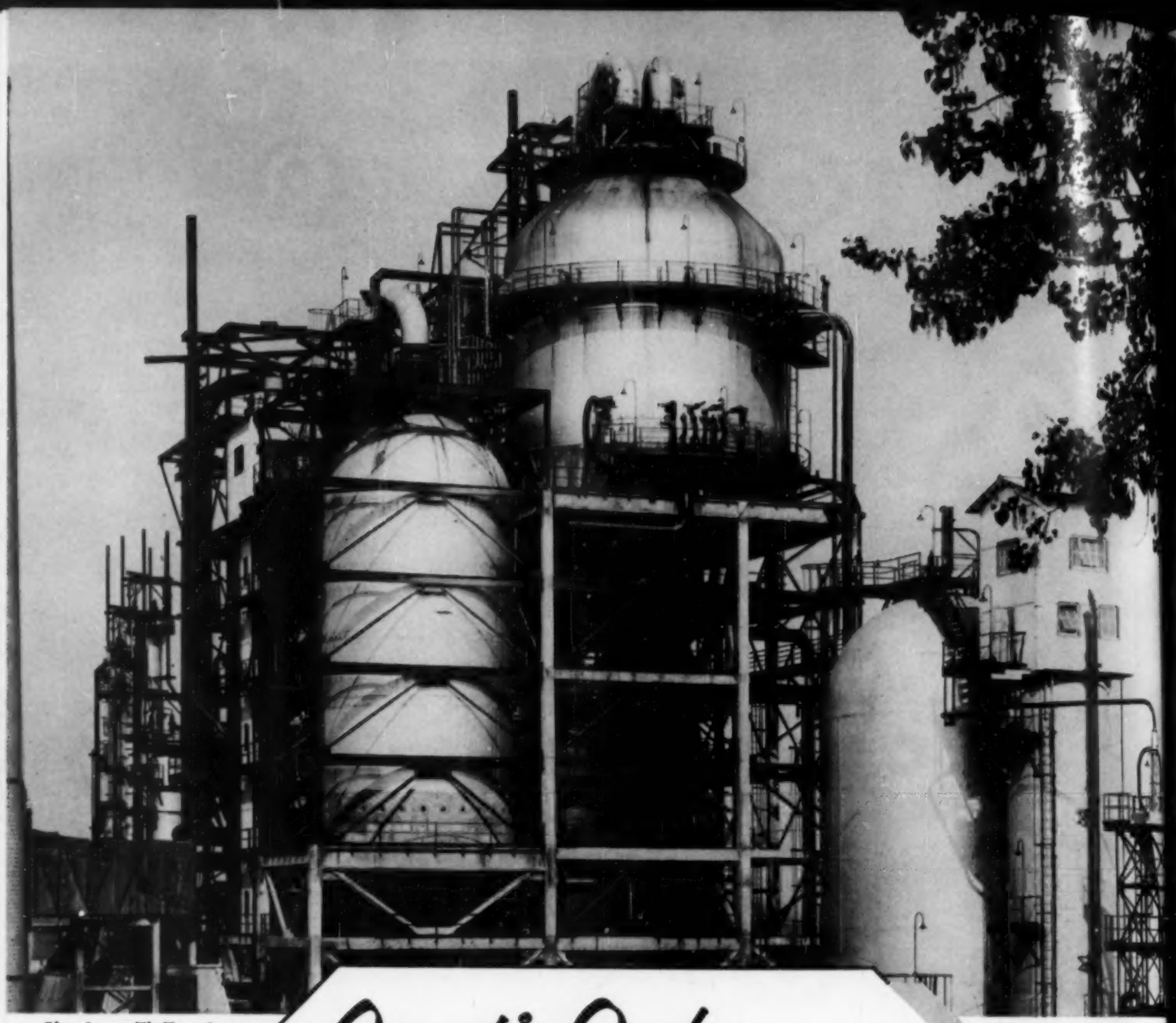

*Photo Courtesy The Texas Company*

# Caustic Soda

## . . . for the Petroleum Industry

**Caustic Soda is an essential chemical used in petroleum refining.**

**Uniformly high quality GLC GRAPHITE ANODES are essential too—in helping the electrolytic industry meet the growing civilian and defense needs for caustic soda and chlorine.**

ELECTRODE DIVISION

**Great Lakes Carbon Corporation**

Niagara Falls, N.Y. GLC Morganton, N. C.

**Graphite Electrodes, Anodes, Molds and Specialties**

**Sales office:** Niagara Falls, N.Y. **Other offices:** New York, N.Y., Oak Park, Ill., Pittsburgh, Pa

Sales Agents: J. B. Hayes, Birmingham, Ala.; George O'Hara, Long Beach, Cal.; Great Northern Carbon & Chemical Co., Ltd., Montreal, Canada

Overseas Carbon & Coke Company, Inc., Geneva, Switzerland; Great Eastern Carbon & Chemical Co., Inc., Chiyoda-Ku, Tokyo

# Corrosion Inhibitors and Polarographic Maxima[1]

HARRY C. GATOS

*Engineering Research Laboratory, Engineering Department, E. I. du Pont de Nemours and Company, Inc., Wilmington, Delaware*

ABSTRACT

Electrical polarization phenomena occurring in corrosion and polarographic processes are compared, and certain similarities are pointed out. On this basis, results of polarographic studies of a number of corrosion inhibitors are presented, particularly for the iron-sulfuric acid system. It is found that these inhibitors considerably suppress one or more of the oxygen, lead, or nickel polarographic maxima. The maxima-suppressing effectiveness of compounds known to inhibit corrosion by adsorption is a function of concentration resembling gas adsorption isotherms. Furthermore, certain inhibitors which function by either anodic or cathodic polarization are also effective in suppressing either anodic or cathodic maxima. Some general inhibitors are general maxima suppressors as well.

Polarography is suggested as a valuable tool in corrosion inhibitor studies.

## INTRODUCTION

Chemical and physical changes responsible for metallic corrosion in liquid media take place mostly on metal surfaces and at metal-liquid interfaces. A thorough understanding of the function of metal surfaces and metal-liquid interfaces, so critical in corrosion, is limited by the facts that (*a*) metal surfaces are very difficult to obtain and maintain chemically pure and physically reproducible, and (*b*) metal-liquid interfaces, due to their extreme thinness and intricate structure, are beyond the sensitivity range of conventional experimental techniques.

Among metals, mercury is unique in that it can be obtained in highly pure chemical form, and its surface-physical characteristics can be easily reproduced, mainly because of its liquid state. These outstanding characteristics of mercury have been primarily responsible for the development of polarography.

Although mercury as a material of construction is of no practical significance, it has been extensively used in obtaining information about metal-liquid interface phenomena, which have been of importance in understanding metal-liquid interfaces in general.

It is the purpose of this paper to point out how some characteristic phenomena occurring at the interface of a mercury microelectrode in contact with electrolyte solutions can be employed for corrosion inhibitor studies.

### *Polarographic Maxima*

By applying an increasing potential between a dropping mercury microelectrode (cathode) and a reference electrode (nonpolarizable anode) in the presence of electroreducible materials, a typical "polarographic wave" (1) is obtained as in Fig. 1 (curve IV).[2] In the presence of $NiCl_2$, the cathode reaction is:

$$Ni^{++} + 2e + Hg = Ni(Hg)$$

The limiting current is proportional to the concentration of the reacting substance, a relationship which is employed in quantitative analysis.

The potential corresponding to one-half the limiting current value is called the "half-wave potential." In contrast to the "decomposition potential," the half-wave potential is a well definable quantity, and it is usually independent of concentration of the reacting material. Hence, it is employed for qualitative analysis.

The dropping mercury electrode is under virtually complete concentration polarization when the limiting current is reached. Thus, the amount of current flowing through the cell is primarily controlled by the diffusion rate of the reacting material to the polarized electrode (diffusion current) and within certain limits is independent of the applied emf. The electrical migration of the reducible ions is minimized by employing a nonreducible electrolyte (supporting electrolyte) such as KCl in the electrolysis solution. The supporting electrolyte is present at considerably higher concentrations than the reducible ions, and thus the transference number of the latter is reduced practically to zero. Under these conditions the limiting current becomes entirely a diffusion current.

The current-voltage curves with the dropping mercury electrode quite often exhibit more or less

[1] Manuscript received January 8, 1954. This paper was prepared for delivery before the Boston Meeting, October 3 to 7, 1954.

[2] Methyl amine (see figure caption) does not participate in the electrode reaction. Its role is discussed later.

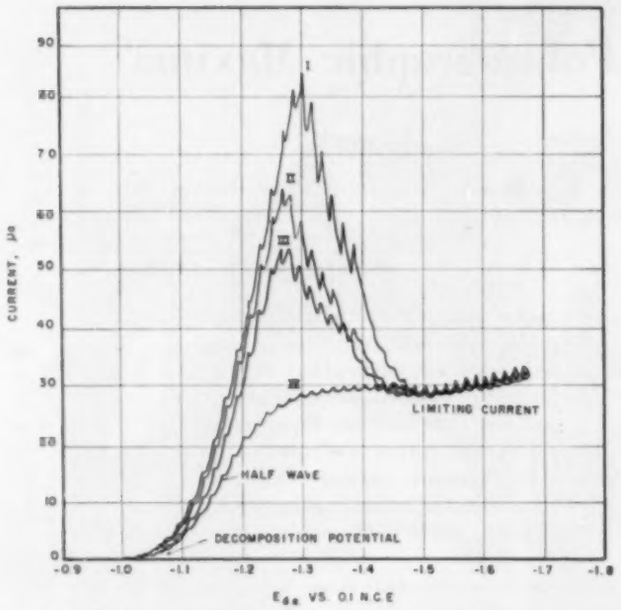


FIG. 1. Polarograms of $NiCl_2$ in 0.1M KCl. $E_{d.e.}$—potential of dropping electrode. Curve I—Ni maximum; curve II—maximum partially suppressed 0.03% methylamine; curve III—maximum further suppressed with 0.06% methylamine; curve IV—Ni "polarographic wave," 0.30% methylamine.

pronounced current maxima (polarographic maxima) before the limiting value for the current is reached (Fig. 1, curve I). These maxima are fairly reproducible, and their shapes are independent of the direction in which the applied voltage is changed. They interfere with determination of the half-wave potential and the limiting current. They are suppressed, however, in the presence of certain substances, e.g., methyl amine, which usually do not affect the limiting current.

The origin and suppression of polarographic maxima have been the subject of extensive investigations (2). It has been shown that the dropping mercury electrode remains depolarized until the peak of the maximum is reached. Beyond this point, concentration polarization sets in and the current reaches its limiting value.

According to Heyrovsky (3), the maxima can be distinguished as positive or negative depending upon the charge of the mercury with respect to the solution at the potential at which the maxima occur. Mercury, when immersed in solutions of capillary-inactive electrolytes, such as potassium chloride, is positively charged. If a cathodic potential is applied to mercury, its charge decreases as the cathodic potential increases to about −0.52 volt vs. the saturated calomel electrode. At this point (electrocapillary zero) mercury is electrically uncharged with respect to the solution, as indicated by its maximum surface tension (Fig. 2). At more cathodic potentials mercury becomes negatively charged, and its surface tension decreases again. Positive maxima appear at potentials below, and the negative above, −0.52 volt.

A considerable amount of work has been reported in connection with the suppression of polarographic maxima (4), and a number of mechanisms have been proposed. Whatever the exact mechanism may be, it appears that, in the presence of the maxima supressors, the microelectrode becomes polarized at emf values at which it is ordinarily depolarized, as indicated by the appearance of polarographic maxima.

### *Corrosion and Polarographic Processes*

It is widely accepted that metallic corrosion in liquid media is under electrochemical control with local electrolytic cells operating during the corrosion process. Anodic, cathodic, or mixed polarization of local cells leads to a decrease or elimination of corrosion, depending on the degree of polarization (5, 6). On the other hand, depolarization of local cells results in promotion of corrosion. It is thus apparent that polarization-depolarization phenomena on metal surfaces in contact with liquids are of paramount importance in corrosion processes. It is believed that a number of substances (in particular organic compounds) inhibit metallic corrosion by adsorbing on the metal surfaces and thus inducing polarization of the active local galvanic cells (7-9).

As mentioned previously, polarography is based on electrode polarization phenomena. Complete polarization of the dropping mercury microelectrode is necessary for the appearance of typical polarographic waves (Fig. 1, curve IV). Lack of complete polarization of the same electrode at certain emf values results in the appearance of polarographic maxima. Substances suppressing these maxima are

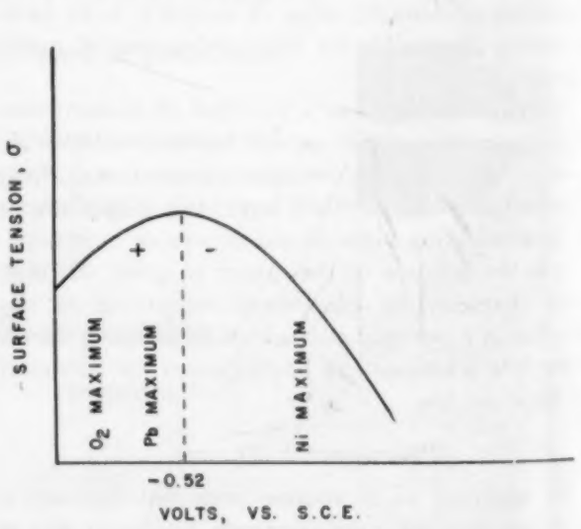


FIG. 2. Electrocapillary curve

believed to polarize microelectrodes at the above emf values. Most probably, this polarization is brought about mainly by adsorption of maxima suppressors on the metal surface (10).

Thus, it becomes apparent that both corrosion and polarographic processes are electrical-polarization dependent. Electrical polarization, therefore, results in corrosion protection and in typical polarographic waves. Lack of polarization usually promotes corrosion and causes polarographic maxima.

At this point, a comparison between polarographic maxima suppressors and corrosion inhibitors becomes of considerable interest. To begin with, a number of polarographic maxima suppressors (11), e.g., organic sulfur derivatives, amines, gelatine, etc., are also well known for their corrosion inhibiting properties. Furthermore, capillary active anions and negative colloids in general preferentially suppress maxima appearing on the positive side of the electrocapillary zero (positive maxima), whereas capillary-active cations and positive colloids are effective with the negative maxima. High molecular weight substances like gelatine suppress maxima of various metal ions on both sides of the electrocapillary zero. This behavior of maxima suppressors appears comparable to that of corrosion inhibitors, since corrosion inhibitors also, according to their nature, are known to act preferentially on anodic or cathodic areas (anodic and cathodic inhibitors, respectively) as well as indiscriminately over the metal surfaces (general inhibitors) (12).

On the basis of the above comparison between polarographic maxima suppressors and corrosion inhibitors, it was felt worth while to investigate their common characteristics and thus better understand similarities between phenomena occurring in polarographic and in corrosion processes. The present broad knowledge of polarographic processes could prove quite useful to corrosion in general and to corrosion inhibitors in particular.

## Experimental

In order to investigate any existing similarities between corrosion inhibition and polarographic processes, the behavior of a number of substances toward various polarographic maxima was studied over a large range of emf values. These substances were reported as possessing corrosion-inhibiting properties. Preference was given to inhibitors for which comparative data in specific environments were available.

*Polarographic maxima.*—Three polarographic maxima were chosen for this investigation corresponding to the following reduction reactions. (The half-wave potential, referred to a saturated calomel electrode, for each reduction is shown in parentheses.)

$$O_2 + 2H^+ + 2e = H_2O_2 \quad (-0.10 \text{ v})$$
$$Pb^{++} + 2e = Pb \quad (-0.40 \text{ v})$$
$$Ni^{++} + 2e = Ni \quad (-1.10 \text{ v})$$

All maxima were obtained in 0.1 molar KCl supporting electrolyte containing the reducible ions. A dropping mercury microelectrode served as the cathode.

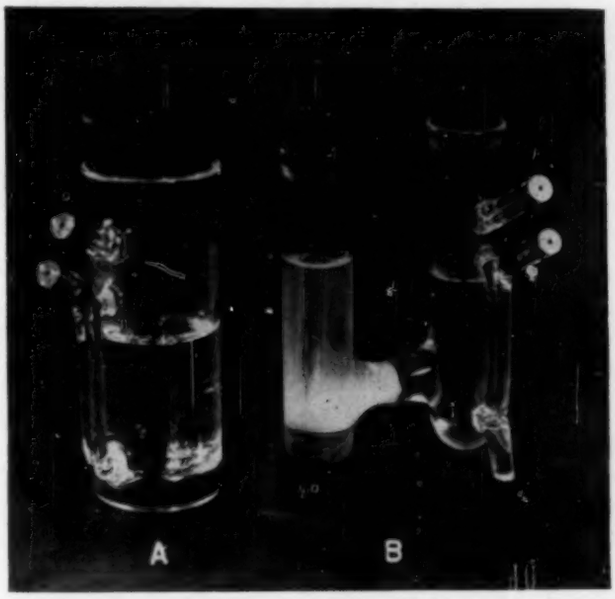


Fig. 3. Electrolytic cells employed with the dropping mercury electrode.

The oxygen maximum was obtained by saturating the 0.1M KCl solution in the electrolytic cell with oxygen immediately before the polarographic run. The lead maximum was obtained from a $4.05 \times 10^{-3}$M solution of $Pb(NO_3)_2$ in 0.1M KCl. Immediately before each run, nitrogen was bubbled through this solution for about 15 min to remove any oxygen present in the solution. Traces of oxygen suppress the lead as well as the nickel maximum. The nickel maximum was obtained from a $3.22 \times 10^{-3}$M $NiCl_2$ solution under conditions described for the lead maximum.

*Electrolytic cell.*—A single-compartment electrolytic cell was used with a pool of mercury as the nonpolarizable electrode (Fig. 3A). A gas inlet and outlet allowed bubbling of gases through the solution, thus maintaining the desirable gas atmosphere over the solution during polarographic runs. The cell was kept at constant temperature (25°C) by means of a constant temperature bath.

*Polarograph.*—Throughout this investigation an automatic recording polarograph[3] was used. Characteristics of the dropping mercury electrode, e.g.,

[3] "Electro-Chemograph, Type E, Leeds and Northrup. Philadelphia, Pa.

dropping time (5.55 sec/drop at zero applied potential) and mercury flow rate (1.240 mg/sec at zero applied potential) were maintained constant through the investigation.

*Inhibitors for Steel in Sulfuric Acid*

A number of inhibitors for steel in sulfuric acid (13) were polarographically tested with the oxygen, lead, and nickel polarographic maxima. For each test, one of the three maxima was obtained by using 15 cc of solution containing the corresponding reducible substance as described previously (blank run). Thereafter, 0.2 cc of a 0.2% aqueous solution of inhibitor was added to the electrolytic cell to determine its effect upon the maximum. The final arbitrarily chosen inhibitor concentration was approximately 27 ppm. In cases of slightly soluble inhibitors, small amounts were added directly to the cell. It was found necessary to run a blank with each test in order to make sure that the maximum was not affected by accidental causes prior to addition of the inhibitors.

Effectiveness of various inhibitors in suppressing polarographic maxima was expressed as "per cent suppression" and was calculated as follows:

$$\% \text{ suppression} = \frac{(M_1 - i_d) - (M_2 - i_d)}{(M_1 - i_d)} \times 100$$

$$= \frac{M_1 - M_2}{M_1 - i_d} \times 100$$

TABLE I. *Inhibitors for steel in sulfuric acid in the approximate order of decreasing effectiveness**

| Inhibitor | % Suppression of maxima | | |
|---|---|---|---|
| | $O_2$ | Pb | Ni |
| 1. Butyl disulfide | 100 | 100 | 7 |
| 2. Phenyl thiourea | 100 | 100 | 23 |
| 3. Thiourea | 100 | 53 | 22 |
| 4. Butyl mercaptan | 100 | 100 | 52 |
| 5. Triamylamine | 100 | 100 | 100 |
| 6. Aldol | 100 | 100 | 100 |
| 7. Phenyl morpholine | 100 | 100 | 100 |
| 8. *p*-Tolualdehyde | 94 | 100 | 38 |
| 9. Phorone | 89 | 100 | 100 |
| 10. Diamylamine | 100 | 100 | 100 |
| 11. Dicyclohexylamine | 100 | 100 | 100 |
| 12. Ethanol morpholine | 8 | 26 | 18 |
| 13. α-Naphthylamine | 100 | 100 | 100 |
| 14. Phenyl hydrazine | 94 | 100 | 100 |
| 15. Benzaldehyde | 64 | 100 | 32 |
| 16. Morpholine | 29 | 37 | 66 |
| 17. Cyclohexanone | 66 | 100 | 100 |
| 18. Dimethylamine | 37 | 100 | 100 |
| 19. Diethylaniline | 65 | 100 | 21 |
| 20. Acridine | 100 | 100 | 100 |
| 21. Ethylenediamine | 4 | 34 | 100 |
| 22. Dimethylaniline | 100 | 100 | 21 |
| 23. Pyridine | 41 | 60 | 35 |

* The tests (13) were run in 4.9% $H_2SO_4$ for 48 hr at 25°C.

TABLE II. *Substances found less effective as inhibitors compared with those in Table I under similar conditions**

| Inhibitor | % Suppression of maxima | | |
|---|---|---|---|
| | $O_2$ | Pb | Ni |
| Diethylamine | 0 | 16 | 35 |
| Butylamine | 5 | 49 | 51 |
| *n*-Amyl alcohol | 12 | 18 | 15 |
| Ethylamine | 12 | 34 | 49 |
| Isopropylamine | 13 | 2 | 30 |
| Methylamine | 20 | 13 | 24 |
| Aniline | 66 | 100 | 13 |

* See reference (13).

where $M_1$ = polarographic maxima in μa, $M_2$ = polarographic maxima in μa after addition of inhibitor, and $i_d$ = diffusion current.

As a rule, diffusion current was not affected by addition of inhibitors at the concentration mentioned above. When it was decreased, the corresponding maximum was totally suppressed. Results obtained with the three maxima are shown in Table I. It can be seen that practically all inhibitors tested suppress considerably one or more of the employed polarographic maxima. Of 23 inhibitors, 18 suppress the lead maximum 100%. The oxygen maximum is suppressed either to the same or lesser extent than the lead maximum, except for thiourea. Since the lead maximum is less anodic than the oxygen, it is perhaps more effectively suppressed under conditions favoring anodic polarization.

In the case of the nickel maximum, which appears at the cathodic side of the electrocapillary zero, it is of interest to notice that the suppressing effectiveness of a large number of inhibitors changes considerably, e.g., it decreases for sulfur derivatives. In other cases it increases. This is consistent with the fact that certain substances are specific in induc-

TABLE III. *Inhibitors for aluminum**

| Inhibitor | % Suppression of maxima | |
|---|---|---|
| | $O_2$ | Ni |
| α-Naphthoquinoline | 100 | 100 |
| Acridine | 100 | 100 |
| Thiourea | 100 | 22 |
| Iodine | 80 | 14 |
| Pyridine | 41 | 35 |
| Dimethylamine | 37 | 100 |
| Nicotinic acid | 20 | 60 |
| Methylamine | 20 | 24 |
| Hexamethylenetetramine | 18 | 20 |
| Sodium chromate | 8 | 100 |
| Phenol formaldehyde | 7 | 86 |
| Butylamine | 5 | 51 |
| Ethylamine | 12 | 49 |
| Diethylamine | 0 | 35 |

* See reference (14).

TABLE IV. *Inhibitors for copper*

| Inhibitor | % Suppression of maxima | |
|---|---|---|
| | $O_2$ | Ni |
| Benzanilide | 100 | 100 |
| Butyl mercaptan | 100 | 52 |
| Rosin | 100 | 71 |
| Aniline | 66 | 13 |
| Sodium benzoate | 50 | 21 |
| Lauryl mercaptan | 49 | 9 |
| Morpholine | 29 | 66 |
| Sodium nitrite | 11 | 13 |
| Potassium dichromate | 9 | 100 |
| Sodium silicate | 6 | 100 |
| Ethylenediamine | 4 | 100 |

ing polarization at either anodic or cathodic metal surfaces.

Some inhibitors reported to be less effective than those of Table I, under similar experimental conditions, were also observed, as a whole, to be relatively less effective maxima suppressors (Table II).

*Other inhibitors.*—A group of inhibitors for aluminum (14) were tested for their effectiveness in suppressing oxygen and nickel polarographic maxima. These experiments were carried out under conditions identical to those described for iron inhibitors. Results are shown in Table III. It can be seen that all inhibitors tested suppressed one or both maxima by at least 20%. Here again the suppressing effectiveness of some of these inhibitors changes sharply from the oxygen to the nickel maximum.

Some compounds relatively ineffective in inhibiting corrosion of iron and at the same time not very effective maxima suppressors (Table II) are, nevertheless, listed among inhibitors for aluminum. Polarographic conditions employed in testing inhibitors for either metal were identical, and no attempt was made at this point to characterize polarographic behavior of inhibitors under varying conditions with reference to specific corrosion systems.

A number of representative inhibitors for copper selected from the literature were tested like the inhibitors for iron and aluminum. Results for oxygen and nickel maxima are shown in Table IV. In addition to the general maxima-suppressing ability of these inhibitors, it is of interest to notice that some of those least effective in suppressing the oxygen maximum are most effective in suppressing the nickel maximum.

### *Effect of Noninhibitors on Polarographic Maxima*

It is difficult to find compounds which are not corrosion inhibitors to some extent under some experimental conditions. However, a few substances were selected which are not commonly reported as effective corrosion inhibitors. Their influence on the polarographic maxima is shown in Table V. It is apparent that these compounds are as a whole considerably poorer maxima suppressors than those reported in Tables I, III, and IV.

TABLE V. *Effect of noninhibitors on polarographic maxima*

| Name of substance | % Suppression of maxima | | |
|---|---|---|---|
| | $O_2$ | Pb | Ni |
| Methyl alcohol | 5 | 18 | 27 |
| Ethyl alcohol | 0 | 15 | 30 |
| Propyl alcohol | 6 | 13 | 13 |
| Butyl alcohol | 7 | 8 | 10 |
| Isoamyl alcohol | 1 | 13 | 13 |
| *tert*-Amyl alcohol | 6 | 12 | 8 |
| Ethyl ether | 0 | 13 | 10 |
| Propyl ether | 14 | 8 | 7 |
| Cane sugar | 0 | 11 | 16 |
| Formic acid | 20 | 27 | 67 |
| Acetic acid | 0 | 6 | 44 |
| Propionic acid | 0 | 5 | 43 |
| Butyric acid | 0 | 7 | 33 |

From results reported to this point it appears that in general the polarizing ability of corrosion inhibitors can be demonstrated polarographically. The conclusiveness of these findings is limited by the fact that inhibitors were tested at a single concentration. Furthermore, corrosion test data for all these inhibitors under identical conditions are not available.

### *Quantitative Approach*

On the basis of the above qualitative experiments, it was felt worth while to extend these studies on a quantitative basis in order to shed some light on common characteristics of polarographic and corrosion inhibition processes.

In the following experiments, the single-compartment polarizing cell was replaced with an H-type cell shown in Fig. 3B. A 0.1*N* calomel electrode was employed as the reference electrode instead of the mercury pool. Electrical contact between the calomel electrode and electrolysis compartment was established through a fritted glass disk and an agar plug. The main advantage of the H-type cell over the single compartment cell is that the potential of the calomel reference electrode is not susceptible to variations.

### *Effect of pH on Polarographic Maxima*

Determining the effect of *p*H on polarographic maxima was considered essential since *p*H of solutions from which the maxima were obtained could change to a different extent by addition of various inhibitors. For this purpose, solutions containing the reducible substances were prepared over a wide *p*H range. Since conventional buffered solutions in

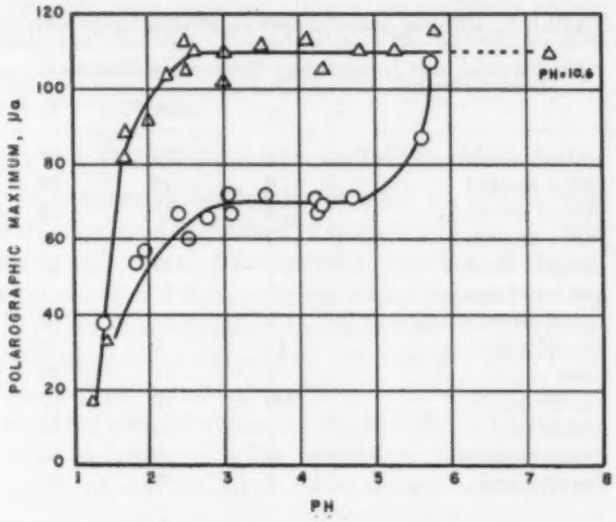


FIG. 4. Effect of *p*H upon the oxygen and nickel maximum. △—oxygen maximum; limiting current 17 μa; ○—nickel maximum; limiting current 25 μa.

general affect polarographic maxima, small amounts of hydrochloric acid and potassium hydroxide solution were employed for *p*H adjustments. Polarographic maxima were then obtained from these solutions. The *p*H was measured with a Beckman *p*H meter. Results obtained for the oxygen and nickel maxima are shown in Fig. 4. Values of the maxima include the corresponding limiting current which remained constant over the employed *p*H range. It is apparent that the oxygen maximum is completely eliminated at about *p*H 1; it increases with increasing *p*H up to *p*H 2.5, and it remains constant for higher *p*H values. The nickel maximum is also considerably suppressed at *p*H 1, and it increases with increasing *p*H. It remains constant, however, only for *p*H values of 3–5 and increases rapidly beyond this range.

Suppression of maxima in high $H^+$ concentrations indicates that the microcathode becomes polarized at the potentials of the maxima. As mentioned previously, the microcathode is not polarized when the maxima appear. This polarization is perhaps brought about by adsorption of $H^+$ on the mercury surface. In this respect, it is of interest to notice that the oxygen maximum occurring at an emf value at which the dropping electrode is positively charged with respect to the solution is somewhat less affected by $H^+$ concentration than the negative nickel maximum. Similar $H^+$ adsorption probably occurs at cathodes of metals corroding in strong acids. This adsorption of $H^+$ on cathodic areas very likely hinders corrosion inhibitors from acting upon local cathodes. Thus, anodic inhibitors would be expected to act more effectively than cathodic ones in low *p*H solutions, a fact widely accepted.

### *Amines as Corrosion Inhibitors and Polarographic Maxima Suppressors*

A number of amines, both aliphatic and aromatic, were employed for a basic comparison of polarization phenomena occurring in polarographic and corrosion inhibition processes. Amines chosen have been extensively studied by Mann and his coworkers (7–9) as corrosion inhibitors for mild steel in 1*N* $H_2SO_4$ at room temperature. Among the various maxima, that of nickel was found most responsive and, in general, more suitable for the study of the above amines.

*Aliphatic amines.*—The following aliphatic amines were studied in connection with maxima suppression: methyl-, ethyl-, propyl-, butyl-, and amylamine. According to Mann (Fig. 5), the effectiveness of these amines in inhibiting corrosion of mild steel in 1*N* $H_2O_4$ at room temperature (25°C) increases with increasing molecular weight for any given amine concentration expressed in per cent nitrogen. The effectiveness of each amine increases with its concentration and eventually levels off. Effectiveness at the leveling-off point is again higher, the higher the molecular weight of the amine. Since the covering power and the ability of normal aliphatic amines to adsorb on metal surfaces increase with increasing chain length, these corrosion inhibition results are in agreement with the widely accepted theory that amines inhibit corrosion by adsorbing on metals.

Effectiveness of the above amines in suppressing the nickel polarographic maximum was studied as a function of concentration. The nickel maximum was obtained from $6.25 \times 10^{-3}$M $NiCl_2$ solution in 0.1M KCl supporting electrolyte. A blank run

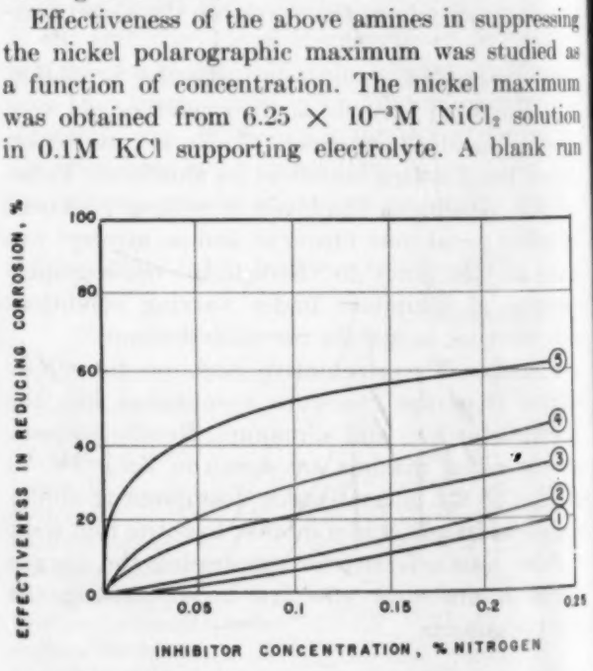


FIG. 5. Inhibition by aliphatic amines of mild steel corrosion in 1*N* $H_2SO_4$ at 25°C (7). Curve 1—methylamine; curve 2—ethylamine; curve 3—propylamine; curve 4—butylamine; curve 5—amylamine.

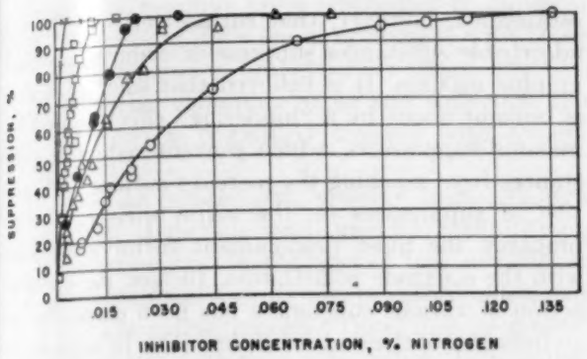


FIG. 6. Suppression of the nickel maximum as a function of concentration of aliphatic amines. ○—methylamine; △—ethylamine; ●—propylamine; □—butylamine; ×—amylamine.

preceded every test. Specific amounts of amine solutions of known concentration were added to the polarizing cell containing the nickel chloride-potassium chloride solution. The amine solutions were also at the same concentration in respect to nickel chloride and potassium chloride as the solution from which the maximum was obtained. In this way, changes in $Ni^{++}$ concentration during testing were avoided. Individual runs were performed for all concentrations of the amines tested. The *p*H of all solutions was adjusted to a value of about 3.0 by means of small amounts of HCl. All experiments were performed at 25° ± 0.1°C.

The effectiveness of the tested aliphatic amines in suppressing the nickel maximum is shown as a function of nitrogen concentration in Fig. 6. There is a striking similarity between the behavior of these amines as corrosion inhibitors and as nickel maximum suppressors. The suppression of the nickel maximum increases with amine concentration and becomes complete above a critical amine concentration. For a given concentration of amine, expressed in per cent nitrogen, the maximum suppression increases with molecular weight of the amines. Inhibitor concentrations in the polarographic and corrosion experiments are not the same since different metals and electrolytes are involved in the two cases.

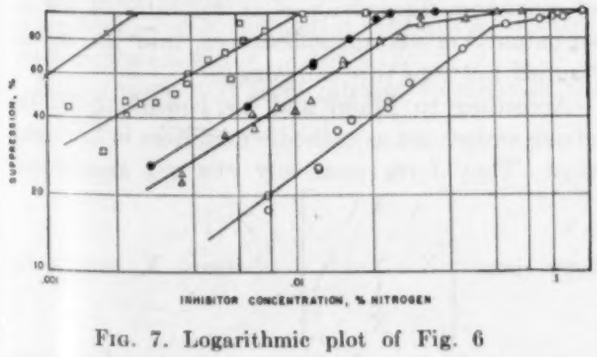


FIG. 7. Logarithmic plot of Fig. 6

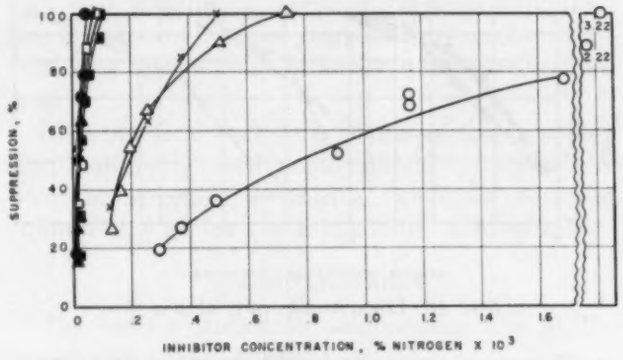


FIG. 8. Suppression of the nickel maximum as a function of concentration of aromatic amines. ○—aniline; △—*p*-toluidine; ×—*o*-toluidine; ■—3,5-xylidine; □—dimethylaniline; ▲—2,3-xylidine; ●—2,6-xylidine.

By plotting the logarithm of the per cent suppression vs. the logarithm of the amine concentration, straight lines result (Fig. 7). Similar curves are obtained from Mann's data for these amines by plotting the logarithm of corrosion inhibiting effectiveness vs. the logarithm of their concentration in per cent nitrogen. In some cases, the slope of the lines changes at certain amine concentrations, suggesting a change in adsorption rates of these compounds at certain concentrations.

*Aromatic amines.*—Seven aromatic amines were selected to study further the polarographic behavior of corrosion inhibitors: aniline, dimethylaniline, *o*-toluidine, *p*-toluidine, 2,6-xylidine, 3,5-xylidine, and 2,3-xylidine. The procedure described for studies of aliphatic amines was employed for aromatic amines also. Polarographic results are shown in Fig. 8, and corresponding corrosion data (7) in Fig. 9. In the case of these amines also, the function

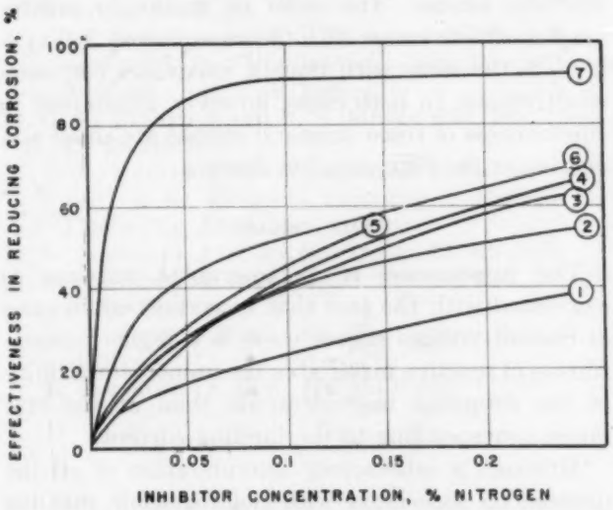


FIG. 9. Inhibition by aromatic amines of mild steel corrosion in 1*N* $H_2SO_4$ at 25°C (7). Curve 1—aniline; curve 2—2,6-xylidine; curve 3—*p*-toluidine; curve 4—*o*-toluidine; curve 5—3,5-xylidine; curve 6—*N*,*N*-dimethylaniline; curve 7—2,3-xylidine.

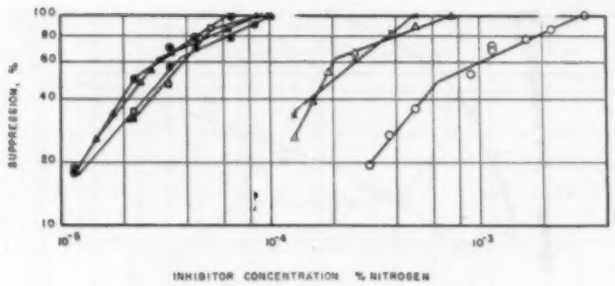


FIG. 10. Logarithmic plot of Fig. 8

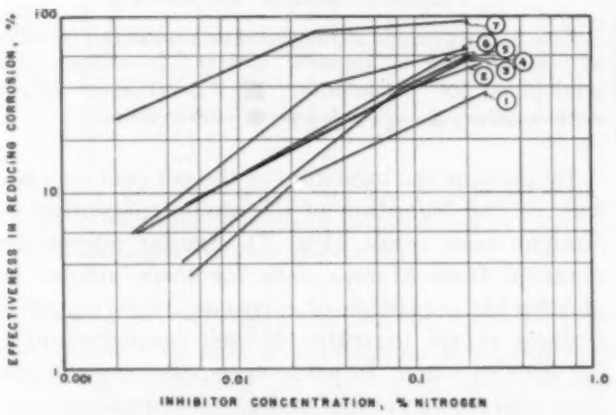


FIG. 11. Logarithmic plot of Fig. 9

of their polarographic maximum suppression effectiveness vs. their concentration resembles gas adsorption isotherms. Corresponding logarithmic plots are shown in Fig. 10. Here again the slope of all but one of the lines changes as it does in five of the corresponding corrosion plots (Fig. 11). Thus, polarographic behavior of the above aromatic amines resembles their behavior as corrosion inhibitors, which in turn is comparable to that of aliphatic amines. The order of maximum polarographic effectiveness, with the exception of 2,6-xylidine, is the same with that of maximum corrosion effectiveness. In both cases, however, differences in effectiveness of some aromatic amines are small and overlap as the concentration changes.

## DISCUSSION

The appearance of polarographic maxima is associated with the fact that at certain emf values of current-voltage curves there is a higher concentration of reactive material in the immediate vicinity of the dropping microelectrode than at the emf range corresponding to the limiting current.

Although a satisfactory interpretation of all the phenomena associated with polarographic maxima is not available, it seems that polarization of the mercury microelectrode at the maxima is not established because an excess supply of reactive material is available at the microelectrode as a result of some specific electrochemical phenomenon. It has been established, however, that surface-active or highly adsorbable substances suppress or eliminate polarographic maxima. It is believed that such an action is brought about by a "hindering" effect caused by maxima suppressors, which prevent reducible substances from reaching the mercury surface. Adsorption of suppressors on the metal surface is very probably the most predominant factor associated with the electrode polarization. In fact, suppressive action of various substances has been employed as an indicator of their adsorbability (15). In some cases the degree of suppression of the maxima has been suggested as a means of quantitative analysis of various substances (16), surface-active ones in particular (17).

With regard to mechanisms of corrosion and corrosion inhibition, electrical polarization and adsorption are of paramount importance according to current theories. It becomes thus apparent that significant similarities exist between the processes involved in polarographic maxima and their suppression on one hand, and in metallic corrosion and its inhibition on the other. On this basis, it is reasonable to believe that polarography constitutes a valuable tool for corrosion and corrosion inhibition studies.

In the present study, it is shown that the behavior of a number of inhibitors in the mild steel-sulfuric acid system is reflected in their action on some polarographic maxima obtained in 0.1M KCl solutions as supporting electrolyte. Particularly for the amines studied, it was demonstrated that their order of relative inhibiting effectiveness is the same as that of their suppressing effectiveness. It was further demonstrated that the inhibiting as well as the suppressing effectiveness is a function of concentration of the adsorption isotherm type. This is in agreement with the proposed (7) thesis that amines inhibiting corrosion adsorb on metal surfaces by means of the active amino-group. Their effectiveness increases with their covering power and concentration. The former increases, within limits, with molecular weight and molecular polarity. The latter affects inhibiting effectiveness according to the gas adsorption isotherm function. Polarographically, the degree of maximum suppression is an indicator of the adsorbability of certain substances, and the amines studied fall into this category.

According to Mann and his coworkers (7) the above amines act as cathodic inhibitors in acid solutions. They form positively charged ammonium-type ions $\left[\begin{array}{c} X \\ | \\ X-N-X \\ | \\ X \end{array}\right]^{+}$ (where X stands for organic radicals or hydrogen atoms) and thus are

attracted by negative poles (cathodes) of the local cells. The present data are in agreement with these views, since amines are generally more effective with the nickel maximum at an emf such that the microelectrode is negatively charged with respect to the solution.

It should be pointed out, however, that, although electrostatic attraction constitutes the main driving force for adsorption in the case of ions or charged colloids, additional factors are probably associated with the adsorption process. Thus, ions in general are preferentially effective with either the negative or positive maxima; in many cases, however, they suppress both types of maxima to a small or great extent. It appears plausible that the nature of various inhibitors, insofar as being anodic, cathodic, or both is concerned, is very probably revealed by their effectiveness in suppressing positive or negative maxima. This correlation does not hold if local cathodes and anodes of a corroding system are either both negatively charged or both positively charged with respect to the corrosive medium. Further systematic studies in that direction should prove of considerable interest.

In comparing processes of corrosion inhibition and maxima suppression, it should be kept in mind that no single mechanism can explain all the phenomena involved in these processes, nor is this necessary. Furthermore, considerably different mechanisms may lead to similar results depending on the substances and experimental conditions involved. Thus, in connection with maxima suppression, Heyrovsky (3) suggested that the suppressing ability of various substances increases with their ability to coagulate colloidal solutions. This holds true in a number of cases, although not in all. In corrosion studies, it has also been suggested (18, 19) that colloidal phenomena are of importance in corrosion protection, especially where corrosion products easily acquire the colloidal state. In such cases, the action of corrosion inhibitors may be due primarily to coagulation of corrosion products to a protective film. The above views on the importance of coagulating properties of some substances in maxima suppression and corrosion inhibition expressed independently could serve as an additional indication of similarities between the two processes.

In this respect, it is of interest to mention the fact that gelatine, a so-called "general inhibitor," has been used for many years as a "general suppressor" over a wide range of anodic and cathodic maxima.

On a practical basis, it is suggested that a polarograph properly used could provide a convenient tool for screening promising candidate corrosion inhibitors, e.g., for the iron-sulfuric acid system.

### Acknowledgment

The author wishes to acknowledge the skillful assistance of C. T. Cinaglia.

Any discussion of this paper will be published in a Discussion Section which will appear in the June 1955 issue of the JOURNAL.

### REFERENCES

1. For an extensive treatment see I. M. KOLTHOFF AND J. J. LINGANE, "Polarography," Interscience Publishers, New York (1952).
2. M. VON STACKELBERG, *Fortschr. chem. Forsch.*, **2**, 229 (1951).
3. J. HEYROVSKY, "A Polarographic Study of the Electrokinetic Phenomena of Adsorption, Electroreduction and Overpotential Displayed at the Dropping Mercury Cathode," Actualités Scientifiques et Industriells, No. 90, Hermann et Cie, Paris (1934).
4. For comprehensive reviews, see reference (1), p. 160, Vol. 1 and reference (2).
5. U. R. EVANS, "Metallic Corrosion, Passivity, and Protection," p. 350, Edward Arnold & Co., London (1948).
6. R. B. MEARS, *This Journal*, **95**, 1 (1949).
7. C. A. MANN, *ibid.*, **69**, 115 (1936).
8. C. A. MANN, B. E. LAUER, AND C. T. HULTIN, *Ind. Eng. Chem.*, **28**, 159, 1948 (1936).
9. S. CH'IAO AND C. A. MANN, *ibid.*, **39**, 910 (1947).
10. E. J. W. VERWEY, *Chem. Revs.*, **16**, 374 (1937).
11. Reference (1), p. 160, Vol. 1.
12. Reference (5), p. 534.
13. G. G. ELDREDGE AND J. C. WARNER, "Corrosion Handbook," (H. H. Uhlig, Editor) p. 905, John Wiley & Sons, Inc., New York (1948).
14. G. G. ELDREDGE AND R. B. MEARS, *Ind. Eng. Chem.*, **37**, 736 (1945).
15. O. H. MÜLLER, "The Polarographic Method of Analysis," p. 58, Chemical Education Publishing Co., Easton, Pa. (1951).
16. G. SEMERANO, *Arch. sci. biol. (Italy)*, **20**, 329 (1934).
17. M. VON STACKELBERG AND H. SCHÜTZ, *Koll. Z.*, **105**, 20 (1943).
18. J. N. FRIEND, *Trans. Am. Electrochem. Soc.*, **40**, 63 (1921).
19. S. YAMAGUCHI, *Koll. Z.*, **126**, 155 (1952).

# Corrosion Properties of Titanium in Marine Environments[1]

H. B. Bomberger, P. J. Cambourelis, and G. E. Hutchinson

*Rem-Cru Titanium, Inc., Midland, Pennsylvania*

ABSTRACT

Data are presented on the behavior of commercially pure titanium and several common structural metals exposed up to five years at Kure Beach, North Carolina. Tests include exposures to the atmosphere, quiet and flowing sea water, jet impingement, stress corrosion, and galvanic couples. These tests indicate that titanium is unaffected by marine environments.

## Introduction

Commercially pure titanium has, in addition to a high strength-to-weight ratio, the desirable property of outstanding corrosion resistance to a number of chemicals. It has excellent resistance to nitric acid solutions (1–5), although violent reaction of a titanium-manganese alloy with red fuming nitric acid (12) suggests that work with any titanium-base material in fuming nitric should be conducted with caution. Especially interesting is the metal's resistance to moist chlorine gas (1), sodium and calcium hypochlorites, chloride salt solutions including cupric and ferric chlorides, and some mixed acids (1, 2). Titanium also has a high resistance to many organic acids and compounds (1, 6), but the metal is attacked by hydrochloric, hydrofluoric, sulfuric, oxalic, trichloroacetic, and unaerated formic acid solutions.

Hutchinson and Permar (1) reported on the apparent immunity of titanium to sea water by atmospheric, jet impingement, and sea water immersion tests.

These results were confirmed by Williams (7) along with additional information. Exposures up to eight months in the atmosphere, in quiescent and rapidly moving sea water, and on jet impingement had a negligible effect. No evidence of stress corrosion was observed after six months on titanium stressed to nearly the yield strength for 0.1% offset.

LaQue (8) reported similar results for titanium subjected to marine environments for extended periods of time under many test conditions. No significant effect was observed under any test condition. Excellent resistance to erosion, corrosion fatigue, stress corrosion, crevice corrosion, and pitting was reported. The galvanic effect of titanium in contact with other materials was found to be about the same as that of the 18-8 stainless steels.

This paper reports additional information on titanium and a number of controls exposed to marine environments at Kure Beach since midsummer of 1948.

## Experimental

Commercially pure, cold-rolled titanium[2] was tested along with the controls listed in Table I. Titanium sheet had a nominal composition of more than 99% titanium, 0.3% carbon, and a few tenths to a few hundredths of 1% oxygen, nitrogen, and iron.

Except in jet impingement and galvanic tests, materials were tested as 6 in. x 1½ in. x 1/32 in. to 1/16 in. strips. After testing, aluminum alloys, stainless steels, Inconel, and titanium were cleaned by swabbing in 65% nitric acid for three minutes. The copper and Monel were swabbed in 20% hydrochloric acid for 10 seconds. Cleaning techniques had negligible effect on the base material.

### *Atmospheric Tests*

Unlike the control specimens, titanium showed no significant weight loss or change in appearance on being exposed to sea air 80 and 800 ft from the ocean for five years, as indicated by Fig. 1. Aluminum alloys acquired a mottled limestone gray appearance, stainless steels became rusty brown, Monel turned dark green, and Inconel became speckled with brown spots. Control specimens from the shore rack were more discolored and corroded more rapidly than those in the main lot 800 ft from the ocean.

Materials exposed to the industrial atmosphere of Bridgeport, Connecticut, for four years and eleven months were similar in appearance to those removed from the main lot at Kure Beach, but the average corrosion rates, given in Table II, were a little higher. The same materials exposed five years to the rural atmosphere north of Wilmington, Delaware, appear by visual examination to be completely un-

[1] Manuscript received November 12, 1953. This paper was prepared for delivery before the Wrightsville Beach Meeting, September 13 to 16, 1953.

[2] Produced by Rem-Cru Titanium, Inc.

TABLE I. *Control alloys tested at Kure Beach, N. C.*

Aluminum alloys

| Alloy | Surface condition | Cu | Fe | Si | Mn | Mg | Cr | Zn | Ti | Al |
|---|---|---|---|---|---|---|---|---|---|---|
| 24S-T3 | Bright | 4.54 | 0.30 | 0.15 | 0.58 | 1.46 | — | — | — | Bal. |
| Alclad 24S-T3: | Bright | | | | | | | | | |
| coating | | 0.27 | 0.13 | 0.07 | 0.01 | 0.13 | — | — | — | Bal. |
| core | | 4.19 | 0.28 | 0.11 | 0.56 | 1.39 | — | — | — | Bal. |
| 52S-1/2H | Bright | 0.02 | 0.15 | 0.12 | 0.05 | 2.53 | 0.21 | — | — | Bal. |
| Alclad 75S-T6: | Bright | | | | | | | | | |
| coating | | 0.09 | 0.36 | 0.07 | 0.01 | 0.15 | — | 1.31 | — | Bal. |
| core | | 1.58 | 0.15 | 0.08 | 0.12 | 2.61 | 0.24 | 5.90 | 0.05 | Bal. |

Stainless steels

| Alloy | Surface condition | Cr | Ni | Mn | P | S | Si | C | Mo | Cb | Fe |
|---|---|---|---|---|---|---|---|---|---|---|---|
| Type 302 | Bright, cold rolled | 18.37 | 8.71 | 0.93 | 0.019 | 0.009 | 0.600 | 0.099 | — | — | Bal. |
| Type 316 | Hot rolled & pickled | 17.36 | 12.68 | 1.60 | 0.024 | 0.023 | 0.44 | 0.053 | 1.89 | — | Bal. |
| Type 347 | Hot rolled & pickled | 18.58 | 11.27 | 1.76 | 0.026 | 0.020 | 0.58 | 0.058 | — | 0.87 | Bal. |

Nickel alloys

| Alloy | Surface condition | Cu | Cr | Ni | Mn | P | S | Si | C | Fe |
|---|---|---|---|---|---|---|---|---|---|---|
| Monel | Cold rolled & annealed | 29.75 | — | 67.85 | 1.04 | 0.029 | 0.008 | 0.127 | 0.072 | 0.98 |
| Inconel | Hot rolled | — | 14.79 | 77.63 | 0.20 | 0.010 | 0.008 | 0.183 | 0.056 | 6.96 |

affected, except Monel which had a green tarnish film and the aluminum alloys which had weathered to a limestone gray. Exposures at these three test sites are being continued indefinitely for future examination.

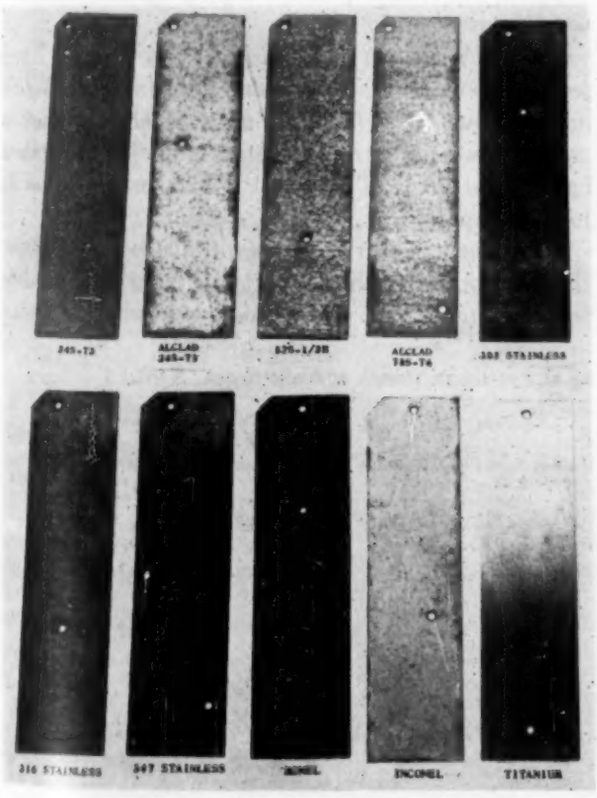


FIG. 1. Materials exposed 80 ft from the ocean for five years

*Immersion Tests*

The titanium specimens immersed in sea water flowing at 3 ft/sec had, after cleaning, essentially the same weight and bright surface that they had when installed 4.5 years earlier. Although all materials were fouled by marine organisms, corrosion was observed only on the control specimens as indicated in Fig. 2 and 3. Inconel, Monel, 24S-T3 aluminum alloy, and Type 347 stainless steel suffered rather heavy localized attack. Corrosion rates and maximum pit depths for these materials are given in Table III. Corrosion rates for control specimens after 483 days were of the same order as those obtained after 618 days and 4.5 years, except for

TABLE II. *Corrosion rates of materials exposed to the atmosphere*

| Materials* | 5 Years at Kure Beach, N. C. | | 4 Years, 11 months in Bridgeport, Conn. |
|---|---|---|---|
| | Shore rack 80 ft from breakers | Main lot 800 ft from breakers | |
| Titanium | Nil | Nil | 0.00008 |
| 24S-T3 | 0.0256 | 0.0028 | 0.0154 |
| Alclad 24S-T3 | 0.0197 | 0.0034 | 0.0122 |
| 52S-1/2H | 0.0139 | 0.0026 | 0.0135 |
| Alclad 75S-T6 | 0.0278 | 0.0034 | 0.0140 |
| 302 Stainless | 0.0009 | Nil | 0.0001 |
| 316 Stainless | 0.0013 | Nil | 0.0003 |
| 347 Stainless | 0.0011 | Nil | 0.0003 |
| Monel | 0.0175 | 0.0107 | 0.0349 |
| Inconel | 0.0014 | 0.0003 | 0.0094 |

* Average corrosion rates from three specimens in mils per year.

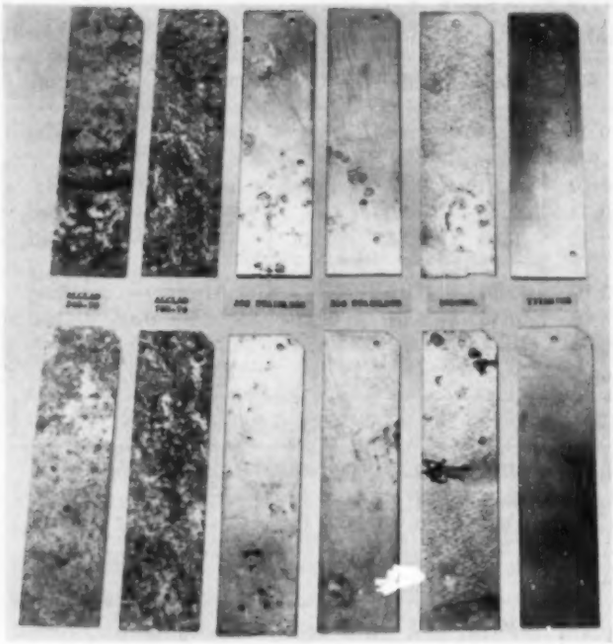

FIG. 2. Materials exposed to flowing sea water for 4½ years

Monel and Type 347 stainless steel where a slight increase was noted. Slightly higher rates were reported for these controls by Hutchinson and Permar for 120-day exposure tests in a trough (1).

Similar results were observed for materials exposed for 480 days in quiet sea water in the basin at Kure Beach as illustrated in Fig. 4. Some materials were heavily attacked by pitting and crevice corrosion. No noticeable change or measurable weight loss could be detected on the six titanium test specimens. Corrosion rates, given in Table IV, are essentially the same as those reported by Hutchinson and Permar for 120-day exposures in the basin.

### *Galvanic Couple Tests*

Although titanium is an inherently reactive metal, it is found at the noble end of the galvanic series

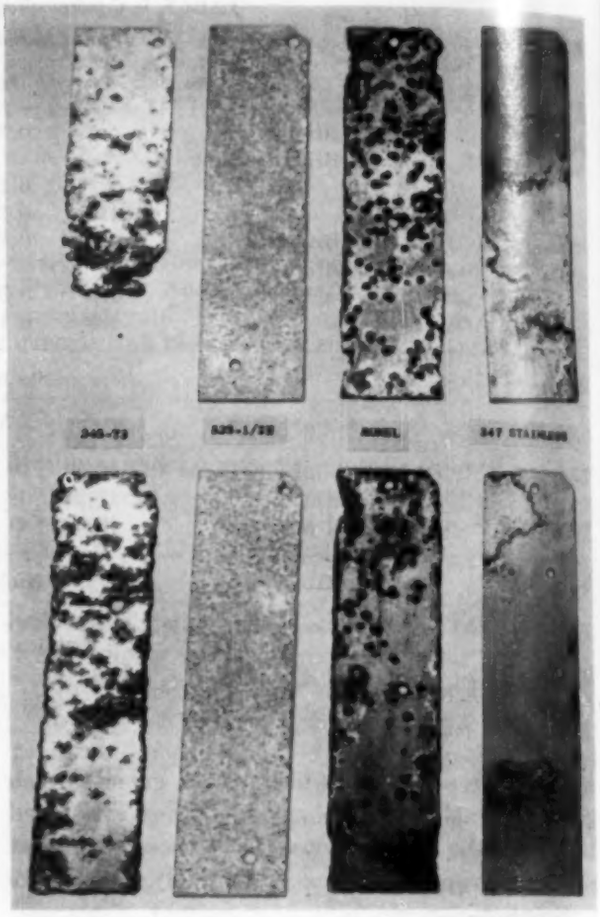


FIG. 3. Materials exposed to flowing sea water one year and 253 days.

for metals in sea water along with silver, Monel, and passive Type 316 stainless steel, and has a steady-state potential of −0.15 volt, vs. saturated calomel, at 25°C. The metal is even more noble at lower temperatures.

Additional potential studies at Kure Beach show that titanium has the property of polarizing readily to the potential of more anodic materials, such as

TABLE III. *Materials immersed in sea water flowing at 3 ft/sec in trough at Kure Beach, N. C.*

| Material* | 483 Days | | | 618 Days | | | 4½ Years | | |
|---|---|---|---|---|---|---|---|---|---|
| | Corr. rate mpy | Max. face pitting, in. | Max. edge pitting, in. | Corr. rate mpy | Max. face pitting, in. | Max. edge pitting, in. | Corr. rate mpy | Max. face pitting, in. | Max. edge pitting, in. |
| Titanium | Nil | None | None | — | — | — | 0.00003 | None | None |
| 24S-T3 | 4.80 | 0.054† | 0.14 | 5.08 | 0.054† | 0.15 | — | — | — |
| Alclad 24S-T3 | 1.10 | None | None | — | — | — | 1.17 | 0.035† | 0.050 |
| 52S-1/2H | 1.52 | 0.046 | 0.10 | 1.47 | 0.035 | 0.040 | — | — | — |
| Alclad 75S-T6 | 1.21 | None | None | — | — | — | 0.781 | 0.035† | 0.20 |
| 302 Stainless | 0.08 | 0.031 | 0.060 | — | — | — | 0.088 | 0.060 | 0.20 |
| 316 Stainless | 0.16 | 0.020 | 0.10 | — | — | — | 0.061 | 0.050 | 0.10 |
| 347 Stainless | 0.28 | 0.068† | 1.5‡ | 3.57 | 0.068† | 1.5‡ | — | — | — |
| Monel | 0.144 | 0.020 | 0.12 | 1.27 | 0.045† | 0.050 | — | — | — |
| Inconel | Nil | 0.008 | None | — | — | — | 0.094 | 0.035† | 0.10 |

* Three specimens of each.
† Specimens perforate with pits.
‡ Maximum depth of crevice corrosion.

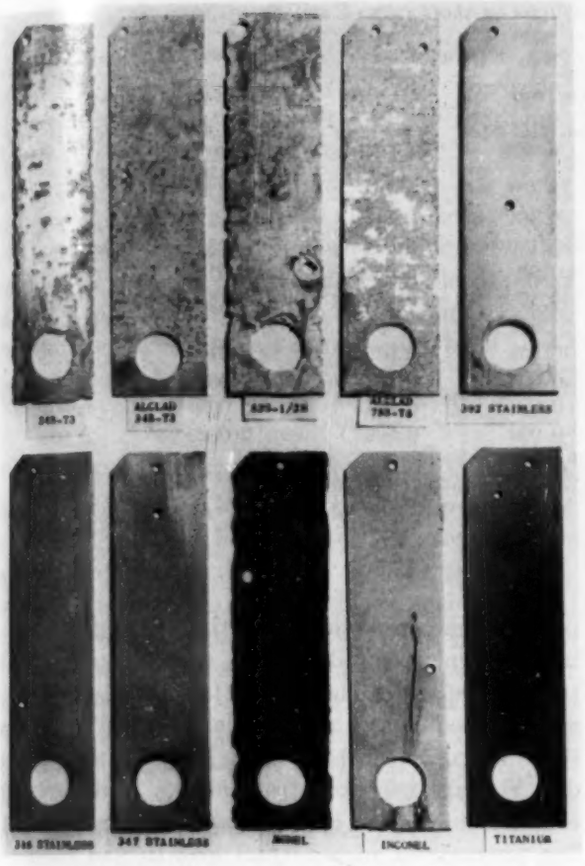


Fig. 4. Materials immersed in quiet sea water 480 days

plain carbon steel, with which it may be in contact (8, 9). The effect of this characteristic was investigated by experiments in which panels of one material were riveted to another with different area relationships. According to LaQue (8), the galvanic contribution of titanium in a couple is about the same as an 18-8 stainless steel, and experiences with this material can be used as a safe guide on replacing stainless steel with titanium.

TABLE IV. *Materials immersed 480 days in quiet sea water in the basin at Kure Beach, N. C.*

| Material* | Average corrosion rate, mpy | Max. face pitting, in. | Max. edge pitting, in. |
|---|---|---|---|
| Titanium | Nil | None | None |
| 24S-T3 | 2.24 | 0.054† | 0.37 |
| Alclad 24S-T3 | 0.612 | 0.001 | 0.001 |
| 52S-1/2H | 0.96 | 0.065† | 0.21 |
| Alclad 75S-T6 | 0.60 | 0.001 | 0.001 |
| 302 Stainless | 0.146 | 0.060 | 0.050 |
| 316 Stainless | 0.24 | 0.060 | 1.50‡ |
| 347 Stainless | 1.43 | 0.067† | 2.50‡ |
| Monel | 1.38 | 0.039 | 0.20 |
| Inconel | 0.49 | 0.034 | 4.75‡ |

* Six specimens of each.
† Specimens perforated.
‡ Maximum depth of crevice corrosion.

In marine atmosphere and sea water tests there were no indications that titanium suffered in any way as a result of being in contact with the common metals and alloys. Corrosion rates for the materials in contact with titanium in the basin at half tide are given in Table V. Titanium coupled with Inconel, silver, and Types 302 and 316 stainless steels appeared to have a negligible effect on these materials. However, a noticeable increase in corrosion occurred with the remaining specimens coupled to titanium. This was especially true for magnesium. In general, rates obtained after 360 days' exposure are similar to or slightly less than those observed after 193 days.

Schlain (10), and Paige and Ketcham (11) re-

TABLE V. *Sea water galvanic couple tests in basin at half tide at Kure Beach*

| Materials | 193-Day exposures | | | 369-Day exposures | | |
|---|---|---|---|---|---|---|
| | Uncoupled corr. rates, mpy* | Coupled corr. rates, mpy | | Uncoupled corr. rate, mpy* | Coupled corr. rate, mpy | |
| | | Metal area 7 × Ti area** | Metal area ½ × Ti area† | | Metal area 7 × Ti area** | Metal area ½ × Ti area† |
| FS-1 Magnesium | 65.06‡ | 920.7§ | Lost | — | — | — |
| Alclad 24S-T3 | 0.55 | 1.20 | 1.70 | 0.233 | 0.89 | Lost |
| 52S-1/2H | 0.457 | 0.91 | 7.42 | Lost | 0.75 | 4.60 |
| Alclad 75S-T6 | 1.21 | 1.38 | 6.12 | 0.633 | 0.83 | Lost |
| Copper | 0.511 | 0.92 | 1.015 | 0.577 | 0.94 | 2.00 |
| Steel (low carbon) | 6.10 | 12.32 | 17.24 | 8.60 | 12.20 | 12.90 |
| Monel | 0.071 | 0.060 | 0.130 | 0.073 | 0.06 | 0.130 |
| Inconel | 0.002 | Nil | 0.002 | Nil | Nil | Nil |
| 302 Stainless | 0.058 | 0.010 | 0.120 | 0.004 | 0.008 | 0.096 |
| 316 Stainless | Nil | Nil | Nil | Nil | Nil | Nil |
| Silver | — | — | — | 0.70 | 1.10 | 1.22 |

* Average of one 6 in. x 1.5 in. specimen and two 1.5 in. x 0.75 in. specimens.
** One 6 in. x 1.5 in. specimen.
† Average of two 0.75 in. x 1.5 in. specimens.
‡ 44 day exposure.
§ Two-day exposure.

TABLE VI. *Atmospheric galvanic-couple tests on shore rack, Kure Beach*

| Material | 360-Day exposure | | | 4 Years & 8 months exposure | | |
|---|---|---|---|---|---|---|
| | Uncoupled corr. rates,* mpy | Coupled corr. rate, mpy | | Uncoupled corr. rates,* mpy | Coupled corr. rate, mpy | |
| | | Metal area 7 × Ti area** | Metal area ⅐ × Ti area† | | Metal area 7 × Ti area** | Metal area ⅐ × Ti area** |
| FS-1 Magnesium | 1.26 | 2.50 | 5.5 | 0.88‡ | 1.17‡ | 3.52‡ |
| Alclad 24S-T3 | 0.06 | 0.277 | 0.86 | 0.0549 | 0.2130 | 0.291 |
| 52S-1/2H | 0.05 | 0.056 | 0.199 | 0.0845 | 0.0362 | 0.0813 |
| Alclad 75S-T6 | 0.10 | 0.460 | 0.99 | 0.0525 | 0.0786 | 0.393 |
| Copper | 0.12 | 0.022 | 0.42 | 0.0852 | 0.1350 | 0.241 |
| Steel (low carbon) | 6.13 | 9.82 | Lost | — | — | — |
| Monel | Nil | 0.020 | 0.032 | 0.0152 | 0.0197 | 0.0320 |
| Inconel | 0.011 | 0.006 | 0.003 | 0.0025 | 0.0029 | 0.0032 |
| 302 Stainless | Nil | 0.009 | 0.023 | 0.0083 | 0.0091 | 0.0015 |
| 316 Stainless | 0.004 | 0.004 | 0.003 | 0.0035 | 0.0029 | 0.0058 |

* Average of one 6 in. x 1.5 in. specimen and two 0.75 in. x 1.5 in. specimens.
** One 6 in. x 1.5 in. specimen.
† Average of two 0.75 in. x 1.5 in. specimens.
‡ Three years and 160 days' exposure.

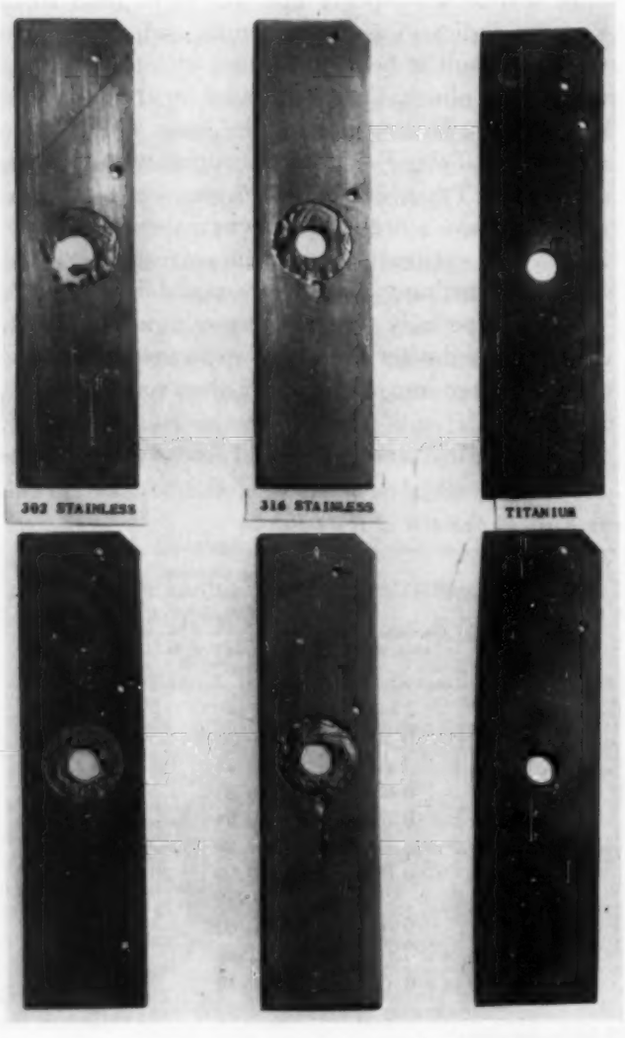


FIG. 5. Materials tested for crevice corrosion in quiet sea water.

ported higher corrosion rates than these for copper, iron, magnesium, aluminum alloys coupled with titanium of the same area in two to three liters of aerated sodium chloride solutions for relatively short times (24–48 hr). These higher rates may be due in part to short test periods and probable changes in solution composition, since rate-controlling phenomena such as film growth and polarization are a function of time and environment. Paige and Ketcham also noted that stainless steel and titanium are similar in their electrochemical behavior.

The galvanic couples tested on the 80-ft shore rack gave similar results, although in this case, as indicated in Table VI, all corrosion rates are significantly less. Again, Inconel and Types 302 and 316 stainless steels appeared to be unaffected by the titanium, and corrosion rates of these materials varied little with time. However, the corrosion of copper, magnesium, and the aluminum alloys was increased by titanium and the rates of these materials decreased with time.

### *Erosion Tests*

Titanium subjected to the action of a submerged jet of sea water for 30 days containing 2.4% by volume of entrained air at a velocity of 12 ft/sec and an average temperature of 23.5°C resulted in no significant weight loss. There was no change in the surface appearance. Titanium specimens whirled through sea water at 30 ft/sec for 60 days suffered negligible attack. Titanium also has an unusually high resistance to cavitation erosion. The metal is said to be superior to conventional propeller alloys and almost as good as stainless steel designed especially for cavitation resistance (8).

### *Crevice Corrosion Tests*

Special tests were designed to determine the susceptibility of titanium to crevice corrosion. In these experiments, fiber, and zinc and cadmium-plated steel washers were bolted to 6 in. x 1.5 in. test strips. After 360 days' immersion in sea water in the basin and four years and eight months exposure on the shore rack no evidence of pitting, crevice corrosion, or any other form of attack could be found on the titanium. However, the nontitanium control specimens suffered from localized attack as illustrated by Fig. 5.

### *Stress Corrosion Tests*

Titanium containing high residual stresses or under static tensile loads does not appear to be susceptible to stress corrosion or corrosion fatigue in sea air and water. Erichsen cup test specimens, stressed as highly as possible without causing failure, were exposed in the basin for 360 days and in the salt air for four years and eight months. In this time there was no evidence of stress corrosion cracking. Titanium tensile specimens with a yield strength of 105,000 psi have been under static loads up to 80,000 psi for over five years in the main lot at Kure Beach without a sign of failure.

There appears to be no difference between the endurance limit of titanium in sea water and in air. The value for titanium in sea water is 60,000 psi. This is well above the values for materials regularly used for pump and propeller shafts (8).

## Summary

Commercially pure titanium exposed to sea, industrial, and rural atmospheres for approximately five years and to sea water up to four and a half years appeared to be completely unaffected. Long-time tests designed to show susceptibility to sea water erosion, crevice corrosion, galvanic corrosion, pitting, stress corrosion, and corrosion fatigue had no noticeable effect on the metal. Titanium coupled to Inconel, silver, and Types 302 and 316 stainless steels had a negligible effect on the corrosion rates of these materials, but the rates of Monel, copper, low-carbon steel, and aluminum alloys were in some cases more than doubled.

## Acknowledgments

The authors are grateful to Mr. F. L. LaQue and the staff of the International Nickel Company, Inc., at the Kure Beach and Harbor Island Test Stations for their advice and assistance in carrying out this work.

Any discussion of this paper will appear in a Discussion Section to be published in the June 1955 issue of the Journal.

## REFERENCES

1. G. E. Hutchinson and P. H. Permar, *Corrosion*, **5**, 319 (1949).
2. L. B. Golden, I. R. Lane, Jr., and W. L. Acherman, *Ind. Eng. Chem.*, **44**, 1930 (1952).
3. E. A. Gee, L. B. Golden, and W. E. Lusby, Jr., *ibid.*, **41**, 1668 (1949).
4. G. C. Kiefer and W. W. Harple, *Metal Progr.*, **63**, 74 (1953).
5. F. H. Beck and M. G. Fontana, *Corrosion*, **9**, 287 (1953).
6. I. R. Lane, Jr., L. B. Golden, and W. L. Acherman, *Ind. Eng. Chem.*, **45**, 1067 (1953).
7. W. L. Williams, U. S. Engineering Experimental Station Report C-3395, C-3501B.
8. F. L. LaQue, Engineering Research and Development Laboratory Symposia, Fort Belvoir, Virginia, 55, August (1952).
9. F. L. LaQue, *Am. Soc. Testing Materials, Proc.*, **51**, 545 (1951).
10. D. Schlain, Bureau of Mines Report of Investigation 4965, April (1953).
11. H. Paige and S. J. Ketcham, *Corrosion*, **8**, 413 (1952).
12. J. F. Scheer, *Metal Progr.*, **64**, 110 (1953).

# Jet Impingement Tests[1]

P. T. Gilbert

*British Non-Ferrous Metals Research Association, London, England*

AND

F. L. LaQue

*International Nickel Company, Inc., New York, New York*

ABSTRACT

This paper describes the operation of jet impingement test apparatus in the laboratories of The British Non-Ferrous Metals Research Association in London and at International Nickel Company's Marine Corrosion Test Station at Harbor Island, N. C. Certain differences in results obtained on the same materials in the two laboratories are discussed with relation to differences in testing conditions. Particular attention is given a comparison between results secured with water that is recirculated and used over and over again, as is the practice in the B.N.F.M.R.A. laboratories, with results obtained with water that is passed through the apparatus only once, as has been the regular practice at Harbor Island. Effects of air bubbles, jet velocity, and other incidental factors are also discussed. The relationship between test results and service experience is considered. It is concluded that test conditions established for use in the B.N.F.M.R.A. laboratory, using recirculated water, are too drastic when applied at Harbor Island, using water that is not recirculated, to permit proper comparisons of materials. The testing conditions at Harbor Island can be modified to yield results in harmony with the B.N.F.M.R.A. results either by reducing the jet velocity or by recirculating the water.

## Introduction

Failure of certain condenser tube alloys as a result of corrosion-erosion produced by salt water moving at moderately high velocity stimulated research on this subject, which has been carried on more or less continuously since the pioneer work of Bengough and May (1). They found that the type of attack encountered in service could be reproduced in the laboratory by subjecting specimens to jets of sea water containing air bubbles of a particular size. Apparatus used and other details of the test procedure have been described (2, 3).

A 24-unit jet impingement apparatus was used with recirculated water in the B.N.F.M.R.A. Laboratory in London, and a similar apparatus was installed at the Harbor Island Test Station for use with sea water that passed through only once. A duplicate apparatus at Harbor Island was arranged so that water could be recirculated as in the B.N.F.M.R.A. Laboratory.

Prior to installation of the B.N.F.M.R.A. type of apparatus at Harbor Island, jet tests were conducted there with apparatus in which air was drawn into the water by aspirating action of a venturi-type nozzle (4, 5). This device produced damage not unlike that observed with the British apparatus, but in comparing results with specimens of several alloys which were exchanged for parallel tests in the two laboratories, considerable difference in behavior was observed. It was thought that this might be due to some peculiar characteristics of the two types of apparatus. Therefore, arrangements were made to operate a duplicate of the British apparatus at Harbor Island.

This paper presents an account of some of the tests made in England and at Harbor Island which illustrate differences in behavior that have been observed with the same apparatus and which show effects of some important variable factors.

## Results of Tests in Two Laboratories

Lack of agreement between results in the two laboratories is illustrated conveniently by comparing relative behavior of Admiralty Brass and Aluminum Brass and by observation of the effects of air bubbles on the extent of impingement attack of Admiralty Brass.

Table I presents data on the average performance of Aluminum Brass and Admiralty Brass under nominally the same testing conditions (except for recirculation of water in the British tests) in the two laboratories. The approximately 8:1 superiority of Aluminum Brass over Admiralty Brass, shown by British tests with air bubbles admitted, was reduced to about 2:1 in Harbor Island tests. This was due to much more severe attack of Aluminum Brass at Harbor Island, since Admiralty Brass

[1] Manuscript received November 4, 1953. This paper was prepared for delivery before the Wrightsville Beach Meeting, September 13 to 16, 1953.

TABLE I. *Results of Jet impingement tests with B.N.F.M.R.A. apparatus at Harbor Island, N. C.*

Velocity of jet: 15 ft/sec
Duration: 28 days

| Water system | % Air added | Temp, °C | Depth of impingement attack (mm) | |
|---|---|---|---|---|
| | | | Arsenical | |
| | | | Admiralty Brass | Aluminum Brass |
| Once through | 3 | 18 | 0.37 | No test |
| | | 20 | 0.36[a] | 0.15[b] |
| | | 24 | 0.22 | 0.16 |
| Once through | 0 | 15 | 0.15 | No test |
| | | 25 | 0.33 | No test |
| Recirculated | 3 | 20[c] | 0.34[c, d] | 0.04[c, e] |
| | | 30 | 0.25 | 0.01 |
| Recirculated | 0 | 25 | 0.27 | 0.00 |

[a] Range 0.20 to 0.61.
[b] Range 0.08 to 0.23.
[c] Test made in England, 30-day run.
[d] Range 0.14 to 0.51.
[e] Range 0 to 0.66 (one specimen out of 20 pitted to depth of 0.66 mm. No impingement attack greater than 0.02 mm.)

was affected to about the same extent at both locations.

Similarity in nature and extent of attack of Admiralty Brass and Aluminum Brass in the apparatus as used at Harbor Island is illustrated by Fig. 1.

Another major difference between the British and the Harbor Island results was the failure of the latter to show any important or consistent effect of air bubbles in aggravating impingement attack on Admiralty Brass under conditions which regularly showed no impingement attack unless air bubbles were present in the British Laboratory. This is illustrated by results of tests on Admiralty Brass as shown in Table I. Fig. 2 shows Admiralty Brass specimens after test with and without air bubbles.

## Tests with Recirculated Water at Harbor Island

Since the principal difference between testing conditions was recirculation of water in the British Laboratory as compared with passing it through the jets only once at Harbor Island, it was decided to modify a test unit at Harbor Island to permit recirculation of water. This change in testing conditions sufficed to bring results more in line with those regularly observed in the B.N.F.M.R.A. Laboratory. A typical comparison of results on Admiralty Brass and Aluminum Brass with once-through and recirculated sea water at Harbor Island is provided by Table I.

It will be seen that when sea water at Harbor Island was recirculated as in the B.N.F.M.R.A. Laboratory, the relative behavior of Aluminum Brass and Admiralty Brass came into line with that ordinarily observed in British tests.

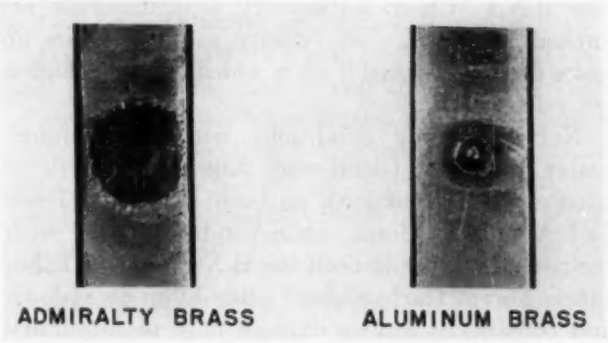


Fig. 1. Admiralty Brass and Aluminum Brass specimens after impingement test with once-through water at 15 ft/sec at Harbor Island.

However, even with recirculated water at Harbor Island, it was not possible to show any strong effect of air bubbles on the extent of impingement attack. Typical results of tests at Harbor Island with and without the admission of air bubbles are shown in Table I.

Without further reference to effects of air bubbles, it became evident that, at least regarding comparison between Admiralty Brass and Aluminum Brass, both the B.N.F.M.R.A. Laboratory and Harbor Island tests with recirculated water rated these alloys more in line with their behavior under many conditions of use than did the more drastic tests at Harbor Island with water that was not recirculated. Apparently what was involved was some sort of trigger effect of erosive conditions created by the jet test. This trigger effect seemed to be a breakdown of protective film. Once this occurred, there would be an abrupt increase in extent of impingement attack to a level which would not be increased much further by greater intensification of erosive forces. In this connection, it has been observed in

Fig. 2. Tests at Harbor Island with once-through water at 15 ft/sec. Impingement attack of Admiralty Brass with and without air bubbles in the jet.

the B.N.F.M.R.A. Laboratory that materials attacked at a certain jet velocity without air are no more deeply attacked if air is added at this or higher jet velocities.

Normal testing conditions with once-through water at Harbor Island were sufficiently drastic to promote film breakdown on both Aluminum Brass and Admiralty Brass, while conditions used with recirculated water in both the B.N.F.M.R.A. Laboratory and at Harbor Island caused film breakdown and consequent serious damage only to Admiralty Brass.

Under these circumstances, it would be easy to understand why the possible mechanical effects of air bubbles might be masked in tests with once-through water at Harbor Island. However, a question remains as to why the effects of air bubbles observed with recirculated water in the B.N.F.M.R.A. Laboratory were not observed also with recirculated water at Harbor Island.

### Tests with Once-Through Water in England

A jet test was operated with once-through sea water in England with the cooperation of Imperial Chemical Industries, Ltd. Results so far obtained are summarized in Table II. The amount of attack produced was in general less than that in once-through tests at Harbor Island, but results were similar in most respects. Thus, Aluminum Brass was attacked only slightly less than Admiralty Brass, and the differences among all materials were slight. There appeared to be some effect of adding air

TABLE II. *Results of tests in England using once-through water*

| Run No. | BA/53 | BB/53 | BC/53 | BD/53 |
|---|---|---|---|---|
| Water speed (ft/sec) | 15 | 15 | 15 | 30 |
| % Air by volume | 3 | 0 | 3 | 3 |
| Average water temp, °C | 7.5 | 9 | 13 | 16 |
| **Material** | **Depth of impingement attack (mm)** | | | |
| 70:30 Cu Ni, 0.04% Fe | 0.05 | 0.03 | 0.09 | 0.10 |
| | 0.06 | 0.04 | 0.07 | 0.08 |
| 70:30 Cu Ni, 0.8% Fe | 0.10 | 0.01 | 0.07 | 0.18 |
| | 0.11 | 0.01 | 0.10 | 0.14 |
| 90:10 Cu Ni, 1% Fe | 0.08 | 0.05 | 0.09 | 0.07 |
| | 0.07 | 0.05 | 0.09 | 0.05 |
| 90:10 Cu Ni, 2% Fe | 0.09 | 0.0 | 0.09 | 0.16 |
| | 0.09 | 0.0 | 0.10 | 0.15 |
| 95:5 Cu Ni, 0.6% Fe | 0.07 | 0.06 | 0.11 | 0.10 |
| | 0.09 | 0.03 | 0.09 | 0.12 |
| 95:5 Cu Ni, 1.3% Fe | 0.08 | 0.07 | 0.12 | 0.23 |
| | 0.07 | 0.06 | 0.13 | 0.25 |
| Arsenical copper | 0.06 | 0.06 | 0.11 | 0.17 |
| | 0.07 | 0.06 | 0.11 | 0.15 |
| Admiralty Brass (70:29:1) | 0.09 | 0.05 | 0.11 | 0.11 |
| | 0.08 | 0.07 | 0.11 | 0.08 |
| Aluminum Brass (76:22:2) | 0.06 | 0.07 | 0.07 | 0.08 |
| | 0.05 | 0.07 | 0.07 | 0.09 |

TABLE III. *Effect of variation of water speed in recirculating jet impingement test without added air bubbles in B.N.F.M.R.A. laboratory*

| Run No. | AD/52 | AG/52 | Z/49 | AB/49 | B/53 | AE/52 | AA/49 | D/53 | A/53 |
|---|---|---|---|---|---|---|---|---|---|
| Water speed (ft/sec) | 10 | 15 | 15 | 15 | 22.5 | 30 | 30 | 15 | 15 |
| % Air | 0 | 0 | 0 | 0 | 0 | 0 | 0 | * | ** |
| **Material** | **Depth of impingement attack** | | | | | | | | |
| 70:30 Cu Ni, 0.04% Fe | 0 | 0 | — | 0 | 0.73 | 0.50 | 0.47 | 0 | 0.35 |
| | 0 | 0 | | 0 | 0.55 | 0.23 | 0.52 | 0 | 0.23 |
| 70:30 Cu Ni, 0.4% Fe | — | 0 | — | — | — | — | — | 0 | — |
| | | 0 | | | | | | 0 | |
| 70:30 Cu Ni, 0.8% Fe | — | 0 | — | — | — | — | — | 0 | — |
| | | 0 | | | | | | 0 | |
| 65:30 Cu Ni, 2% Fe | 0 | 0 | 0 | 0 | 0 | 0 | 0 | 0 | 0 |
| | 0 | 0 | 0 | 0 | 0 | 0 | 0 | 0 | 0 |
| 90:10 Cu Ni, 1% Fe | — | 0 | — | — | — | — | — | 0 | — |
| | | 0 | | | | | | 0 | |
| 90:10 Cu Ni, 2% Fe | 0 | 0 | 0 | 0 | 0 | 0 | 0 | 0 | 0 |
| | 0 | 0 | 0 | 0 | 0 | 0 | 0 | 0 | 0 |
| 95:5 Cu Ni, 0.6% Fe | — | 0 | — | — | — | — | — | 0 | — |
| | | 0 | | | | | | 0 | |
| 95:5 Cu Ni, 1.3% Fe | — | 0 | 0 | 0 | — | — | 0 | 0 | — |
| | | 0 | 0 | 0 | | | 0 | 0 | |
| Arsenical copper | 0 | 0.23 | — | 0.38 | 0.16 | 0.18 | 0.89 | 0.41 | 0.11 |
| | 0 | 0.17 | | 0.39 | 0.16 | 0.15 | 0.73 | 0.38 | 0.13 |
| 70:30 Brass | 0 | 0.02 | — | 0.27 | 0.44 | 0.43 | 0.70 | 0.32 | 0.32 |
| | 0 | 0.03 | | 0.35 | 0.39 | 0.56 | 0.70 | 0.32 | 0.31 |
| Admiralty (70:29:1) Brass | 0 | 0 | 0 | — | 0.61 | 0.67 | — | 0 | 0.38 |
| | 0 | 0 | 0.01 | | 0.64 | 0.68 | | 0 | 0.36 |
| Aluminum Brass (76:22:2) | — | 0.01 | — | <0.01 | — | — | 0 | 0 | — |
| | | 0.03 | | <0.01 | | | 0 | 0 | |

* Air bubbled into the bath instead of passing through the jets.

** Air bubbled into the bath and nitrogen (3%) passed through jets; depth of attack in mm.

bubbles with some of the cupro-nickels, but not with the brasses, and, in general, addition of air had much less effect than in tests made at B.N.F.M.R.A. with recirculated water. Tests made in the B.N.F.M.R.A. laboratories with recirculated sea water taken from the site of the once-through test equipment gave results similar to other recirculating tests and quite different from once-through tests.

Sea water in once-through tests was filtered through nylon cloth before passing through the jets. The first two runs in Table II were carried out in winter, and it was observed that appreciable quantities of fine silt came through the filter. During the runs carried out in spring and summer much less silt passed, but considerable quantities of small marine organisms came through the jets and grew on the sides of the containing basin, specimen holders, etc.

### Effects of Air Bubbles in Tests with Recirculated Water

B.N.F.M.R.A. investigators developed data to indicate the severity of erosive forces with respect to the jet velocity above which air bubbles were not required to produce impingement attack. Several alloys were tested with recirculated water, giving the data summarized in Table III.

Referring to data on Admiralty Brass, B.N.F.M.R.A. tests indicate that air bubbles are not essential for impingement attack when jet velocity is 22.5 ft/sec or greater. However, a similar critical velocity must be below 15 ft/sec with recirculated water at Harbor Island since, as shown by Table I, as much attack occurs with this jet velocity without air bubbles as with them. Up to now, sufficient tests have not been made under those circumstances to establish whether there is a jet test velocity with recirculated water at Harbor Island such that air bubbles exert a controlling effect. One run without air bubbles at a jet velocity of 7.5 ft/sec developed attack of Admiralty Brass to a depth of 0.19 mm. This was less attack than the 0.27 mm depth in a companion test without air bubbles at a jet velocity of 15 ft/sec. However, it appears that the jet test velocity at which zero attack of Admiralty Brass would occur in the absence of air bubbles in recirculated water at Harbor Island would be under 7.5 ft/sec and, therefore, well under the 22.5 ft/sec critical velocity indicated by British results.

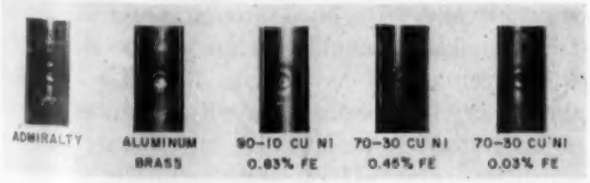


Fig. 3. Jet impingement attack of condenser tube alloys with once-through water at 15 ft/sec at Harbor Island.

Data in the last two columns of Table III are particularly significant in showing that the effect of air bubbles observed in British tests is mechanical rather than chemical, since saturation of water with air outside the jets did not promote impingement attack, whereas admission of nitrogen through the jets did do this.

### Tests of Common Condenser Tube Alloys

As indicated by data for Admiralty Brass and Aluminum Brass in Table I, standard testing conditions with once-through water at Harbor Island may be so severe as to cause film breakdown on most of the common condenser tube alloys and thus tend to mask differences that show up under less drastic testing conditions and in common practical service. The appearance of specimens after test with once-through water at Harbor Island is shown in Fig. 3. Similar, but less severe effects occurred in once-through tests in England as shown in Table II.

Results of tests at 15 ft/sec velocity with recirculated water in the B.N.F.M.R.A. Laboratories and in once-through water at Harbor Island involving a number of common condenser tube alloys are summarized in Table IV.

While tests with once-through water at Harbor Island placed alloys in roughly the same order of merit as did the British tests, attack on the more resistant materials was much greater than in the British tests. Additional data are given in Tables V and VI. This was further evidence that Harbor

TABLE IV. *Comparison of results of tests of condenser tube alloys in the B.N.F.M.R.A. laboratories and at Harbor Island*

*Testing conditions*

Velocity of jet, 15 ft/sec
Air added, 3% by volume
Duration, 28 days
Water recirculated at B.N.F.M.R.A.
Not recirculated at Harbor Island

| Material | Average depth of attack (mm) | |
|---|---|---|
| | B.N.F.M.R.A. | Harbor Island Run 12 |
| Arsenical Admiralty Brass | 0.34 | 0.28 |
| Arsenical 70:30 brass | 0.31 | 0.43 |
| Arsenical copper | 0.30 | — |
| 70:30 Cupro nickel, 0.04% Fe | 0.11 | 0.23 |
| Aluminum Brass | 0.04* | 0.20 |
| 70:30 Cupro nickel, 0.8% Fe | 0.02 | 0.10** |
| 90:10 Cupro nickel, 2% Fe | 0.00 | 0.15 |

* One specimen out of 20 pitted to a depth of 0.66 mm No other specimen greater than 0.02 mm.

** Iron content, 0.45%.

TABLE V. *Typical results in recirculating jet impingement test with added air bubbles in B.N.F.M.R.A. laboratory*

| Run No. / Water speed (ft/sec) / % Air by volume | N/53 10 3 | Y/50 15 1.5 | J/50 15 3 | W/53 15 3 | M/50 30 3 | B/50 30 5 |
|---|---|---|---|---|---|---|
| Material | Depth of impingement attack | | | | | |
| 70:30 Cu Ni, 0.04% Fe | 0 | 0.11 | 0.06 | 0.04 | 0.56 | 0.46 |
| | 0.01 | 0.11 | 0.06 | 0.05 | 0.47 | 0.45 |
| 65:30 Cu Ni, 2% Fe | — | 0 | 0 | 0 | 0 | 0.02 |
| | | 0 | 0 | 0 | 0 | 0.07 |
| 70:30 Cu Ni, 0.8% Fe | 0 | | | 0 | | |
| | 0 | — | — | 0 | — | — |
| 90:10 Cu Ni, 2% Fe | 0 | 0 | 0 | 0 | 0 | 0 |
| | 0 | 0 | 0 | 0 | 0 | 0 |
| 95:5 Cu Ni, 0.6% Fe | 0 | | | 0 | | |
| | 0 | — | — | 0 | — | — |
| 95:5 Cu Ni, 1.5% Fe | 0 | 0 | 0.02 | 0 | 0.03 | 0.06 |
| | 0 | 0.08 | 0.04 | 0 | 0.01 | 0.06 |
| Arsenical copper | 0 | 0.25 | 0.10 | 0.50 | 0.62 | — |
| | 0 | 0.20 | 0.10 | 0.50 | 0.67 | |
| 70:30 Brass, 0.03% As | 0.59 | 0.22 | 0.28 | 0.49 | 0.61 | 0.61 |
| | 0.74 | 0.20 | 0.26 | 0.49 | 0.62 | 0.67 |
| 70:29:1 Brass, 0.03% As | 0.42 | | | 0.44 | | |
| | 0.05 | — | — | 0.45 | — | — |
| Aluminum Brass (76:22:2 + 0.03% As) | 0 | 0 | 0 | 0.01 | 0 | 0.34 |
| | 0 | 0 | 0 | 0.01 | 0 | 0 |

TABLE VI. *Summary of a number of results with the recirculating jet impingement test at 15 and 30 ft/sec with 1.5–5% added air in B.N.F.M.R.A. laboratory*

| Material | 15 ft/sec | | | 30 ft/sec | | |
|---|---|---|---|---|---|---|
| | Range of Depths mm | Average Depth mm | No. of Runs* | Range of Depths mm | Average Depth mm | No. of Runs* |
| 70:30 Cu Ni, 0.04% Fe | 0.03–0.31 | 0.11 | 11 | 0.11–0.73 | 0.40 | 7 |
| 70:30 Cu Ni, 0.8% Fe | 0.00–0.07 | 0.02 | 9 | 0.00–0.14 | 0.02 | 9 |
| 65:30 Cu Ni, 2% Fe | 0 | 0 | 11 | 0.00–0.07 | <0.01 | 7 |
| 90:10 Cu Ni, 2% Fe | 0 | 0 | 11 | 0.00–0.57 | 0.05 | 7 |
| 95:5 Cu Ni, 1.5% Fe | 0.00–0.09 | 0.03 | 11 | 0.00–0.23 | 0.05 | 7 |
| 95:5 Cu Ni, 1.5% Fe Aged 600°C/30 min | 0.01–0.30 | 0.14 | 8 | 0.07–0.71 | 0.29 | 4 |
| Arsenical Copper | 0.08–0.61 | 0.30 | 7 | 0.17–0.67 | 0.50 | 3 |
| 70:30 Brass (0.03% As) | 0.20–0.44 | 0.31 | 10 | 0.50–1.16 | 0.66 | 6 |
| 70:29:1 Brass (0.03% As) | 0.14–0.51 | 0.34 | 6 | 0.04–0.55 | 0.31 | 6 |
| 76:22:2 Aluminum Brass (0.03% As) | 0.00–0.66** | 0.04** | 10 | 0.00–0.34 | ~0.05 | 7 |

* Normally two specimens in each run.

** One specimen out of 20 pitted to a depth of 0.66 mm. No other specimen greater than 0.02 mm.

TABLE VII. *Effect of jet velocity on impingement attack of Admiralty Brass and 90:10 cupro nickel alloy with once-through water in B.N.F.M.R.A. apparatus at Harbor Island*

*Testing conditions*

Air added, 3% by volume
Temperature, 20°C
Duration, 28 days

| Jet Velocity (ft/sec) | Depth of Impingement Attack (mm) | |
|---|---|---|
| | Admiralty Brass | 90:10 Cupro Nickel, 2% Fe |
| 15 | 0.28 | 0.15 |
| 12 | 0.35 | 0.13 |
| 9 | 0.26 | 0.13 |
| 7.5 | 0.18 | 0.06 |
| 6 | 0.25 | 0.05 |
| 4 | 0.15 | 0.03 |

Island tests were much more drastic—perhaps too drastic to permit ready evaluation of difference in resistance to impingement attack among compositions that performed well in British tests.

### Tests at Reduced Water Velocity

An effort was made to discover whether, by reducing jet velocity, the extent of damage to the more resistant alloys by once-through water at Harbor Island could be brought into line with results secured with recirculated water in the B.N.F.M.R.A. Laboratory. Data obtained with Admiralty Brass and an iron-modified 90/10 cupro-nickel alloy as shown in Table VII illustrate results of this series of experiments.

It was evident from these results that tests with

TABLE VIII. *Impingement attack of condenser tube alloys as tested in several ways*

| Material | 15 ft/sec B.N.F.M.R.A. Lab. | 15 ft/sec Once-through water in England | Depth of Impingement Attack (mm) | | |
|---|---|---|---|---|---|
| | | | 15 ft/sec Once-through water at Harbor Island | 15 ft/sec Recirculated water at Harbor Island | 4 ft/sec Once-through water at Harbor Island |
| Arsenical Admiralty | 0.34 | 0.11 | 0.28 | 0.28 | 0.15 |
| 70:30 Cupro Nickel, 0.04% Fe | 0.11 | 0.08 | 0.23 | 0.14 | — |
| Arsenical Aluminum Brass | 0.04 | 0.07 | 0.20 | 0.01 | — |
| 90:10 Cupro Nickel, 1.5% Fe | 0.00* | 0.10* | 0.15 | 0.02 | 0.01 |
| 70:30 Cupro Nickel, 0.45% Fe | 0.02** | 0.09** | 0.10 | 0.01 | 0.01 |

* 2% Iron.
** 0.8% Iron.

once-through water at Harbor Island might be brought into line with those obtained with recirculated water in the B.N.F.M.R.A. Laboratory if the jet velocity at Harbor Island were reduced sufficiently, e.g., to 4 ft/sec. That such was the case is shown by data for some common condenser tube alloys tested with once-through water at Harbor Island at 4 ft/sec jet velocity (Table VIII). Included in this table for convenient comparison are results for the same alloys as tested in once-through water in England and in recirculated water at both Harbor Island and the B.N.F.M.R.A. Laboratory. Appearance of specimens after these tests at Harbor Island is shown in Fig. 4 which should be compared with Fig. 3.

## Relation of Test Results to Performance in Service

Results of jet impingement tests made in the laboratory of B.N.F.M.R.A. have provided a satisfactorily reliable guide in establishing relative merits of condenser tube alloys under practical conditions in marine and power plant condensers. For example, they were the basis for commercial development of Aluminum Brass as a condenser tube alloy having resistance to impingement attack superior to that of Admiralty Brass. They also demonstrated the advantage of iron additions to cupro-nickel alloys as summarized in a recent paper (6). Therefore, since the relative performance of materials in practical service seems to be reflected better by jet impingement tests at the level of severity obtained in B.N.F.M.R.A. tests with recirculated sea water than by more drastic tests with once-through sea water at the same jet velocity (15 ft/sec) at Harbor Island, it is in order to lessen the severity of the latter testing conditions either by reducing jet velocity of once-through water to about 4 ft/sec or by recirculating water at 15 ft/sec. Of the two possibilities, use of once-through water at the lower velocity might be preferable since, in ordinary practice, sea water used for cooling passes through heat exchanger tubes only once. However, the final choice will be influenced by additional data to be accumulated at Harbor Island.

While use of a 15 ft/sec jet velocity with once-through water at Harbor Island may be too drastic to rate materials for normal service conditions, it could be of value for qualifying them for exceptionally severe conditions. For example, Fig. 5 shows specimens of three alloys that remained free from impingement when tested with once-through water at 15 ft/sec at Harbor Island. Presumably these alloys will perform well where service conditions are too severe for ordinary condenser tube compositions.

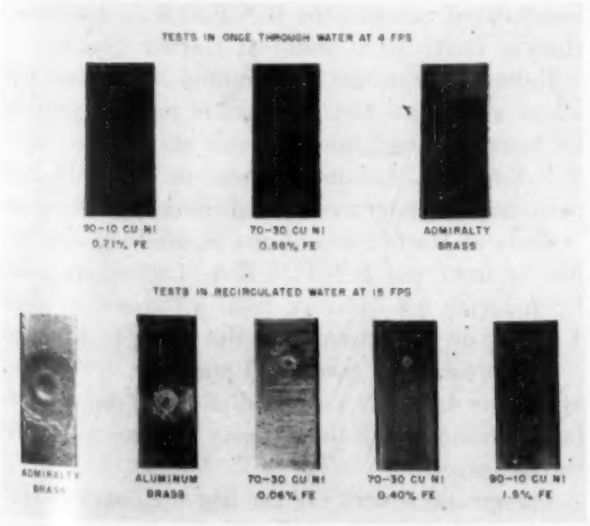
TESTS IN ONCE THROUGH WATER AT 4 FPS
90-10 CU NI 0.71% FE
70-30 CU NI 0.58% FE
ADMIRALTY BRASS
TESTS IN RECIRCULATED WATER AT 15 FPS
ADMIRALTY BRASS
ALUMINUM BRASS
70-30 CU NI 0.05% FE
70-30 CU NI 0.40% FE
90-10 CU NI 1.5% FE

Fig. 4. Tests at Harbor Island

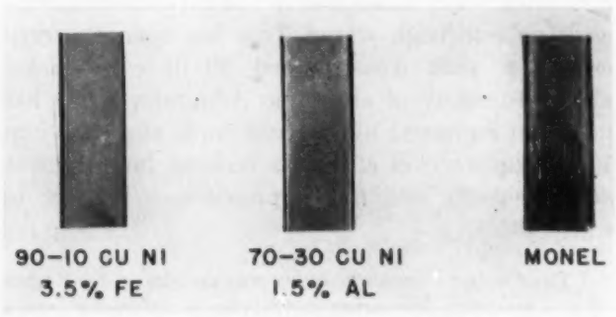


Fig. 5. Alloys resistant to jet impingement attack with once-through water at 15 ft/sec at Harbor Island.

FIG. 6. Pitting of Aluminum Brass around supports in recirculated water to which silt was added at Harbor Island.

## CAUSES OF DIFFERENCE BETWEEN ONCE-THROUGH AND RECIRCULATED WATER AT HARBOR ISLAND

In view of difference in behavior of certain alloys in once-through and recirculated water as illustrated by Table VIII, there have been many speculations as to the underlying cause or causes. Measurements of *p*H and the Copper Corrosion Index[2] in once-through and recirculated water showed no variations in these factors that would account for the difference in results. However, there was a strong feeling that the critical factor was in some way affected by biological influence. This would be based on the abundance of plankton in the once-through water and its scarcity in recirculated water from which it settled out in the tests at Harbor Island or was filtered out in tests in the B.N.F.M.R.A. Laboratory. These organisms could exert both chemical and mechanical effects, the latter through abrasive action of the animals or their hard skeletons, e.g., the silicious material in diatoms. At present, there has been insufficient opportunity to settle the matter, but experiments at Harbor Island introducing silt that had settled from flowing water indicated that organic material in suspension may be important. A method for increasing and controlling the amount of suspended matter in recirculated water has not yet given reproducible results. However, there have been strong indications that the presence of suspended organisms or their skeletons may make recirculated water as aggressive toward some materials as is once-through water. This has been observed especially with iron-modified 90/10 cupro-nickel alloys. Intensity of attack on Admiralty Brass has not been increased by silt additions, and high-iron 70/30 cupro-nickel alloy has resisted impingement attack equally well in the presence or absence of added silt.

[2] The Copper Corrosion Index was developed by Rogers (7) as a means of comparing corrosivity of different samples of sea water, particularly as it might be influenced by contaminants resulting from biological activity.

Presumably the principal effect of suspended matter is to promote removal of protective films under action of the jet. In addition, there appear to be some chemical effects, principally in the form of severe corrosion of Aluminum Brass specimens in crevices that exist where they are attached to their specimen holders (Fig. 6).

The reason for the anomalous situation that tests with recirculated water give better correlation with practical experience than once-through tests may be connected with the fact that ships normally steam at full power for long periods only in the open sea where there is little suspended matter. Occurrence of fine silt and small marine organisms capable of causing abnormal corrosive effects may be confined mainly to coastal waters.

Results of all tests given in this paper were obtained using clean or relatively clean sea water. Very different effects and much more severe attack have been obtained from time to time in the B.N.F.M.R.A. Laboratory using naturally polluted sea water samples.

## CONCLUSIONS

Severity of jet impingement tests with once-through sea water at Harbor Island was much greater than with recirculated sea water under otherwise similar testing conditions in laboratories of the British Non-Ferrous Metals Research Association. Materials that were badly attacked in recirculated water were, however, no more severely attacked in once-through water.

Tests with once-through water in England gave less severe attack than those with once-through water at Harbor Island, but results otherwise were very similar.

Under severe impingement test conditions it was not necessary to have air bubbles in the water for attack to occur. Air bubbles had more effect in recirculated water in the B.N.F.M.R.A. Laboratory than in recirculated water at Harbor Island.

Relative behavior of common condenser tube alloys when tested at the level of severity provided by tests with recirculated water at 15 ft/sec in the B.N.F.M.R.A. Laboratory was in line with their performance under many conditions of practical use.

Tests at Harbor Island can be made to duplicate results from the B.N.F.M.R.A. Laboratory either by reducing jet velocity from 15 ft/sec to about 4 ft/sec, or by recirculating the water at 15 ft/sec.

The presence of suspended plankton in the water at Harbor Island is suspected as being the principal factor in increasing the severity of tests with once-through water.

The greater severity of the test with once-through water at Harbor Island should provide a means for

qualifying materials to resist exceptionally severe conditions of impingement attack in practical service.

## Acknowledgment

Several past and present staff members of The British Non-Ferrous Metals Research Association assisted in carrying out part of the work reported in this paper, and their help is gratefully acknowledged. Thanks are also due the Director and Council of the Association for permission to publish results.

The authors wish to acknowledge the help of the staff at International Nickel Company's Harbor Island Test Station in performing tests that were undertaken there.

Any discussion of this paper will appear in a Discussion Section to be published in the June 1955 issue of the JOURNAL.

## REFERENCES

1. G. D. BENGOUGH AND R. MAY, *J. Inst. Metals*, **32**, 81 (1924).
2. R. MAY, *ibid.*, **40**, 141 (1928).
3. R. MAY AND R. W. DEVERE STACPOOLE, *ibid.*, **77**, 331 (1950).
4. F. L. LAQUE AND W. C. STEWART, *Metaux & corrosion*, **23** [274], 147 (1948).
5. F. L. LAQUE AND J. F. MASON, JR., Paper presented before Corrosion Session, American Petroleum Institute, Division of Refining, May 1950.
6. G. L. BAILEY, *J. Inst. Metals*, **79**, 243 (1951).
7. T. H. ROGERS, *ibid.*, **76**, 597 (1950).

# Effect of Rapid Cathode Rotation and Magnetic Fields on Crystal Orientation in Electrodeposited Metals

LING YANG

*Metals Research Laboratory, Carnegie Institute of Technology, Pittsburgh, Pennsylvania*

ABSTRACT

Crystal orientations in metals electrodeposited on a cathode rotating at 3000 rpm were studied by electron diffraction; results were compared with those on a stationary cathode. It was found that orientation could (*a*) be destroyed, (*b*) be changed to another type, or (*c*) remain unchanged. These observations were satisfactorily explained by considering the effect of the forced convection of rotation on the nature of the diffusion layer surrounding the cathode and, thus, on the amount of hydrogen codeposited, the latter being known as an important factor controlling the crystal orientation in electrodeposited metals. Under bath conditions used in this work, presence of a magnetic field of 5400 gauss strength, either perpendicular or parallel to the cathode, had no effect on the types of crystal orientation in iron, nickel, and cobalt deposits. However, when the field was perpendicular to the cathode, the surface of these deposits became very rough and covered with projections protruding in the direction of the field. A possible explanation of this observation was given.

## INTRODUCTION

In previous investigations (1–12) of how various factors affect the crystal orientation in electrodeposited metals, attention has chiefly been paid to factors normally present during electrodeposition, such as bath temperature, bath composition, and current density. It seems to be of interest to extend the study to factors which are not always present but which are imposed purposely. Attempts have been made to study the effect of two of these factors—high speed rotation of the cathode and the presence of a magnetic field.

## EFFECT OF HIGH SPEED ROTATION OF CATHODE

### *Experimental*

The cathode was a brass disk 1 mm thick and 2 cm in diameter. A small brass nut was soldered to the center of one face of the disk, through which the disk could be screwed to the axis of the driving motor, while the other side of the disk (the working side) was polished and degreased. All the metal parts in contact with the electrolytic solution, except the working side of the disk, were covered with a thin layer of polythene to prevent deposition. The driving motor was held vertical and the disk cathode was screwed to its axis with the polished working side downward facing a horizontally disposed stationary anode (5 cm x 5 cm x 1 mm) about 3 cm away. The bath container was a one-liter beaker about three-fourths filled with the desired electrolyte and the cathode was about 5 cm below the liquid level. During deposition, the electric connection to the rotating cathode was made through a slip ring. Motor speed was 3000 rpm, as measured with a Hasler tachometer. For comparison, each experiment was run twice, one on a rotating cathode and the other on a stationary cathode under the same bath conditions.

Crystal orientation in the deposited metal was studied by electron diffraction for two reasons. Firstly, owing to the low penetration of electron beam, the structures of the deposit could be studied without interference from the substrate. Secondly, because of the high intensity of the diffraction pattern shown on the fluorescent screen, different regions of the deposit surface could readily be examined by moving the focused beam across it.

Electrolytic baths were all prepared from chemically pure reagents and further purified by electrolysis. Anodes were all electrolytic metals. Compositions of the baths in grams per liter are: (*a*) nickel, $NiSO_4 \cdot 7H_2O$ 240, $H_3BO_3$ 30, *p*H = 2.9; (*b*) iron, $FeSO_4 \cdot (NH_4)_2SO_4 \cdot 6H_2O$ 350, $H_2SO_4$ 2.5; (*c*) silver, AgCN 35, KCN 37, $K_2CO_3$ 38; (*d*) copper$_1$, $CuAc_2 \cdot 2H_2O$ 25, $Na_2SO_3 \cdot H_2O$ 50, KCN 35, $Na_2CO_3$ 10; (*e*) copper$_2$, $CuSO_4 \cdot 5H_2O$ 200, $H_2SO_4$ 30; (*f*) antimony, $SbCl_3$ 200, HCl (conc) 300 cc.

### *Results and Discussions*

In all cases studied (see Table I and Fig. 1 and 2), orientations of crystals deposited on the rotating cathode, as compared with those on stationary cathode, fall into three categories according to whether (*a*) crystal orientation was destroyed, (*b*) crystal orientation was changed to the type in which the most densely packed lattice plane was parallel to

[1] Manuscript received July 23, 1953.

TABLE I *Influence of rotation of cathode (3000 rpm) on the crystal orientation of electrodeposited metals*

| Deposit | Bath temp (°C) | Current density (amp/dm²) | Current efficiency (%) | Orientation |
|---|---|---|---|---|
| Ni* | 20 | 1.25 | 90 | (110) |
| Ni† | 20 | 1.25 | 45 | Random |
| Ni* | 52 | 1.25 | 95 | (100) |
| Ni† | 52 | 1.25 | 55 | Random |
| Fe* | 20 | 3.75 | 90 | (111) |
| Fe† | 20 | 3.75 | 25 | Random |
| Fe† | 20 | 7.50 | 85 | (111) |
| Ag* | 20 | 3.00 | 80 | Weak (110) |
| Ag† | 20 | 3.00 | 100 | Weak (111) |
| $Cu_1$* | 80 | 0.75 | 75 | (110) |
| $Cu_1$† | 80 | 0.75 | 90 | (111) |
| $Cu_2$* | 20 | 1.25 | 98 | (110) |
| $Cu_2$† | 20 | 1.25 | 98 | (110) |
| Sb* | 20 | 0.10 | 100 | Amorphous |
| Sb† | 20 | 0.10 | 100 | Amorphous |
| Sb* | 75 | 0.65 | 92 | (100) |
| Sb† | 75 | 0.65 | 93 | (100) |

Note: Deposit thickness, 2.5–5 μ.
* Deposit on stationary cathode.
† Deposit on rotating cathode.

the substrate, or (*c*) crystal orientation was unaffected.

For all three cases, the type and the degree of the orientation persisted over the whole cathode surface. This indicates that at 3000 rpm the influence of rotation of the cathode on the crystal orientation of the deposited crystals could not be due to the centrifugal forces produced by the rotation. If this were the case, observed changes in crystal orientation in (*a*) and (*b*) would vary with the radial position of the crystals on the disk cathode. These changes, however, were found to be accompanied always by a pronounced change in current efficiency, suggesting a modification of the nature of the diffusion layer contiguous to the cathode surface by the forced convection introduced by rotation. This is discussed below in the light of examples under headings of the three above-mentioned cases.

### *Crystal Orientation Destroyed*

Data for nickel and iron indicate that, where rotation of the cathode decreases current efficiency, crystal orientation may be destroyed by rotation. Loss of crystal orientation in these cases is, therefore, probably due to disturbances caused by the excessive amount of codeposited hydrogen on the rotating cathode.

The relation between current efficiency and rotation of the cathode can be explained as follows. It was first postulated by Nernst and later proved experimentally by many investigators that a thin layer of liquid surrounds the surface of the cathode and that ionic concentrations there differ from those in the bulk of the solution. Replenishment of the ions used up at the cathode surface must be made by diffusion and transport through this layer. Although this theory has been criticized by Eucken (13), Levich (14), and Agar (15), the idea is still useful for the present qualitative explanation of results. Based on this theory, actual concentrations of the deposited ions at the cathode surface are therefore determined, on the one hand, by the rate of removing them by deposition and, on the other hand, by the rate of replenishment through the diffusion layer. The latter is usually less than the former at the beginning of the deposition, and they do not

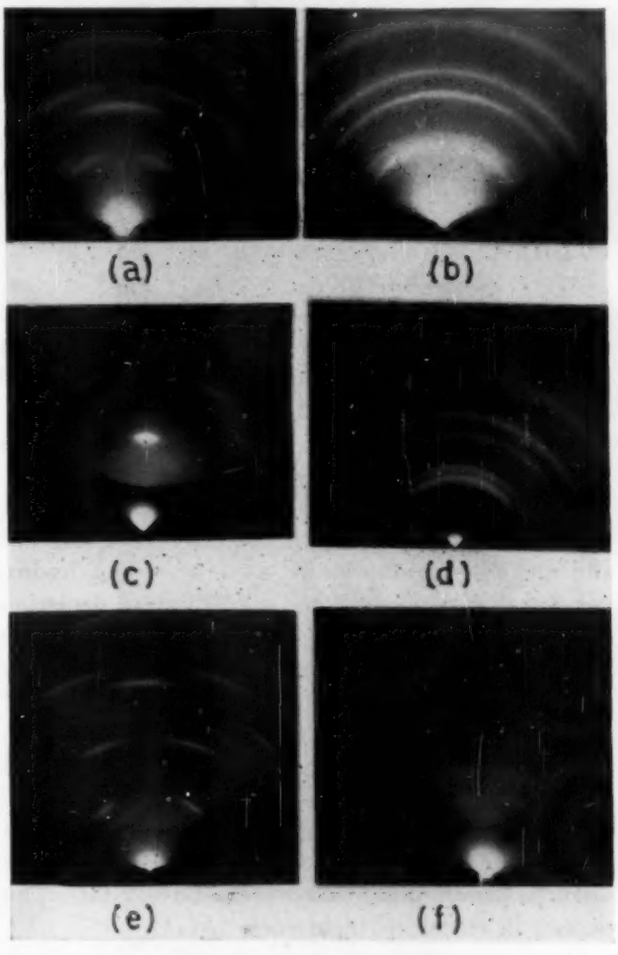


FIG. 1. Examples of crystal orientation destroyed by rotation of cathode. Left hand column, stationary cathode; right hand column, rotating cathode, 3000 rpm. Top, nickel: sulfate bath, 20°C, 1.25 amp/dm², 5 x $10^4$ Å thick; (*a*) (110) current efficiency 90%; (*b*) random, current efficiency 45%. Center, nickel:sulfate bath, 52°C, 1.25 amp/dm², 4 x $10^4$ Å thick; (*c*) (100) current efficiency 95%; (*d*) random, current efficiency 55%. Bottom, iron:sulfate bath, 20°C, 3.75 amp/dm², 5 x $10^4$ Å thick; (*e*) (111) current efficiency 90%; (*f*) random, current efficiency 25%.

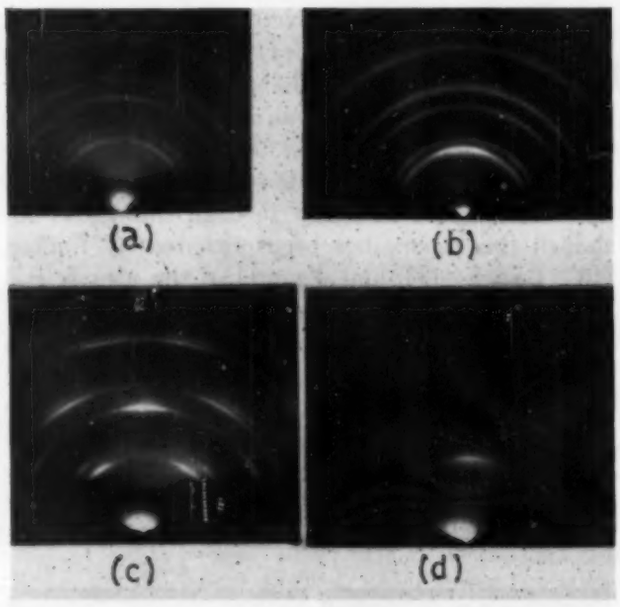


FIG. 2. Examples of crystal orientation changed by rotation of cathode. Left hand column, stationary cathode; right hand column, rotating cathode, 3000 rpm. Top, silver: cyanide bath, 20°C, 3 amp/dm², 3.5 x 10⁴ Å thick; (*a*) weak (110), current efficiency 80%; (*b*) weak (111), current efficiency 100%. Bottom, copper:cyanide bath, 80°C, 0.75 amp/dm², 2.5 x 10⁴ Å thick; (*c*) (110), current efficiency 75%; (*d*) (111), current efficiency 90%.

become equal until a steady state has been reached in which concentrations of the depositable ions at the cathode surface are more or less impoverished and give rise to concentration polarization.

Under conditions such that hydrogen ions can codeposit with metal ions, both types of ions are impoverished at the cathode surface, but the extent of their impoverishment may not be equal. For the nickel and iron baths used here, the hydrogen ion is apparently more susceptible to depletion than metal ions, as indicated by the facts that the amount of codeposited hydrogen is decreased by increasing the current density, and that the *p*H value of the solution at the cathode surface is so high that basic metal hydroxides are precipitated and included in the deposit (16, 17). This low hydrogen ion concentration at the cathode surface lessens the amount of codeposited hydrogen and hence the disturbances to the growth of metal crystals. The deposit is, therefore, highly oriented.

However, if the cathode is rotated at high speed, forced convection produced by rotation decreases the thickness of the diffusion layer. For a circular disk rotating about an axis passing through its center, Levich (18) has shown that the thickness of the diffusion layer is inversely proportional to the square root of the speed of rotation. This decrease of thickness of the diffusion layer increases the rate of ion supply, particularly hydrogen ion, to the cathode surface. As a result, hydrogen ion concentration at the cathode surface and the amount of codeposited hydrogen increase. Thus, there is increasing disturbance to the growth of deposited crystals. When the disturbance is severe enough, deposited crystals become randomly disposed.

If this explanation is true, a higher current density would outweigh the increased rate of diffusion of hydrogen ions to the cathode surface because of cathode rotation. In other words, increased current efficiency may give oriented deposits even when the cathode is rotated. This was the case. Iron deposited from the sulfate bath at 20°C and 3.75 amp/dm² on a cathode rotating at 3000 rpm in randomly arranged crystals, the current density being 25%; by increasing current density to 7.50 amp/dm², current efficiency increased to 85% and the deposited crystals showed (111) orientation.

### *Crystal Orientation Changed*

If rotation of the cathode causes a marked increase in current efficiency, deposited crystals may change from the type of orientation characteristic of prevailing bath conditions on a stationary cathode to the type in which the most densely packed lattice plane is parallel to the substrate. This is illustrated in Table I by the cases of silver and copper deposited from their cyanide baths.

This change of orientation can be explained in the same way as that in the previous section. In these cyanide baths, it is the metal ions which are more susceptible to depletion than the hydrogen ion, as shown by the fact that current efficiency decreases rapidly when current density is increased. Since the forced convection caused by rotation of the cathode decreases the thickness of the diffusion layer on the cathode surface, the metal ion concentration near the cathode surface is increased, and so is the current efficiency. Decrease in codeposited hydrogen diminishes the disturbance to the growth of the deposited crystals and, consequently, these crystals show a preferred orientation with the most densely packed lattice plane parallel to the substrate. The latter is the type of orientation developed in most metals deposited under bath conditions involving little or no disturbance to the growth of crystals.

### *Crystal Orientation Unaffected*

If rotation of the cathode causes little or no change in the current efficiency of the deposition, then the crystal orientation of the deposit likewise remains unchanged, no matter whether the cathode is rotating or stationary. This is illustrated by copper deposited from a sulfate bath and antimony deposited from a chloride bath, as shown in Table I.

### Effect of Magnetic Field

Various attempts to study the influence of a magnetic field on the mode of crystal growth have almost all led to negative results. For example, Bergala and Gorskii (19) found that the rates of crystallization of water, salol, and diphenylamine were unchanged by fields up to 17,000 gauss. Steacie and Stevens (20) reported that a field of 5000 gauss had no effect on the rate of crystallization of sodium thiosulfate from its supersaturated solution, but for nickel sulfate a slightly increased rate was noted. Bozorth (2) could not find any change in the amount of crystal orientation of electrodeposited nickel when deposition was carried out in a magnetic field of unspecified strength. Cobalt was electrodeposited in a magnetic field of several hundred oersted strength (21) and iron, nickel, and cobalt were electrodeposited in a magnetic field of 12,000 oersted strength (22), but the crystal orientations of the deposit were not studied. The purpose of the present work was to find out whether the presence of a magnetic field of 5400 gauss strength could modify the crystal orientation of electrodeposited iron, nickel, and cobalt.

#### *Experimental*

A horse-shoe permanent magnet having a field strength of 5400 gauss was used. The poles were

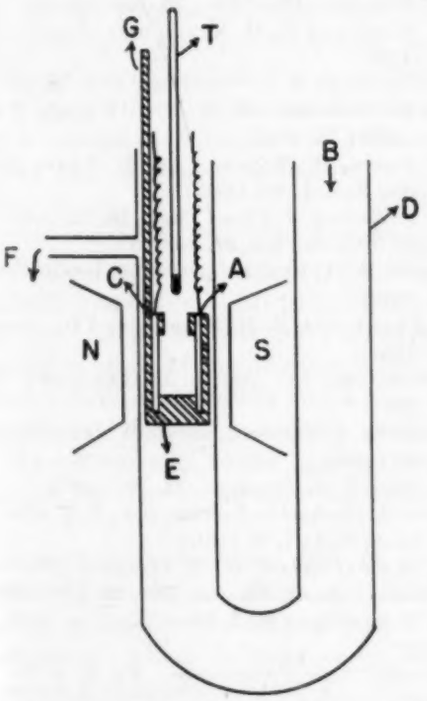


Fig. 3. Arrangements for electrodeposition in a magnetic field. A—anode; B—entrance for fresh solution; C—cathode; D—tube containing electrolytic solution; E—Bakelite frame for supporting electrodes; F—exit for used solution; G—arm of Bakelite frame; N, S—poles of magnet; T—thermometer.

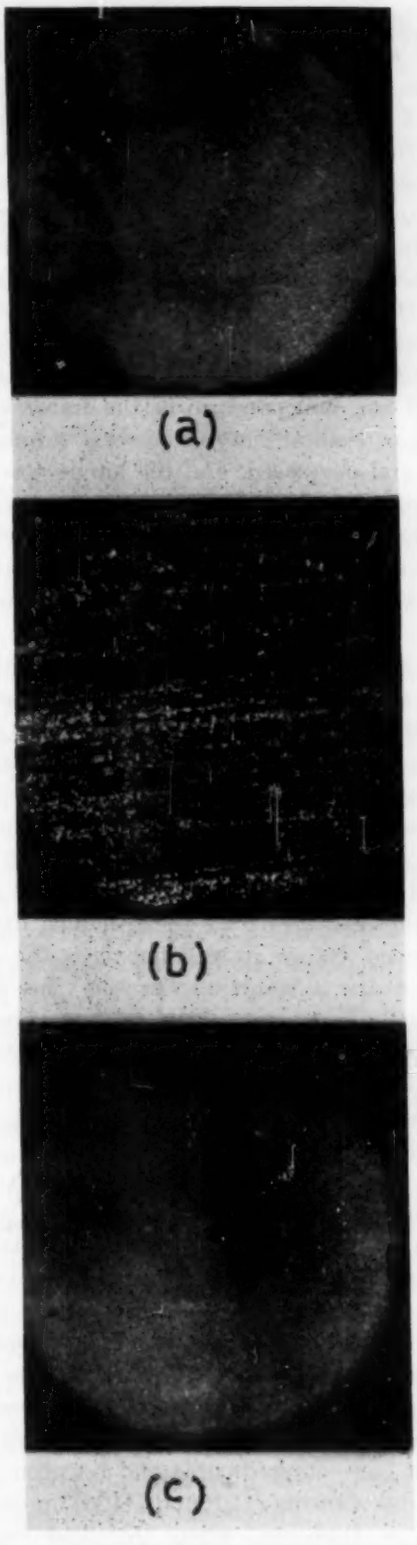


Fig. 4. Appearance of iron electrodeposited on brass from a sulfate bath at 80°C and 3.75 amp/dm². (a) In the absence of magnetic field; (b) specimen surface is perpendicular to the direction of a magnetic field of 5400 gauss strength; (c) specimen surface is parallel to the direction of the magnetic field. Time of deposition, 10 min. 15×.

circular (diameter 2.0 cm) and the pole gap was 1.2 cm. The small size of the pole gap limited the dimensions of the solution container which was a U-tube of 1 cm diameter. One of its arms containing the electrodes was put into the pole gap of the magnet. Through the other arm, fresh solution was introduced slowly, after passing the lower part of the U-tube immersed in a constant temperature bath, to displace the solution which had been impoverished of the deposited ions (Fig. 3). The electrodes, both of which were 0.4 cm x 0.6 cm x 0.1 cm, were fixed rigidly on a Bakelite frame, at a distance of about 0.4 cm, and one arm of the frame was held by a copper clamp. The cathode was a brass plate, polished and degreased, and the anode was a piece of electrolytic metal of the kind to be deposited. Electrodes were immersed about 1 cm below the liquid level and all immersed surfaces of the electrodes, except the facing areas, were coated with collodion.

Compositions of the nickel and iron baths used were the same as described above, while the cobalt bath contained 200 g of $CoSO_4 \cdot (NH_4)_2SO_4 \cdot 6H_2O$ and 30 g of $H_3BO_3$/l ($pH$ = 3.0). Deposition of nickel was carried out at 1.25 amp/dm², 20° and 60°C; that of iron at 3.75 amp/dm², 20° and 80°C; and that of cobalt at 2.50 amp/dm² and 20°C.

Crystal orientations in the deposits were studied by electron diffraction, but the specimen had to be demagnetized before it was put into the camera because of the interaction between the electron beam and the magnetic field of the specimen. Each experiment was done in three ways: without magnetic field; with field parallel to the surface of the electrodes; and with field perpendicular to the surface of the electrodes.

## Results

No change in the types of crystal orientation of nickel, iron, and cobalt deposits was observed as a result of the presence of a magnetic field of 5400 gauss. The iron deposit showed (111) orientation at 20°C and (110) orientation at 80°C; the nickel deposit showed (110) orientation at 20°C and (100) orientation at 60°C; and the cobalt deposit was a mixture of face-centered-cubic and hexagonal-close-packed forms showing (110) and $(11\bar{2}0)$ orientations, respectively. However, when the field was perpendicular to the surfaces of the electrodes, the deposit surface became very rough and covered with projections protruding in the direction of the field. This is evident from Fig. 4(*a*), (*b*), and (*c*), showing photomicrographs of the surfaces of iron deposited from a sulfate bath at 80°C and 3.75 amp/dm² for 10 min, (*a*) with no field, (*b*) with a magnetic field normal to the deposit surface, and (*c*) with a magnetic field parallel to the deposit surface. The deposit seemed to grow predominantly on the ridges resulting from the polishing of the substrate. If the deposit was made on an iron substrate instead of on a brass one, this tendency was even more pronounced. No such phenomenon was observed, however, for copper deposited from an acid sulfate bath and antimony from a chloride bath.

It is tentatively suggested that the effect is due in part to the magnetic lines of force being more concentrated near the projecting parts on the surface of the brass substrate after the latter had been coated with ferromagnetic deposits. It is possible that this uneven distribution of field along the cathode surface causes an uneven distribution of $Fe^{++}$, $Ni^{++}$, and $Co^{++}$ concentrations there, since these ions are paramagnetic, with the result that metal ion concentration is higher near these projecting regions and thus facilitates deposition there. The fact that the crystal orientation of the deposit is not affected suggests that this outgrowth is merely a macroscopic phenomenon and that the tendency of the growth of the crystal nuclei in iron, nickel, and cobalt deposits is not affected by a magnetic field of the strength used.

Any discussion of this paper will appear in a Discussion Section to be published in the June 1955 issue of the Journal.

## References

1. R. Glocker and E. Kaupp, *Z. Physik*, **24**, 121 (1924).
2. R. M. Bozorth, *Phys. Rev.*, **26**, 390 (1925).
3. G. I. Finch and C. H. Sun, *Trans. Faraday Soc.*, **32**, 852 (1936).
4. G. I. Finch and A. C. Williams, *ibid.*, **33**, 564 (1937).
5. W. Hume-Rothery and M. R. J. Wyllie, *Proc. Roy. Soc.*, **A181**, 331 (1943).
6. G. I. Finch, H. Wilman, and L. Yang, *Discussion Faraday Soc.*, **1**, 144 (1947).
7. M. R. J. Wyllie, *J. Chem. Phys.*, **16**, 52 (1948).
8. L. Yang, *This Journal*, **97**, 241 (1950).
9. W. Smith, J. H. Keeler, and H. J. Read, *Plating*, **36**, 355 (1949).
10. G. L. Clark and S. H. Simonsen, *This Journal*, **98**, 110 (1951).
11. H. Leidheiser, Jr., and A. T. Gwathmey, *ibid.*, **98**, 225 (1951).
12. A. Brenner, V. Zentner, and C. W. Jennings, *Plating*, **39**, 865 (1952).
13. A. Eucken, *Z. Elektrochem.*, **38**, 341 (1932).
14. B. Levich, *Discussion Faraday Soc.*, **1**, 37 (1947).
15. J. N. Agar, *ibid.*, **1**, 26 (1947).
16. D. J. Macnaughtan, G. E. Gardam, and R. A. F. Hammond, *Trans. Faraday Soc.*, **29**, 729 (1933).
17. G. E. Gardam and D. J. Macnaughtan, *ibid.*, **29**, 755 (1933).
18. B. Levich, *Acta Physicochim., U. R. S. S.*, **17**, 257 (1942).
19. R. Ya Berlaga and F. K. Gorskii, *J. Exp. Theor. Phys., U. R. S. S.*, **4**, 527 (1934).
20. E. W. R. Steacie and C. F. B. Stevens, *Canadian J. Res.*, **10**, 483 (1934).
21. A. Perrier and C. Mermod, *Helv. Phys. Acta*, **11**, 362 (1938).
22. A. Perrier, C. Mermod, and E. Besse-Walter, *Helv. Chim. Acta*, **26**, 1861 (1943).

# Role of Sulfur in the Luminescence and Coloration of Some Aluminosilicates[1]

RUSSELL D. KIRK

*Dielectrics Branch, Solid State Division, Naval Research Laboratory, Washington, D. C.*

ABSTRACT

Certain complex, sulfur-containing sodalite-type silicates, synthesis of which is described, exhibit under 3650 Å excitation an emission extending from 5000 Å to beyond 7000 Å, the spectrum varying with composition. The band structure of this emission at −196°C is similar to the emission structure shown by a mixture of $Na_2S_x$ and $Na_2SO_4$. It is concluded that luminescence is due to the presence of $Na_2S_x$, which replaces part of the NaCl normally present in sodalite.

Synthetic sodalites containing both NaCl and $Na_2S$ are tenebrescent, coloring purple on irradiation with 2537 and 3650 Å ultraviolet.

## INTRODUCTION

The orange-yellow luminescence of certain forms of the mineral sodalite has long been known (1). The variety of sodalite known as hackmanite is not only luminescent, but is tenebrescent as well. It colors rapidly from white to red-purple on exposure to a short-wave ultraviolet source (2–4). Visible light causes a bleaching of the color. Medved (5) prepared sodalite which colored under 2537 Å ultraviolet by firing synthetic sodalite in hydrogen.

The purpose of this investigation was to duplicate the luminescence and tenebrescence of natural sodalite with synthetic products and to obtain more information concerning the centers involved.

Since it is known that sulfur compounds are often present in natural sodalite, it was suspected that sulfur may play a role in luminescence and tenebrescence.

Gobrecht and Hahn (6), who first reported and described the luminescence of polysulfides, prepared a large number of alkali polysulfides and partially reduced alkali sulfates by various methods. They found in many of the products a red luminescence under 3650 Å excitation and a blue emission on exciting with 2537 Å radiation. These workers ascribe the red emission to the presence of polysulfide ion and the blue to alkali metal activation of sulfate.

The present work confirms some of the results obtained by Gobrecht and Hahn and describes the preparation and properties of a group of sodalite-type compounds which, in some cases, show both luminescence and tenebrescence.

[1] Manuscript received November 12, 1953. This paper was prepared for delivery before the New York Meeting, April 12 to 16, 1953.

## EXPERIMENTAL METHODS

### *Preparation*

Sodalite has the composition $3(Na_2O \cdot Al_2O_3 \cdot 2SiO_2) \cdot 2NaCl$, the natural sulfate analog (the mineral noselite), $3(Na_2O \cdot Al_2O_3 \cdot 2SiO_2) \cdot Na_2SO_4$. The synthetic sodalite-type compounds prepared for this work contain, in place of NaCl, combinations of NaCl, $Na_2SO_4$, and $Na_2S_x$ in varying amounts such that they have the general composition $3(Na_2O \cdot Al_2O_3 \cdot 2SiO_2) \cdot X NaCl \cdot Y Na_2S_x \cdot Z Na_2SO_4$, where $X + 2(Y + Z) = 2$. Thus within the parameters of this formula, one $Na_2SO_4$ or one $Na_2S_x$ replaces 2NaCl.

The following reagents were used in the preparations: Linde "A" aluminum oxide, Mallinckrodt's Special Bulky grade silicic acid, and the usual C.P. grades of sodium carbonate, sodium chloride, and sodium sulfate.

Dry mixing methods were used for the sodalite products, since traces of nonvolatile residues introduced by milling in organic liquids caused some reduction of the sulfate on firing, and some of the components are water soluble. Desired quantities of the starting compounds were mixed by stirring together the dry powders, prefiring in silica dishes at 750°C in air, and grinding the resulting cake in an automatic mortar. Prefiring and grinding operations were repeated several times to insure intimate mixing and complete reaction.

When $Na_2S$ was to be introduced into the sodalites, this was done by hydrogen reduction of the $Na_2SO_4$ which had been prefired into the mixture.

The final firing, whether in helium, hydrogen, or air, was for two hours at 900°C.

Several sodalite sample series were prepared with varying ratios of $Na_2S/Na_2SO_4$ and of ($Na_2S$ +

$Na_2SO_4$)/NaCl within the series. Thus, end members of a particular series had the composition $3(Na_2O \cdot Al_2O_3 \cdot 2SiO_2) \cdot X NaCl \cdot Y Na_2S$ and $3(Na_2O \cdot Al_2O_3 \cdot 2SiO_2) \cdot X NaCl \cdot Z Na_2SO_4$. Intermediate members were made by grinding together the previously fired end members in the desired ratios and firing the mixtures in dried helium. Only the end member sulfide-containing sodalites fired in hydrogen are believed to contain sulfide as $Na_2S$. Products prepared by firing an end member containing $Na_2S$ with one containing $Na_2SO_4$ are, for reasons stated in the discussion section, believed to contain $Na_2S_x$, where $x > 1$. Since the amount of $Na_2S_x$ formed is not known, compositions given in the text and figures hereafter will, for simplicity, refer to the mole ratio of components used in the preparation and are not intended to represent the final chemical composition.

In this paper, the terms "sodalite compounds" and "sodalites" will be used to describe the sodalites with sodium sulfate or sodium sulfides substituting partially or completely for sodium chloride. Strictly speaking, these are not sodalite, although they are closely related crystallographically and chemically.

Sodium polysulfide-sulfate mixtures were prepared in a manner similar to that used by Gobrecht and Hahn, i.e., by heating $Na_2S_2O_3 \cdot 5H_2O$ or $Na_2SO_3$ in air at 900°C until most of the polysulfide sulfur first produced was oxidized. This state is reached when the solidified melt is translucent, has a very pale yellow color, and shows a yellow luminescence under a 3650 Å source. The time necessary to reach this stage depends upon empirical conditions such as the amount of exposed surface and the degree of air circulation in the furnace.

A polysulfide mixture with a red visible emission under 3650 Å excitation was prepared from $Na_2SO_3$ by the same method, except that the heating was stopped while a large proportion of polysulfide was still present in the melt. The resulting solidified mixture is opaque yellow in visible light.

$Na_2S_2O_3$ is known to decompose on heating into $Na_2S_x$ and $Na_2SO_4$. $Na_2SO_3$ disproportionates on heating into $Na_2SO_4$ and $Na_2S$, the latter oxidizing readily in air to polysulfide and other products, even at room temperature. Since the ratio of $Na_2S_x$ to $Na_2SO_4$ in the decomposition products is not known, the mixture, for the sake of brevity, will be designated as $Na_2S_x \cdot n Na_2SO_4$.

All products made by heating $Na_2S_2O_3$ or $Na_2SO_3$ which luminesced either yellow or red gave a positive test for polysulfide with the reagent used by Gobrecht and Hahn. The formation of a purple color with this complex cobaltic-dimethylglyoxime-aniline reagent is claimed by the discoverers, Beato and Brügger (7) to be a specific test for the polysulfide ion.

### *Physical Measurements*

Luminescence of the preparations was observed under a 100-watt, high-pressure mercury lamp with red-purple Corex + Corning #5860 filters unless otherwise specified. Emission spectra were obtained with an automatically recording spectroradiometer with the above exciting source and filters.

Excitation spectra were determined in the usual manner with a Beckman hydrogen lamp and monochromator. The spectra illustrated are corrected to equal energy of excitation.

Tenebrescence was observed after exposure to various sources. 1850 Å + 2537 Å radiation was obtained from an unfiltered, low-pressure, silica-envelope mercury arc; 2537 Å radiation, from the same lamp with a Corning #9863 filter. The 3650 Å source was the above-mentioned high-pressure mercury lamp and filters; the soft x-ray irradiation used was that from a Machlett Type OEG 60 tube with a tungsten target.

Reflection spectra were obtained by means of an automatically recording apparatus described by Schulman and Klick (8).

Visual observations on the luminescence and tenebrescence of the synthetic products described in this paper are summarized in Tables I and II, respectively.

Excitation curves for sodium polysulfide-sulfate from $Na_2S_2O_3$ and all the synthetic sodalite products were identical. The relative excitation spectra extend from 2500 to 5000 Å with a single peak at 4000 Å as shown for a typical sample in Fig. 1.

TABLE I. *Luminescence properties of synthetic sodalites*

| $3(Na_2O \cdot Al_2O_3 \cdot 2SiO_2)$ with: | Emission color, 3650 Å excitation | Color in white light |
|---|---|---|
| NaCl | None | White |
| $Na_2SO_4$ | None | White |
| $Na_2S$ | None† | Gray |
| NaCl + $Na_2S$ | None† | Gray |
| $Na_2SO_4$ + $Na_2S$* | Orange-yellow | White‡ |
| NaCl + $Na_2SO_4$ | None | White |
| NaCl + $Na_2S$ + $Na_2SO_4$* | Orange-yellow | White‡ |
| NaCl + $Na_2SO_4$ fired in sulfur vapor | Orange-yellow | White |

* Starting composition. As stated in the text, this composition is believed to produce $Na_2S_x$ on firing.

† When ordinary reagent grade aluminum oxide was used in place of Linde "A" in the $Na_2S$-containing preparations, a weak green luminescence with afterglow was observable. This may possibly be the iron activated $Na_2S$ luminescence described by Tiede and Reinicke (9).

‡ Samples containing both sulfate and sulfide occasionally had small amounts of blue or green ultramarine on the outside of the cake.

TABLE II. *Tenebrescence properties of synthetic sodalites*

| 3($Na_2O \cdot Al_2O_3 \cdot 2SiO_2$) with: | Firing atmosphere | X-rays | Radiation | | | Daylight |
|---|---|---|---|---|---|---|
| | | | 1850+2537 Å | 2537 Å | 3650 Å | |
| NaCl | Air | + | − | − | − | − |
| NaCl, $Na_2SO_4$ | Air | + | + | − | − | − |
| NaCl, $Na_2S$ | $H_2$ | + | + | + | + | + |
| NaCl, $Na_2S$, $Na_2SO_4$ | He | + | + | + | + | − |
| NaCl, $Na_2SO_4$ | S vapor + He | + | + | − | − | − |
| $Na_2SO_4$ | Air | − | − | − | − | − |
| $Na_2S$ | $H_2$ | − | − | − | − | − |

+ = purple color after exposure.
− = no color after exposure.

The sodium polysulfide-sulfate prepared from thiosulfate or sulfite exhibits, in addition to the yellow-appearing, 3650 Å-excited emission, a blue luminescence under 2537 Å irradiation. The excitation peak for the blue emission was found to be at 2450 Å, the emission maximum, at 4600 Å. These results are similar to those obtained for "alkali-metal-activated" alkali sulfates by Gobrecht and Hahn, who found an excitation band from 2400 to 2900 Å and emission from 3600 to 5150 Å, peaking at 4300 Å. This blue emission and its excitation band can be found in products prepared by heating $Na_2S_2O_3$ or $Na_2SO_3$ until the solidified melt is white and no emission is observable under 3650 Å excitation. The synthetic sodalites do not show this blue emission.

Emission spectra of the synthetic sodalites and of $Na_2S_x \cdot nNa_2SO_4$ from the thiosulfate are shown in Fig. 2 and 3 for 20°C and −196°C, respectively. Although the luminescence colors are yellow and red at the two respective temperatures, the emission

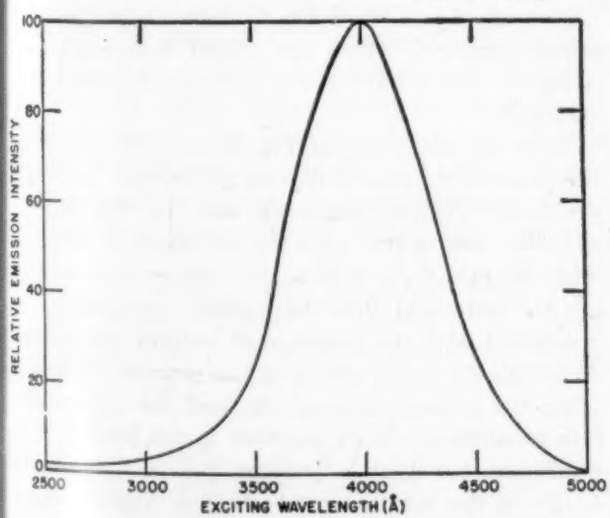


FIG. 1. Excitation spectrum of $3(Na_2O \cdot Al_2O_3 \cdot 2SiO_2)$ $1.0NaCl \cdot 0.25Na_2S \cdot 0.25Na_2SO_4$.

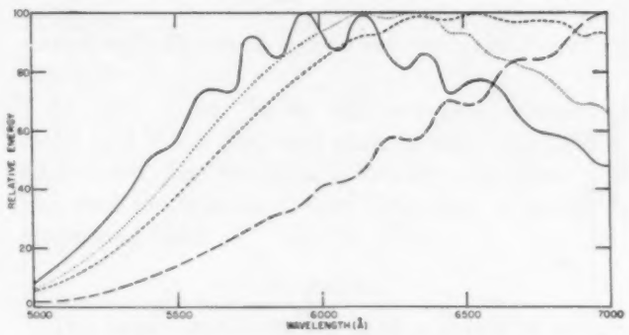


FIG. 2. Emission spectra at 20°C with 3650 Å excitation. .....$3(Na_2O \cdot Al_2O_3 \cdot SiO_2)$ $1.8\ NaCl \cdot 0.05Na_2S \cdot 0.05Na_2SO_4$; – – – – –$3(Na_2O \cdot Al_2O_3 \cdot 2SiO_2)1.0NaCl \cdot 0.25Na_2S \cdot 0.25Na_2SO_4$; — — — $3(Na_2O \cdot Al_2O_3 \cdot 2SiO_2)$ $0.5Na_2S \cdot 0.5Na_2SO_4$; ——— $Na_2S_x \cdot n\ Na_2SO_4$ from $Na_2S_2O_3$.

is broad in both cases, extending from about 5000 Å to beyond 7000 Å. Gobrecht and Hahn mention the yellow emission of the polysulfide-sulfate prepared from sodium thiosulfate, but give no emission spectrum of this particular material.

The small amount of structure shown by the sodalites at room temperature becomes clearly resolved at the low temperature into a series of maxima spaced about 200 Å apart; the observed emission color shifts from yellow or orange-yellow to red. At about 150°C and above the orange-yellow sodalite emission color changes to pale yellow.

It will be observed that the progressive substitution of $1(Na_2S + Na_2SO_4)$ for 2NaCl in the sodalite compounds shifts the emission maximum to longer wave lengths, e.g., when equimolecular concentrations of $Na_2S$ and $Na_2SO_4$ are used in a chloride-free preparation, the product at room temperature shows a maximum beyond 7000 Å, as compared to peaks at 6150 and 6350 Å for the high NaCl composition.

When the NaCl remains constant, e.g., in the series $3(Na_2O \cdot Al_2O_3 \cdot 2SiO_2)1.0NaCl \cdot 0.5(Na_2S + Na_2SO_4)$, the emission brightness slowly increases

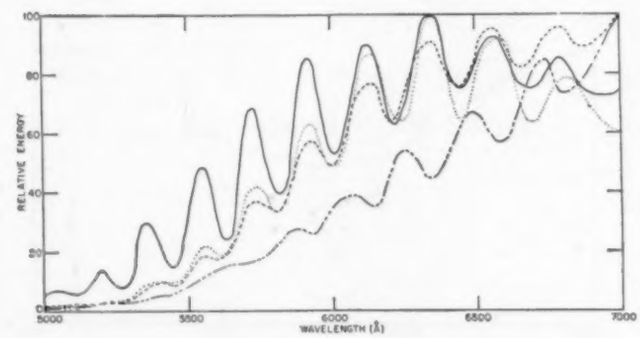


FIG. 3. Emission spectra at −196°C with 3650 Å excitation. . . . . $3(Na_2O \cdot Al_2O_3 \cdot 2SiO_2)$ $1.8NaCl \cdot 0.05Na_2S \cdot 0.05Na_2SO_4$; – – – – – $3(Na_2O \cdot Al_2O_3 \cdot 2SiO_2)1.0NaCl \cdot 0.25Na_2S \cdot 0.25Na_2SO_4$; — — — — $3(Na_2O \cdot Al_2O_3 \cdot 2SiO_2)0.5Na_2S \cdot 0.5Na_2SO_4$; ——— $Na_2S_x \cdot n\ Na_2SO_4$ from $Na_2S_2O_3$.

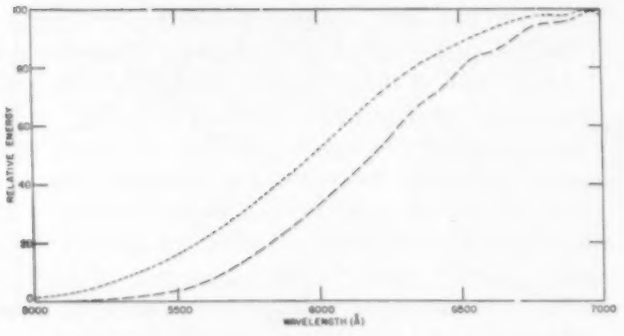


FIG. 4. Emission spectra of $Na_2S_x \cdot n\ Na_2SO_4$ from $Na_2SO_3$ (early stage of heating) with 3650 Å excitation. - - - - - 20°C; — — — —196°C.

with increasing $Na_2SO_4/Na_2S$ ratio. Maximum brightness was obtained with a starting $Na_2SO_4/Na_2S$ mole ratio of 5.7; increase of this ratio to a value greater than 7 caused a rapid decrease in brightness.

In this series, decreasing the $Na_2SO_4/Na_2S$ ratio to less than one appeared to cause the position of the emission maximum to shift toward the red, e.g., the emission maximum of the product with $Na_2SO_4/Na_2S = 0.1$ was 500 Å farther toward the red than that of the product with $Na_2SO_4/Na_2S = 1$. This may be only an apparent shift due to an internal filtering effect, since the high $Na_2S$ members rapidly colored pink under the exciting source.

Spectrographic analysis of some of the early synthetic sodalite products disclosed the presence of traces of several heavy metals. Therefore, an attempt was made to determine whether the band structure emission of the sodalites was due to the presence of metal activators. Emission spectra of $3(Na_2O \cdot Al_2O_3 \cdot 2SiO_2)$ 0.5 $Na_2S \cdot 0.5Na_2SO_4$ fired with mole ratios of $10^{-3}$, $10^{-4}$, and $10^{-5}$ of salts of each of the following metals, Mn, Pb, U, Sm, Ce, and Eu, were examined. None of these activators

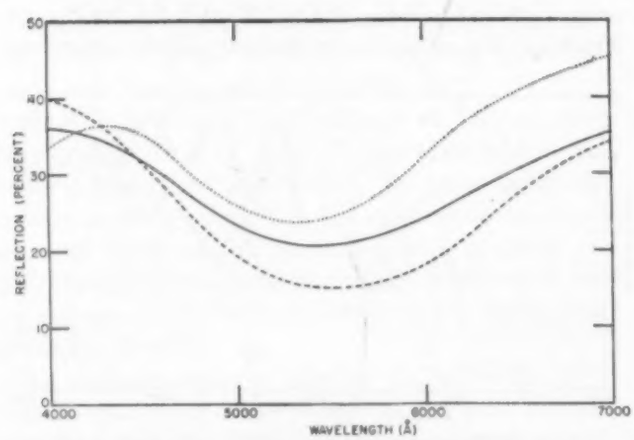


FIG. 5. Reflection spectra of natural hackmanite and synthetic products after coloring by 2537 Å radiation. . . . . Hackmanite; ——— $3(Na_2O \cdot Al_2O_3 \cdot 2SiO_2)$ $1.8NaCl \cdot 0.05Na_2S \cdot 0.05Na_2SO_4$; - - - - - $3(Na_2O \cdot Al_2O_3 \cdot 2SiO_2)$ $1.0NaCl \cdot 0.25Na_2S \cdot 0.25Na_2SO_4$.

effected any change in the structure of the emission at either 20° or −196°C.

Fig. 4 illustrates the emission spectra at 20° and −196°C of the sodium polysulfide-sulfate mixture formed by heating $Na_2SO_3$ for only a short period so that little polysulfide oxidation occurs, as described in the preparation section. The luminescence appears red to the eye, with practically no structure discernible in the emission spectra obtained by the author; low temperatures cause a shift to longer wave lengths with only very slight resolution into band structure. This emission is similar to that recorded by Gobrecht and Hahn for pure polysulfides with the exception that they found no evidence of structure at either 20° or −180°C.

Reflection spectra for the visible range, as recorded for two typical tenebrescent synthetic products and for natural hackmanite, are shown in Fig. 5. These, after coloring by ultraviolet, show only a single reflection minimum in the range of 5300 to 5500 Å. Medved found an absorption maximum at 5300 ± 50 Å for natural hackmanite colored by exposure to 2537 Å radiation.

## DISCUSSION

There appear to be two distinct types of 3650 Å-excited luminescence of sodium polysulfides: (*a*) a nearly structureless emission, appearing red to the eye and peaking in the infrared; this was obtained by the author from $Na_2S_x \cdot nNa_2SO_4$ from $Na_2SO_3$ after the early stages of heating, and also by Gobrecht and Hahn from pure polysulfides; (*b*) the yellow appearing emission with line structure shown by sodium polysulfide-sulfate prepared from $Na_2S_2O_3$ and from $Na_2SO_3$ in the final stages of heating. Reasons for this emission difference are not known but may be related to the $Na_2S_x$:$Na_2SO_4$ ratio or to the value of $x$ in $Na_2S_x$, since only the polysulfide-sulfate mixtures which are almost completely oxidized to sulfate have the yellow emission with line structure.

From an inspection of Fig. 3 it can be seen that the peaks of the band structure of the emission of the synthetic sodalite materials and of the $Na_2S_x \cdot nNa_2SO_4$ are nearly identical in spectral position. Thus it appears likely that the luminescence centers are the same and that the sodalite luminescence is connected with the presence of sodium polysulfide. Although the exact nature of the reaction occurring when the sodium monosulfide- and the sodium sulfate-sodalites are fired together is not known, it is quite possible that a sodium polysulfide-sodalite is one of the reaction products, the $Na_2SO_4$ acting as an oxidizing agent for the $Na_2S$.

From Table II it can be seen that the ability of the synthetic sodalites to color under radiation of

2537 Å or longer wave length is apparently due to the combined presence of $Na_2S$ and NaCl in the sodalite-type aluminosilicate lattice. Sodalites containing only one of these compounds do not color strongly under this radiation nor do sodalites containing only $Na_2SO_4$ or $Na_2SO_4$ + NaCl. The red-purple color of the $Na_2S$-containing sodalites bleaches rapidly under a tungsten light source.

Medved (5) reported formation of 2537 Å-sensitive products by heating NaCl-sodalite in hydrogen at 1060°C. In trials by the author, sodalite containing NaCl with no sulfur compounds added was fired in hydrogen at 900° and at 1060°C. The products were found to give an extremely weak coloration under 2537 Å radiation. It is believed by this author that these products contained traces of sulfur. Medved detected $Cl^-$ in the effluent gas and attributed its presence to replacement by hydrogen of part of the chlorine in NaCl to produce NaH and HCl. Attempts by this author to duplicate Medved's work at 1060°C caused extensive loss of NaCl. Thus, a two-hour firing at 1060° in hydrogen resulted in a weight loss of 55% of the contained NaCl, 99% of which could be condensed on a water-cooled silica tube.

It is not unlikely that sodalites containing $Na_2SO_4$ could be reduced to sodalites with $Na_2S_x$ by firing in sulfur vapor. Such reduction could not produce $Na_2S$ as long as excess sulfur is present. Tables I and II illustrate that sodalites which contain both NaCl and $Na_2SO_4$ are neither luminescent under 3650 Å nor tenebrescent under 2537 Å. When these sodalites are fired in sulfur vapor, it can be seen that they are still nontenebrescent under 2537 but have become luminescent (now contain $Na_2S_x$).

Unlike the luminescence, the tenebrescence of the sodalites could not be duplicated by the simple salt system without the aluminosilicate lattice. Incorporation of the $Na_2S$ and NaCl into the sodalite crystal structure is apparently requisite for the color formation. Mixtures of NaCl and $Na_2SO_4$ fired in graphite crucibles in $H_2$ until all the $Na_2SO_4$ was reduced to $Na_2S$ were nontenebrescent under ultraviolet. X-raying of these NaCl-$Na_2S$ mixtures caused only the weak yellow coloration of F-centers in NaCl.

As seen from Table II, sodalites containing NaCl and $Na_2SO_4$ colored under x-rays and 1850 Å ultraviolet. The resulting coloration was bluer and bleached much more slowly than that of sodalites containing $Na_2S$.

## Summary

The luminescence emission of a group of sulfur-containing, synthetic sodalites exhibits at −196°C a series of bands spaced about 200 Å apart. These bands are similar in spectral position to a previously undescribed band emission from sodium polysulfide at −196°C, leading to the conclusion that the sodalite luminescence is due to the presence of sodium polysulfide.

When the synthetic sodalites contain sodium monosulfide and sodium chloride they are tenebrescent, coloring to a red-purple color under ultraviolet radiation.

## Acknowledgments

The author wishes to express his gratitude to Dr. James H. Schulman, Dr. Clifford C. Klick, and Mr. Robert J. Ginther of this laboratory for their helpful discussions of this work.

Any discussion of this paper will appear in a Discussion Section to be published in the June 1955 issue of the Journal.

## References

1. Th. Liebisch, *Sitzber deut. Akad Wiss. Berlin*, **13**, 229 (1912).
2. L. H. Borgström, *Geol. Fören. Stockholm Förh.*, **23**, 563 (1901).
3. E. Vredenburg, *Records Geol. Survey India*, **31**, 43 (1904).
4. O. I. Lee, *Am. Mineralogist*, **21**, 764 (1936).
5. D. B. Medved, *J. Chem. Phys.*, **21**, 1309 (1953).
6. H. Gobrecht and D. Hahn, *Z. Physik*, **132**, 111 (1952).
7. J. Beato and M. D. Brügger, *Anales soc. españ. fis. y quim.*, **27**, 822 (1929); *C.A.*, **24**, 1051 (1930); original work not consulted.
8. J. H. Schulman and C. C. Klick, *J. Opt. Soc. Amer.*, **43**, 516 (1953).
9. E. Tiede and H. Reinicke, *Ber.*, **56**, 666 (1923).

# Preparation and Properties of Lead Telluride[1]

EDWARD L. BRADY

*Research Laboratory, General Electric Company, Schenectady, New York*

ABSTRACT

Single crystals of lead telluride, PbTe, have been prepared and their resistivity and Hall coefficients determined. Both *n*- and *p*-type lead telluride have been produced, but they were not of high resistivity. Charge carrier concentration in every case has been 1–5 × $10^{18}$/cm³. Hall mobility of *n*- and *p*-type carriers was found to be about 2240 and 860 cm²/volt-sec, respectively.

Material of *p*-type was converted to *n*-type by allowing lead to diffuse into the crystal at 500°C. The value of the diffusion coefficient of Pb in PbTe at this temperature is estimated to lie between 5.6 × $10^{-8}$ and 9.2 × $10^{-8}$ cm²/sec.

## INTRODUCTION

In recent years, a great deal of experimental work has been done with the series of compounds PbS, PbSe, and PbTe, stimulated by the observations that these compounds are photoconductive in the infrared (1) and that they exhibit transistor action (2, 3). Preparation of these compounds as single crystals is described by Lawson (4), and some of their electrical and optical properties are reported by Smith (1), Chasmar and Putley (5), Gibson (6, 7), and Putley (8). The present work had the following purposes: (*a*) determination of the ease of preparation of PbTe in pure, stoichiometric form; (*b*) determination of methods of producing *p*- and *n*-type PbTe at will; (*c*) measurement of the resistivity, Hall effect, and rectification properties of *p*- and *n*-type PbTe; and (*d*) obtaining information about the chemical stability of PbTe.

## EXPERIMENTAL

### *Preparation of Lead Telluride*

Lead telluride was prepared following a modification of the procedure described by Lawson (4). Elementary lead and tellurium were weighed with an accuracy of about one part in 20,000 to 50,000. The lead was spectrographically standardized grade.[2] The analysis states that total impurities are less than 2 × $10^{-3}$%. The following elements were detected spectrographically: bismuth, copper, cadmium, silver, calcium, aluminum, and sodium. The bars of lead as received are covered with an oxide layer, which was removed by electrolytic etching in a mixture of perchloric and acetic acids. After removal from the acid bath, the bar was washed with distilled water, dried rapidly with lens paper, and stored in a nitrogen atmosphere until weighed. For weighing purposes the bar was cut into pieces weighing 50–100 mg, and the final weight was adjusted by removing slivers of lead from the pieces with a scalpel. When necessary, the weight could easily be adjusted to 0.1 mg. Although the surface of the lead must have become at least partly oxidized during the weighing procedure, there was no observable change in weight of the pieces of lead while standing in air for a time comparable to that required for weighing.

Before it was used, the tellurium[3] was distilled in vacuum in a three-bulb distillation train, and was finally sealed off in vacuum until used. Tellurium prepared in this way was *p*-type and had a resistivity of 0.4 ohm-cm. Intrinsic tellurium is reported to have a resistivity of 0.56 ohm-cm and 0.29 ohm-cm, depending on orientation (9), and has a carrier concentration of about $10^{16}$/cm. For use, the tellurium was broken into pieces weighing 20–50 mg and then weighed. Here again, there was no weighable oxidation during the weighing procedure. The approximate desired quantity of tellurium was weighed, and the weight of lead was adjusted to the required amount.

The container for the reaction was either a graphite cup or a fused quartz tube. Graphite was used to eliminate complications from traces of oxygen left in the system, since room temperature equilibrium conditions for reactions of carbon with oxides of lead and tellurium are far toward the side of the formation of carbon dioxide accompanied by reduction of lead and tellurium. Furthermore, no compounds of carbon with lead have been reported. Carbon ditelluride is reported in an electric arc reaction, but would not be expected to form under the conditions of this experiment. When quartz was used, the tube was filled with about 30–35 cm of hydrogen and heated to glowing before addition of lead and tellu-

[1] Manuscript received March 17, 1954. This paper was prepared for delivery before the New York Meeting, April 12 to 16, 1953.

[2] Obtained from Johnson, Mathey and Company.

[3] Obtained from A. D. Mackay, Inc., 99.9% Te by company specifications.

rium. If this was not done, lead telluride stuck to the quartz tube, and, on cooling, both the tube and the lead telluride cracked badly.

The reaction of lead with tellurium proceeds rapidly with evolution of sufficient heat to maintain the reaction once it is started, if the reactants are intimately mixed. When the reaction is carried out with lumps of both reactants, pieces of lead swell as the reaction takes place and on occasion have cracked the graphite crucible. To avoid this difficulty, the tube containing the unreacted lead and tellurium was inserted into a furnace at a temperature 50°–60°C above the melting point of 905°C. All carbon cups in which the reaction was carried out were heated in a hydrogen furnace at 1100°C prior to use. The cup containing the unreacted elements was sealed into a fused quartz tube at a pressure of about $10^{-5}$ mm after the system had been pumped at this pressure for several hours. Sometimes the tube was sealed with a few centimeters of helium; an estimate of the rate of transmission of helium through the silica glass indicates that the pressure drops by about a factor of two per day at 900°C. The estimate also indicates that helium pressure in the tube sealed in high vacuum will increase to a pressure of about 1 $\mu$ during the time of the experiment. Permeation of oxygen through the glass is not fast enough to be an important consideration.

When a carbon cup was not used, the reactants were placed initially in the Pyrex arm of a Y-tube constructed with one Pyrex arm and one silica glass arm. The Y-tube was fitted with a ball joint so that rotation about the joint would cause the reactants to drop into the silica glass tube. Hydrogen was admitted to the system at a pressure of 30–35 cm and the silica arm heated with a torch to a glowing temperature. The line was pumped out to about $5 \times 10^{-5}$ mm, keeping the tube hot. After the tube had cooled, lead and tellurium were transferred to the silica arm by rotating the Y-tube about the ball joint. The tube was then sealed off about two inches above the reactants. In none of the experiments to be described was there any observable correlation between properties of lead telluride and type of container used.

Production of single crystals of PbTe was accomplished without difficulty by lowering the melt through a temperature gradient of about 20°/cm starting about 50°C above the melting point and ending about 50°C below. The lowering rate was 1 cm/hr. The equipment used is indicated in Fig. 1.

Before the crystal was grown, the tube was maintained at a temperature of 955°–965°C for three or four hours to ensure thorough mixing of the contents. During this time, the tube was agitated occasionally by moving it up and down inside the furnace. After

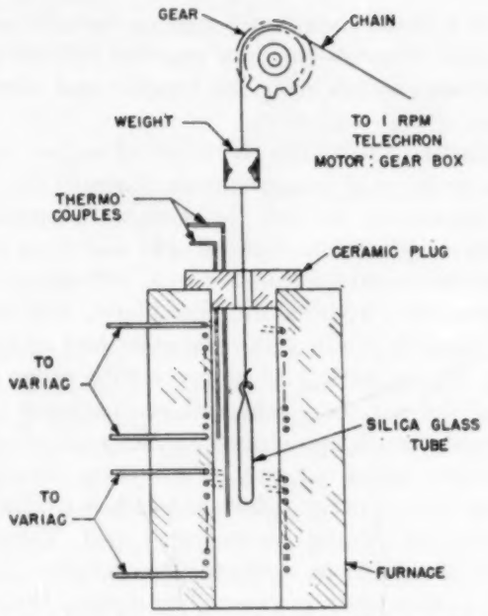


FIG. 1. Apparatus for producing single crystals of lead telluride.

the tube had been lowered about 12 cm (the crystal was usually 3–4 cm long), temperature was decreased to room temperature over a period of about eight hours to permit annealing. However, there was no apparent difference in crystals when the current was shut off and the furnace allowed to cool to room temperature at its natural rate.

The free volume in all tubes used to prepare crystals was kept as small as possible in order to minimize composition changes due to volatility and partial decomposition of lead telluride. Vapor pressure of PbTe at 950°C is claimed to be several centimeters (4), although no accurate measurements could be found in the literature. In all experiments in which a carbon cup was sealed in a silica glass tube, lead telluride condensed on the silica. Occasionally a small amount of solid was found in the bottom of the tube. Evidence for partial decomposition of PbTe is given by the characteristic yellowish color of tellurium vapor observed over lead telluride above its melting point. Thermodynamic data required for an estimate of the dissociation constant are not available in the literature.

Ingots of lead telluride have a bright, silvery appearance with a large number of small pits in the surface. In each of these pits there is usually one or more flat surfaces, and, if the ingot is a single crystal, these are all oriented in the same direction. Reflections from these surfaces provide fairly good evidence that the ingot is composed of a single crystal, but this visual indication was checked occasionally with x-rays. Lead telluride has the sodium chloride structure and cleaves fairly easily, but not controllably. For this reason the material was difficult to

saw to a shape suitable for making electrical measurements. Some of the data reported here were obtained with rather irregular samples and therefore are not of high accuracy.

In order to minimize the effect of surface conditions on electrical measurements of semiconductors, it is customary to etch the surface to produce a smooth bright finish. Various acid and base treatments were used on lead telluride without success. Hydrochloric, hydrofluoric, perchloric, and acetic acids alone or mixed with each other had no visible effect. Dilute nitric acid alone or with other acids turned the surface black, and concentrated nitric produced a much lighter gray surface and converted the black surface to gray. Presumably the black coating is elementary tellurium which is oxidized to tellurium dioxide by concentrated acid. Tellurium dioxide is soluble in a strong base solution, but a bright surface was not obtained by dipping the gray-coated solid in potassium hydroxide solution. A mixture of sodium hydroxide and sodium acetate had no visible effect on the surface. Electrolytic etching in a mixture of concentrated perchloric and glacial acetic acid produced a black coating when the lead telluride was the anode and no visible effect when the PbTe was the cathode. A bright etch can be achieved only by use of a technique which removes lead and tellurium equally rapidly from the surface. Perhaps thermal evaporation in vacuum would be successful; experiments to be described later indicate that partial volatilization in a hydrogen atmosphere produces a dull gray finish. The surface can easily be polished to a mirror finish by standard polishing techniques, but an x-ray examination of a polished surface reveals residual irregularities which a properly etched surface would not have. No difference in properties was observed between crystals with a mirror polish and those obtained with a diamond saw cut. Because of the difficulties with the etching procedure, measurements reported here were obtained with blocks which had a saw-cut surface smoothed with 2/0 emery polishing paper.

Another procedure often used to minimize the effect of surface conditions is to solder electrical contacts to the surfaces. It was found that a physically strong, nonrectifying contact could be achieved with ordinary soft solder by using a drop of concentrated hydrofluoric acid as flux. However, heating lead telluride in air changes its surface properties, and, since contacts could be obtained with no difficulty by pressure alone, all electrical measurements in this report were obtained with pressure contacts.

Resistivity and Hall coefficient data were obtained using equipment and techniques previously described by Dunlap (10).

*Electrical Properties of Lead Telluride Ingots*

When lead and tellurium were mixed in a nearly stoichiometric proportions as possible and a single crystal prepared as previously described, the ingot was invariably found to have the following properties. Almost all of the outside surface was $n$-type, as determined by a thermoelectric effect probe, but over most of the crystal the $n$-type character was present to a depth of only .002–.010 cm. The bulk of most of the crystal was $p$-type and only the last 5–10% of the crystal was $n$-type throughout. Typical values of electrical resistivities and Hall coefficients of $p$- and $n$-type material are presented in Table I, together with the mobilities and carrier concentrations calculated from these data.

An attempt was made to prepare high resistivity lead telluride by recrystallization of the ingots after discarding 5–10% of the crystal from each end. After the first recrystallization, the $n$-type region at the end of the crystal was very much smaller than before; the bulk of the crystal (except for the $n$-type skin) was $p$-type with about the same resistivity and Hall coefficient as before. Two more recrystallizations had very little effect on the electrical properties; resistivity and Hall coefficient were not significantly different from the values in Table I.

From an ingot prepared from fresh materials a section was cut out which was $n$-type on one face and $p$-type on the opposite, as determined by the thermoelectric probe. The resistivity of this block was 0.0147 ohm-cm and the Hall coefficient was +4.02. This resistivity is about a factor of four higher than that of the $p$-type samples, a result which is to be expected qualitatively since, in at least part of the block, $n$-type carriers should balance $p$-type. The boundary between $n$- and $p$-types was very sharp. A region of intermediate resistivity could not be detected with the thermoelectric probe when resistivity was judged qualitatively by the galvanometer response.

After each crystallization, small crystals that had deposited from the vapor were collected from the wall of the quartz tube. These crystals ranged in linear dimensions from about 0.1 mm up to 1 to 2 mm, were a few hundredths of a millimeter thick, and were always rectangular in shape, quite often square. These crystals were invariably $n$-type on

TABLE I. *Properties of typical* PbTe

| | $p$-type | $n$-type |
|---|---|---|
| Resistivity (ohm-cm) | 0.005 | 0.00090 |
| Hall coef. ($cm^3$/coulomb) | +4.2 | −2.0 |
| Mobility ($cm^2$/volt-sec) | 840 | 2220 |
| Concentration ($cm^{-3}$) | $1.5 \times 10^{18}$ | $3.1 \times 10^{18}$ |

TABLE II. *Effect of hydrogen on electrical properties of lead telluride*

| Sample | Temp (°C) | Time heated (hr) | Type by thermoelectric effect | Hall coef. ($cm^3$/coul) | Remarks |
|---|---|---|---|---|---|
| 1 | — | 0 | *n* on one side, *p* on others | +4.02 | — |
| 1 | 500 | 6 | *n*, all surfaces | +3.67; +5.26 | *n*-Type layer very thin |
| 1 | 845 | 6 | — | — | Sample completely volatilized |
| 2 | — | 0 | *p*, all surfaces | +2.12 | — |
| 2 | 600 | 6 | *n*, all surfaces | +3.11 | *n*-Type layer removed by light sanding |
| 2 | 695 | 6 | *n*, all surfaces | +3.30 | *n*-Type layer removed by light sanding |

both sides by thermoelectric measurements. The *n*-type character is consistent with the hypothesis that the vapor is partly decomposed at the melting point and that, since tellurium is more volatile than lead, the condensate has a stoichiometric excess of lead, which furnishes electrons to the crystal, making it *n*-type. However, the solid collected from the bottom of the tube, composed of material which also had come through the vapor phase, was *p*-type on the surface in contact with the quartz tube and *n*-type on the exposed surface.

*Treatment of p-Type Lead Telluride with Hydrogen*

If *p*-type lead telluride is treated with hydrogen, the material will be converted to *n*-type if the hydrogen can react with and remove *p*-type impurities or excess tellurium, or if hydrogen can dissolve in lead telluride and provide electrons. To discover the effect of hydrogen, a number of experiments were carried out in which a block of PbTe was heated at various temperatures in a stream of hydrogen. The tank hydrogen[4] was passed through a Deoxo unit and a Drierite tube before it came in contact with the lead telluride. Results obtained are listed in Table II. It is apparent from these results that treatment with hydrogen will convert *p*-type PbTe to *n*-type, but that the effect of the hydrogen does not penetrate more than a few mils in several hours at a temperature low enough to prevent appreciable volatilization of lead telluride. Hydrogen treatment dulled the surface of lead telluride considerably, probably indicating that some reaction with the surface had occurred rather than a dissolution of hydrogen into the solid.

*Distillation of p-Type Lead Telluride*

Since lead telluride condensed from the vapor was usually *n*-type, a vacuum distillation of the *p*-type material was carried out in order to prepare bulk *n*-type material. The *p*-type material in a carbon cup was placed in a silica tube with the end of the tube extending outside the furnace. Pumping was continued while the tube was heated to a final maximum temperature of 980°C, which was maintained for one-half hour. The solid which condensed on the cooler portion of the tube was almost black and was *n*-type thermoelectrically. A portion of this solid was placed in a silica tube and about 10 cm of hydrogen admitted to the system. When the tube was heated, the color of the solid changed from black to the silvery gray characteristic of the bulk ingots. The line was pumped out and the heating with hydrogen repeated. The line was again pumped out and the usual procedure for producing a single crystal followed. This crystal was *p*-type everywhere, including the surface. Hence, the sublimation procedure seems useful for producing small flat *n*-type crystals, but does not seem promising as a means of obtaining a quantity of *n*-type lead telluride which can be recrystallized to an *n*-type ingot.

*Diffusion of Lead Into Lead Telluride*

It is well known that lead sulfide containing excess lead is an *n*-type semiconductor, while with excess sulfur it is *p*-type (11). Similar observations have been reported for lead selenide (12) and lead telluride (4). Anderson and Richards (12) have measured the diffusion coefficient of lead in powdered, pressed lead sulfide and report that the diffusion coefficient, *D*, is given by

$$D = (1.38)(e^{-42{,}000/RT})\ \text{cm}^2/\text{sec}$$

At 500°C, this equation gives $D = 2.2 \times 10^{-12}$ $cm^2$/sec. Since tellurium ions are considerably larger than sulfide ions, one would expect the activation energy of the diffusion of lead in lead telluride to be lower than in lead sulfide and the value of *D* correspondingly greater. Hence it seems feasible to convert *p*-type lead telluride to *n*-type by allowing lead to diffuse into it at a moderate temperature for a few hours.

To test this point, a disk cut from a single crystal of *p*-type lead telluride was heated in vacuum between two disks of lead for 6.5 hr at a temperature of 290°C. After this period, the three disks had not changed in weight, and the lead telluride was still *p*-type.

[4] Produced by the General Electric Company.

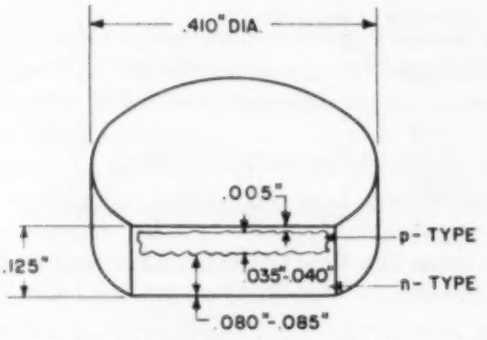


FIG. 2. Disk of lead telluride after diffusion of lead

The temperature was maintained below the melting point of lead in order to minimize solubility of lead telluride in the lead. At the melting point of lead, 327°C, the solubility of tellurium in lead is reported to be about 0.05% (13). Since no effect was observed at 290°C, a similar experiment was carried out at 500°C. In this experiment, the same disk of lead telluride was placed above a lump of spectrographic lead in a small carbon cup. Enough lead was used to ensure contact of the whole area of the flat surface of lead telluride with lead, so that diffusion through lead telluride would be uniform.

The silica glass tube containing the carbon cup with the lead telluride and lead was evacuated (to about 0.05 $\mu$) and heated to 500°C. After 40 min at this temperature, a dark deposit was observed on the cooler parts of the tube. To reduce evaporation and consequent changes in composition, the tube was filled with 35 cm of helium and the temperature maintained at 500° ± 5°C for a total of 7 hr (including the time in vacuum). At the conclusion of the experiment, the disk of lead telluride could not be easily removed from the lead. Separation of the two was accomplished by heating in a helium atmosphere with the lead resting on a nichrome grid. Above the melting point of the lead-tellurium solution (almost that of pure lead) the solid and liquid phases separated easily. No measure was obtained of the completeness of separation, but there was a thin fringe, apparently mostly lead, projecting from the edge of the disk, and the surface of the disk which had been in contact with the lead was shiny and irregular. The top surface was somewhat duller, but there was no major change in appearance. Several measurements of the thickness of the disk averaged to 0.326 cm, whereas the initial thickness had been 0.305–0.310 cm.

From the phase diagram, the solubility of tellurium in lead at 500°C is estimated to be 1%. Since the weight of lead taken was 7.05 g, the solubility of tellurium would be about 0.070 g, corresponding to 0.184 g of lead telluride. The original weight of the lead telluride was 2.124 g, large enough so that the amount of lead telluride dissolved would be only a small fraction of the total. The solid phase in equilibrium with liquid at 500°C is reported to contain 25 weight % (34 atom %) tellurium, and lead should diffuse into the stoichiometric lead telluride until this composition is reached. At equilibrium, a total of 1.05 g of lead would have diffused into the lead telluride.

All exposed surfaces of the disk had changed to $n$-type, including the top, which had had no direct physical contact with the lead. The disk was sawed perpendicular to the top surface and the freshly exposed face probed with a thermoelectric-effect needle in a micromanipulator. The $n$- and $p$-type character of the exposed face is indicated in Fig. 2. It is seen that the lead had penetrated sufficiently deeply into the lead telluride to convert most of it to $n$-type. Surface diffusion or deposition of lead from the vapor phase was rapid enough to convert the whole surface to $n$-type and to penetrate about 0.01 cm into the interior.

An estimate of the diffusion coefficient of lead in lead telluride can be obtained from the data indicated in the figure. The solution of the diffusion equation for one-dimensional diffusion with the boundary conditions of the present situation is given by (14):

$$C(x, t) = C_o\left[1 - \frac{2}{\sqrt{\pi}}\int_0^{x/2\sqrt{Dt}} e^{-y^2}\, dy\right],$$

in which $C(x, t)$ is the concentration at the distance $x$ and the time $t$, $C_o$ is the constant concentration at $x = 0$, and $D$ is the diffusion coefficient. In the present problem, $C_o$ is taken to be the difference in concentration (atoms/cc) between solid lead telluride saturated with lead at 500°C and stoichiometric lead telluride. The distance $x$ is taken to be the furthest distance from the boundary surface at which conversion to $n$-type has occurred, and $t$ is the time of heating at 500°C. The concentration, $C(x, t)$, is more difficult to estimate. It must be at least equal to the concentration of $p$-type carriers in the original material, and may be a good deal higher. The diffusion coefficient will be calculated on the assumptions that $C(x, t)$ is roughly equal to the original hole concentration, and that it is roughly ten times greater. The correct value of the diffusion coefficient should lie between these two values.

Since no data are available for the density of lead telluride saturated with lead, it is assumed that the density is equal to that of the stoichiometric compound. With this assumption, $C_o$ equals $3.5 \times 10^{21}$/cm$^3$. A reasonable value for the hole concentration is $3.5 \times 10^{18}$/cm$^3$. Rearranging the diffusion equation, one can obtain:

$$\frac{2}{\sqrt{\pi}}\int_0^{x/2\sqrt{Dt}} e^{-y}\, dy = 1 - \frac{C}{C_o} = 1 - \frac{1}{1000} = 0.999$$

Tables of the error function (the left side of the above equation) give a value of:

$$\frac{x}{2\sqrt{Dt}} = 2.326$$

The depth of penetration, $x$, equals about 0.175 cm after correction is made for the lead telluride that dissolved in the lead, and $t = 7$ hr $= 2.52 \times 10^4$ sec. When the above equation is solved for $D$, a value of $D = 5.61 \times 10^{-8}$ cm²/sec is obtained. When a ratio of $c/c_s = 0.01$ is assumed as a reasonable upper limit, a value of $D = 9.15 \times 10^{-8}$ cm²/sec is obtained. This range of values for the diffusion coefficient of Pb is considered to be of a reasonable order of magnitude. It is seen that they are $2.5 \times 10^4 - 4 \times 10^4$ times greater than the value for the diffusion coefficient of lead in lead sulfide.

The foregoing discussion is all based on the assumption that the substance which diffuses into the lead telluride is excess lead. There is no proof that lead is responsible for the conversion to $n$-type; one of the impurities present in the spectrographic lead may have caused the change. If this were the case, the diffusion coefficient would be of the order of $10^2$ to $10^3$ times greater than that calculated above.

When the hot point of the thermoelectric probe rested in contact with an $n$-type region, the potentiometer deflection decreased in a few minutes, often changing sign. This effect was observed over almost all of the $n$-type surface. The region closest to the lead did not change sign but only exhibited a change in magnitude. During a period of about 1.5 hr of standing in air at room temperature, about two-thirds of the $n$-type surface had changed to $p$-type, and after about three hours only a small fraction of the surface remained $n$-type. The original pattern was recovered, however, by light sanding with fine emery paper. Changes in type are almost certainly associated with oxidation of the surface. When a stream of oxygen was directed on the surface, the rate of change from $n$- to $p$-type was increased considerably. With a stream of hydrogen on the surface an entirely different effect was obtained; the initial contact of the probe with the surface was $p$-type and remained $p$-type as long as the stream of hydrogen was maintained. On removal of the hydrogen, the surface reverted to $n$-type.

An attempt was made to observe rectification across the $n$-$p$ barrier in the lead telluride. One electrical contact was made with a small aluminum vise used to hold the sample, which was in contact with both $n$-type flat surfaces. The other contact was established with the $p$-type region of a freshly sanded surface, by use of a brass probe. With the probe in very light contact and with a potential difference of 1 v, slight rectification was observed—apparently all associated with the probe contact, since an increase in pressure caused the oscilloscope trace to become ohmic in character. Since the conductivity of the material is so high and the $n$-$p$ boundary so sharp, the potential drop across the $n$-$p$ boundary may exceed the Zener breakdown potential.

When an ohmic trace was obtained and the lead telluride surface illuminated with the light from a flashlight, the current through the solid increased significantly. No quantitative measurements were obtained.

### *Nonstoichiometric Lead Telluride*

Lawson (4) has reported that lead telluride prepared from the pure elements will always be $p$-type even when 2–5% excess lead is used, unless the reaction tube is treated with hydrogen and the reactants melted in hydrogen before reaction. His technique leads to an indeterminate but probably small loss of tellurium before reaction. Lawson's procedure was modified somewhat in an attempt to simplify the procedure and avoid loss of tellurium. The equipment consisted of the Y-tube with one silica glass arm previously described and preparations were made as described.

After preparation of the ingot, a block was sawed from the middle portion, and resistivity and Hall coefficient measurements made. In the samples containing excess lead, it was found that the portion of the ingot that crystallized last was invariably $n$-type (as was the surface) and that the thickness of the $n$-type region was 1 to 2 mm. Samples containing excess tellurium showed no $n$-type regions anywhere. Results of electrical measurements are presented in Table III.

Considering the irregularities in the samples due to cleavage during sawing, results are considered to be identical within the limit of accuracy of the measurements. The bulk of each of the samples is $p$-type, even with 2% excess lead, just as Lawson observed.

TABLE III. *Electric properties of nonstoichiometric lead telluride*

| Sample | Resistivity (ohm-cm) | Hall coefficient (cm³/coul) | Mobility (cm²/volt-sec) | Carrier concentration (1/cm³) (× $10^{18}$) | Thermoelectric type |
|---|---|---|---|---|---|
| % | | | | | |
| 0.5 Te | 0.00493 | +4.16 | 845 | 1.50 | $p$ |
| 0.1 Te | 0.00379 | +3.46 | 914 | 1.81 | $p$ |
| 0.1 Pb | 0.00726 | +5.93 | 817 | 1.05 | $p$ |
| 0.5 Pb | 0.00468 | +5.47 | 1170 | 1.14 | $p$ |
| 0.5 Pb* | 0.00553 | +4.26 | 773 | 1.47 | $p$ |
| 1.0 Pb | 0.00475 | +3.78 | 795 | 1.65 | $p$ |
| 2.0 Pb | 0.00380 | +2.81 | 740 | 2.22 | $p$ |

* Sample crystallized in 20 cm helium. All others in vacuum.

Lattice spacings in the samples containing 0.5% excess tellurium and 0.5% excess lead have been determined.[5] Results obtained were 6.4579 ± 0.0030 Å and 6.4576 ± 0.0019 Å, respectively. The difference, of course, is not significant. The literature value is 6.453 Å. It is believed that the value obtained here is more accurate than the literature value.

## Discussion

The study of electrical properties of lead telluride is hindered by its chemical behavior and by limitations of measuring methods; no volumetric or gravimetric measuring technique is adequate to prepare a mixture of the two components in exactly stoichiometric ratio. Furthermore, no adequate means of ensuring sufficient purity in the initial reactants is available, necessitating purification of the compound after formation. Recrystallization from the melt, a technique that produces adequate purity in elementary semiconductors, is complicated by relatively high vapor pressure and partial decomposition of the compound at its melting point, so that loss of material and change of composition must be minimized by operating in a closed system with a free volume as small as possible. With these restrictions, recrystallization as carried out in the present experiments leads either to ineffective rejection of impurities or to a nonstoichiometric compound, or to both.

The *p*-type character of most of the lead telluride (all but about the last 10% to crystallize) indicates that the solid phase of PbTe is not in equilibrium with a liquid of exactly the same composition, and, indeed, there is no reason to expect such a condition to exist. If it is assumed that the solid is in thermal equilibrium both with empty lead sites and empty tellurium sites, it seems reasonable that the concentration of empty lead sites should be greater than that of empty tellurium sites, since the energy required to create an empty lead site is undoubtedly considerably less than that required for a tellurium defect. Electrical neutrality in the crystal can be maintained, by assuming either that excess tellurium is zerovalent (or monovalent) or that excess telluride ion is balanced by the abstraction of electrons from divalent lead. Any description in terms of a purely onic lattice, however, is certainly an oversimplification.

Therefore, in the usual case, crystallization from the melt is expected to lead to a nonstoichiometric compound, although in principle the composition of the melt could be adjusted so that the solid phase would have the desired composition. In general, this would require extremely delicate control not only of the liquid phase composition, but also of all other variables affecting the solid phase, such [illegible] crystal growth rate and thermal environment.

Since the presence of impurities cannot [illegible] distinguished from deviations from stoichiomet[illegible] by experiments of the type described here, it is i[illegible] possible to decide definitely at present which of the[illegible] sources of donors and acceptors is responsible for [illegible]he electrical properties. However, it is believed that deviations from stoichiometry are probably responsible for the electrical behavior of the ingots prepared in the present work.

Another aspect of the chemical behavior of lead telluride which contributes to the difficulties of making significant reproducible electrical measurements is its reactivity with oxygen. The change of an *n*-type surface to *p*-type when exposed to air at room temperature indicates that the compound should be handled at all times in an inert atmosphere.

Properties of the material obtained in the present research confirm results obtained with the material prepared by Lawson. In his paper on the absorption spectra of lead sulfide, selenide, and telluride, Gibson (7) reports carrier concentrations of $1 \times 10^{18}$ to $2 \times 10^{18}$ for *p*-type lead telluride and $1\text{–}6 \times 10^{18}$ for *n*-type, essentially identical with those obtained here. However, Gibson has worked with lead telluride containing only $5 \times 10^{16}$ carriers/cm³ (6). Putley (8) reports the best values of hole mobility and electron mobility at 290°K to be 840 cm²/volt-sec and 2100 cm²/volt-sec, respectively. Values obtained for the room-temperature mobilities of holes and electrons in the present research were 860 cm²/volt-sec and 2240 cm²/volt-sec.

## Acknowledgments

The author wishes to acknowledge many helpful discussions with Dr. W. C. Dunlap and Dr. L. Apker. Many of the electrical measurements were made by Miss Sally Schwartz.

Any discussion of this paper will appear in a Discussion Section to be published in the June 1955 issue of the Journal.

[5] By Mrs. B. F. Decker.

## REFERENCES

1. R. A. Smith, "Semi-Conducting Materials," (H. K. Henisch, Editor) pp. 198–207, Butterworths Scientific Publications Ltd., London (1951).
2. H. A. Gebbie, P. C. Banbury, and C. A. Hogarth, *Proc. Phys. Soc., London*, **B63**, 371 (1950).
3. C. A. Hogarth, *ibid.*, **B64**, 822 (1951); **B65**, 958 (1952).
4. W. D. Lawson, *J. Appl. Phys.*, **22**, 1444 (1951); **23**, 495 (1952).
5. R. P. Chasmar and E. H. Putley, "Semi-Conducting Materials," (H. K. Henisch, Editor) pp. 208–217, Butterworths Scientific Publications Ltd., London (1951).
6. A. F. Gibson, *Proc. Phys. Soc., London*, **B65**, 196 (1952).
7. A. F. Gibson, *ibid.*, **B65**, 378 (1952).

8. E. H. Putley, *ibid.*, **B65**, 388 (1952).
9. V. E. Bottom, *Science*, **115**, 570 (1952).
10. W. C. Dunlap, *Phys. Rev.*, **79**, 286 (1950).
11. For a review of the information on PbS see K. Hauffe, *Ergeb. exakt. Naturw.*, **25**, 243 (1951).
12. J. S. Anderson and J. R. Richards, *J. Chem. Soc.*, 1946, 537.
13. W. Hofmann, "Blei und Bleilegierungen," pp. 52–55, Julius Springer, Berlin (1941); republished by J. W. Edwards, Ann Arbor, Michigan (1944). G. O. Hiers, "Metals Handbook," (Taylor Lyman, Editor) ASM, Cleveland (1948).
14. R. M. Barrer, "Diffusion In and Through Solids," p. 12, Cambridge University Press, London (1951).

# Crystal Structure and Thermodynamic Studies on the Zirconium-Hydrogen Alloys[1]

EARL A. GULBRANSEN AND KENNETH F. ANDREW

*Westinghouse Research Laboratories, East Pittsburgh, Pennsylvania*

ABSTRACT

The phase diagram of zirconium-hydrogen alloys was studied on alloys prepared at low temperature and for alloys in the composition range of $ZrH_{0.025}$ to $ZrH_{1.963}$. Decomposition pressure studies were made over the composition range and for a series of temperatures. Results of these measurements were in complete agreement with crystal structure studies on the major phases.

Results show presence of two major hydride phases, namely, the $\delta$- and $\epsilon$-phases as described by Hägg. No evidence was found for either the $\gamma$- or $\beta$-phases of Hägg, although the latter phase was found only at high temperature by Hägg. The $\epsilon$-phase was found to have a wide range of homogeneity from $ZrH_{1.965}$ to about $ZrH_{1.65}$. The $\delta$-phase was found to have a composition near $ZrH_{1.50}$ and a range of homogeneity from $ZrH_{1.4}$ to $ZrH_{1.66}$.

A new minor transitional phase was found having the face-centered tetragonal structure and existing only in the presence of $\alpha$-Zr and $\delta$-phases. It has been designated as the $\gamma'$-phase since its composition is probably near that of Hägg's $\gamma$-phase.

The free energy of formation of the $\delta$-phase in contact with $\alpha$-Zr containing hydrogen was determined from decomposition pressure data.

## INTRODUCTION

The reaction of zirconium with hydrogen has been the subject of a number of experimental studies. The literature was reviewed by Smith (1) in 1948 and more recently by Gulbransen (2) in 1953. An analysis of the literature shows some confusion concerning the phases present in the zirconium-hydrogen system and in the interpretation of the absorption isotherms.

Since hydrogen has been found to embrittle zirconium under certain conditions for concentrations as low as 10 ppm (3) and since zirconium is rapidly becoming an industrially important metal, it is of interest to reexamine the role of hydrogen in the metal.

This communication will present both thermodynamic studies on the formation of hydrogen alloys from the metal and crystal structure studies of these alloys. Studies are made for alloys prepared at temperatures below 300°C and for compositions of $ZrH_{0.025}$ to $ZrH_{1.985}$.

It has been known for a long time that zirconium can absorb considerable quantities of hydrogen and still show a metallic appearance. Winkler (4, 5) first observed the large capacity of zirconium for absorption of hydrogen and proposed that definite gaseous and solid hydrides were formed. Gaseous hydrides were not confirmed by Wedekind (6), nor by Schwarz and Konrad (7). The formation of the hydride $ZrH_2$ was suggested by Weiss and Neumann (8) and Wedekind (9) from studies of the absorption of hydrogen by zirconium.

Smith (1) has designated zirconium as belonging to the class of exothermic occluders. These metals absorb hydrogen in large quantities, form alloys of greater complexity, exhibit solid solution phenomena, and form one or more secondary phases.

*Absorption isotherms.*—Sieverts and Roell (10) first studied absorption isotherms on samples of metal powders containing 91% zirconium at 800° and 1100°C and an absorption isobar at 760 mm of Hg hydrogen pressure. Consistent results were difficult to attain by their methods.

Hall, Martin, and Rees (11) recognized the role of surface contamination and eliminated surface oxide by heating to high temperature in vacuo before studying the absorption of hydrogen. Absorption isotherms show strong "kinks" for compositions between $ZrH_{1.0}$ and $ZrH_{1.4}$ and the shapes of the curves show a resemblance to those found for the palladium-hydrogen system where a two-phase region has been noted. Hall, Martin, and Rees (11) interpret the shape of the curves in terms of two solution processes occurring together, only one of which is rate-determining.

*Crystal structure studies.*—Hägg (12) has studied zirconium-hydrogen phases on specimens prepared at high temperature and cooled to room tempera-

[1] Manuscript received March 19, 1954. This paper was prepared for delivery before the Chicago Meeting, May 2 to 6, 1954.

TABLE I. *Crystal structure data on* Zr-H *system*

| Atom % H | Lattice structure and dimensions kX units | Reference |
|---|---|---|
| 0 $\alpha$-phase | h.c.p.; $a$ = 3.228 | 13 |
| | $c$ = 5.140 | |
| Transition temp. °C | 862° ± 5°C | |
| 0 $\beta$-phase | b.c.c.; $a$ = 3.61 at 900°C | |
| 0–5 | $\alpha$-phase; h.c.p. | 12 |
| | $a_{max}$ = 3.247 | |
| | $c_{max}$ = 5.173 | |
| 20 | $\beta$-phase; f.c.c. | |
| | $a$ = 4.66 | |
| 33 | $\gamma$-phase; h.c.p. | |
| | $a$ = 3.335–3.339 | |
| | $c$ = 5.453–5.455 | |
| 50 | $\delta$-phase; f.c.c. (fluorite) | |
| | $a$ = 4.765–4.768 | |
| 66.7 | $\epsilon$-phase; f.c. tetrag. | |
| | $a$ = 4.964 | |
| | $c$ = 4.440 | |
| | $c/a$ = 0.894 | |
| 66.0 | $\epsilon$-phase; f.c. tetrag. | 15 |
| | $a$ = 4.87 | |
| | $c$ = 4.58 | |

ture. Although no details of his preparation procedures are given, many of the samples were prepared above the $\alpha$-$\beta$ transformation temperature for zirconium, the existence of which Hägg was probably unaware. Five phases were noted by Hägg (12), including the $\beta$-phase $Zr_4H$ which is stable only at high temperatures.

Table I shows a compilation of crystal structures of the two zirconium phases and the several zirconium-hydrogen phases. Data for pure metal phases are averaged values of the published literature given by van Arkel (13). The dimensions of the unit cells are given in kX units. A value of 1.00202 has been set (14) as the conversion factor for kX units into Angstrom units. Criticism has been raised by Smith (1) concerning the existence of some of Hägg's phases on the grounds that stresses were set up in the sample on cooling through the transition temperature and that inhomogeneities might occur in the method of preparation. Hägg probably realized many of these difficulties and has not suggested that the work was complete.

## Experimental

*Vacuum microbalance.*—A vacuum microbalance and associated apparatus is used for preparing all specimens and for studying decomposition pressures of these specimens. The construction and use of the microbalance has been described (16).

Specimens are sheets of zirconium 0.0125 cm thick. For convenience two sizes are used. The first size weighs 0.05 g and has an area of 1.25 cm². These specimens are used for preparing and studying hydrogen alloys of compositions above $ZrH_{0.10}$. The second size weighs 0.50 g and has an area of about 12 cm². They are used for preparing and studying hydrogen alloys below $ZrH_{0.10}$.

TABLE II. *Analyses of zirconium samples*

| | Foote Zr Typical |
|---|---|
| Si | .01 |
| Fe | .04 |
| Al | .01 |
| Cu | <.01 |
| Ti | .03 |
| Mn | <.001 |
| Ca | .01 |
| Mg | <.003 |
| Pb | <.001 |
| Mo | <.001 |
| Ni | .01 |
| Cr | .001 |
| Sn | .001 |
| W | <.001 |
| N | <.01 |
| O | <.01 |
| H | <.02 |
| C | <.001 |
| Hf | 2.40 |

The sensitivity of the balance was 0.79 $\mu$g/division (0.001 cm) and the weight change was estimated to ¼ of a division or ($0.20 \times 10^{-6}$ g).

*Vacuum system.*—Vacuum and reaction systems are of critical importance in studying reactions of highly reactive metals such as zirconium. The vacuum system used in this study is of all glass construction and can be evacuated readily to pressures considerably lower than $10^{-6}$ mm of Hg. A mullite furnace tube (17) which contains the specimen is sealed directly to the Pyrex apparatus. Previous studies (17) have shown that pressures less than $10^{-8}$ mm of Hg can be achieved in this system with the furnace tube at 900°C after pumping over night.

*Preparation of gases.*—Pure hydrogen is prepared by diffusing purified electrolytic hydrogen through a hot palladium tube. Experience has shown that gas purity is also a critical factor in the study of the zirconium-hydrogen reaction. Reproducible results are obtained only with the purest preparations of hydrogen.

*Samples and sample preparation.*—High purity iodide process zirconium is used for all experiments. Spectrographic and chemical analyses are given in Table II. The largest impurity is 2.4% of hafnium.

All specimens are abraded starting with 1/0 polishing paper and finishing with 4/0. The last two papers are used with purified kerosene. Samples are then cleaned successively with soap and water,

distilled water, petroleum ether, and absolute alcohol. After a preliminary weighing, specimens are placed in a desiccator until ready for use.

*X-ray diffraction apparatus.*—An iron target x-ray tube was used as a source of x-rays. The x-ray beam was monochromatized to give $FeK_\alpha$ radiation. A 9-cm Unicam powder camera was used to record reflections. Ilford x-ray film was used in the camera.

To reduce the background the camera was evacuated to 0.01 mm of Hg pressure. An exposure time of one day was used to bring out the weak lines of minor phases present in some samples.

A pure NaCl specimen was used for calibrating the camera at a 2 $\theta$ value of 90°C.

## Method

*Preparation of samples.*—The vacuum microbalance was well suited for the preparation of hydrogen alloys of definite composition. The weighed sample was placed on the supporting wire and suspended from one end of the balance beam. After closing off the system, the apparatus was partially evacuated and the liquid nitrogen trap put in place. The evacuation was now completed and the system pumped for 16 hr or longer at a pressure below $10^{-6}$ mm of Hg.

To remove the room temperature oxide a furnace at 700°C was placed around the furnace tube for 2 hr, after which the sample was cooled to the reaction temperature in vacuo to prepare the particular hydrogen alloy. During this heating cycle some pick-up of gases from the vacuum system would be expected to occur. This was found to be of the order of 2 to 3 $\mu$g or less which was negligible for our purposes. To assure homogeneity the specimen was homogenized for 20 hr or longer at the preparation temperature. For specimens prepared above 150°C this treatment appeared to give a uniform composition throughout. Weight changes occurring during this treatment were 2 to 3 $\mu$g or less.

*Decomposition pressure studies.*—Zirconium reacts with hydrogen to form at least two stable hydrides in addition to the $\alpha$-phase of zirconium containing hydrogen. The phase diagram of the zirconium–hydrogen system can be determined by measuring decomposition pressures at a series of temperatures over the complete composition range. Decomposition pressure was determined by closing off the sample from the vacuum pumps and reading the hydrogen pressure by means of a calibrated McLeod gauge. Readings were made on both the decomposition (heating) cycle and on the absorption (cooling) cycle. In this way true equilibrium values could be obtained. Extreme care was used to avoid contamination. If contamination occurred, readings were erratic and nonreversible.

*Crystal structure studies.*—Special sam es were made for x-ray diffraction analyses follo ing the method described above (Vacuum micro alance). Brittle specimens were ground to a pow ler and placed in a 0.3 mm glass capillary havin a wall thickness of 0.01 mm. Strips were cut from the ductile specimens of 0.013 × 0.05 × 1.0 m size. X-ray diffraction patterns were made directly on these samples.

Since the absorption coefficient of the $K_\alpha$ iron x-ray radiation by Zr was large, the outer surface of the specimen contributes mainly to the x-ray diffraction pattern. This makes it possible to test the presence of surface contamination or inhomogeneities in the specimen by the use of etching processes. Thus, some of the specimens were etched in a mixture of 1 cc conc. $HNO_3$, 10 cc of 48% HF, and 90 cc of $H_2O$. The etching process required 5 to 30 sec time, the 30-sec etch removing about 50% of the material.

## Results and Discussion

### *Decomposition Pressure Studies*

Twenty-one compositions were prepared and studied in the range of $ZrH_{0.025}$ to $ZrH_{1.74}$. Decomposition pressures were measured in the temperature range of 325° to 550°C directly after preparation to avoid contamination.

Fig. 1 to 4 show typical results. Decomposition

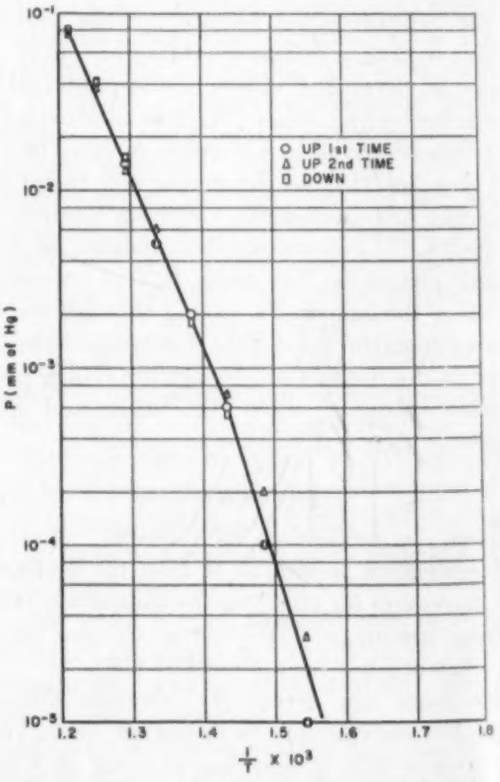


Fig. 1. Decomposition pressure of $ZrH_{0.99}$

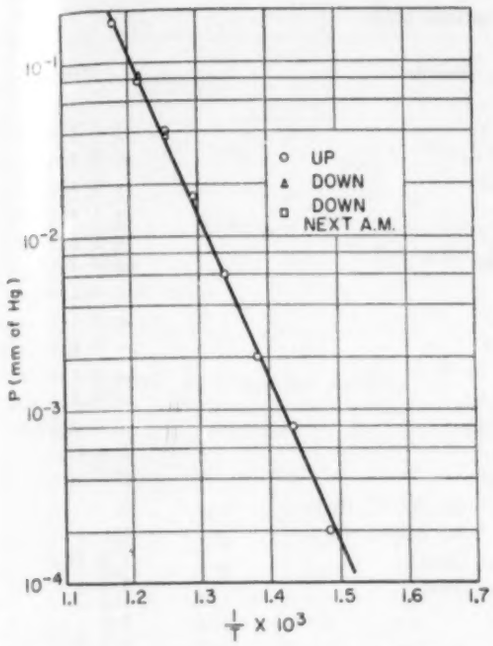


FIG. 2. Decomposition pressure of $ZrH_{1.83}$

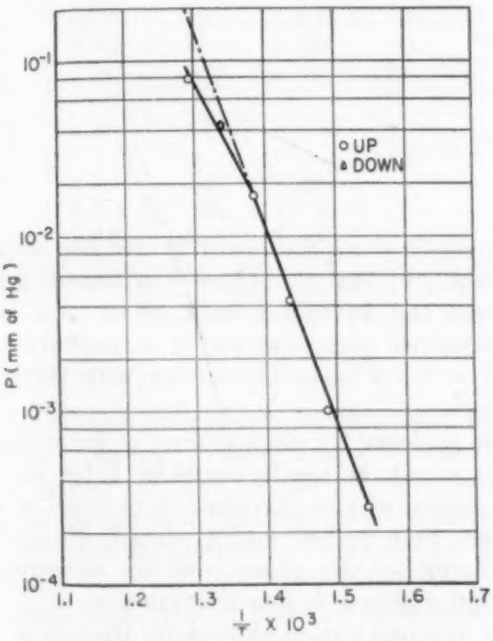


FIG. 3. Decomposition pressure of $ZrH_{1.51}$

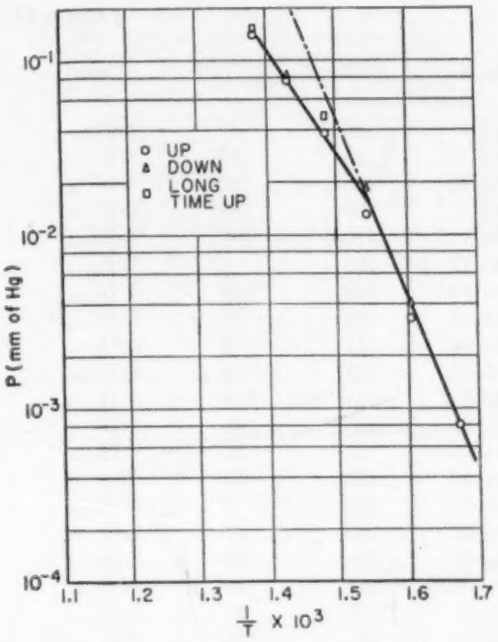


FIG. 4. Decomposition pressure of $ZrH_{1.74}$

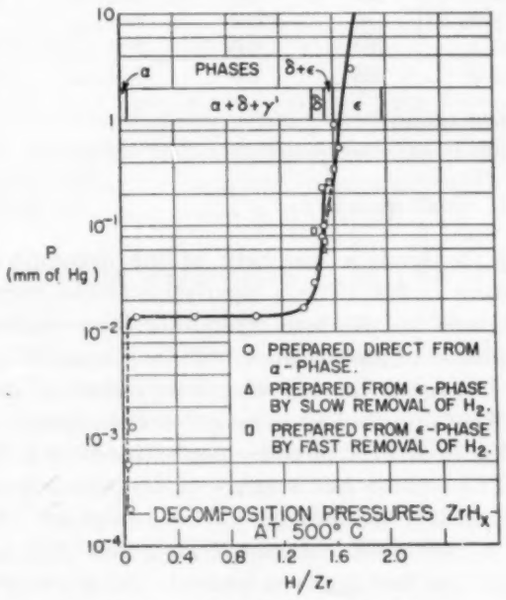


FIG. 5. Decomposition pressure $ZrH_x$

pressures are plotted on a logarithmic scale against $1/T$. Fig. 1 shows a plot of results for the composition $ZrH_{0.99}$. A reversible process was noted. Since the total quantity of hydrogen was small for the 0.05 g samples, the composition of the alloy changes for pressure readings above $10^{-2}$ mm of Hg. For Fig. 1 this change in composition has no effect on the straight line character of the plot at this point. This suggests that the composition $ZrH_{0.99}$ is in a two-phase region where the pressure is independent of composition. This can be seen in Figure 5.

Fig. 2 shows a similar plot for the composition $ZrH_{1.36}$. This plot also shows a reversible character and individual measurements are nearly identical with those for the composition $ZrH_{0.99}$. The straight line character of the curve persists above $10^{-2}$ mm of Hg which suggests that the composition $ZrH_{1.36}$ is also in a two-phase region.

Fig. 3 shows the plot for the composition $ZrH_{1.51}$. Here, a break occurs in the plot between 1 and $2 \times 10^{-2}$ mm of Hg. Decomposition pressure is dependent upon the composition which suggests a single-phase region.

Fig. 4 shows a similar type of plot for the composition $ZrH_{1.74}$. This composition is also in a single phase region.

TABLE III. *Summary of x-ray data (25°C)*

| Exp. No. | Temp, °C | Preparation time, min | Compn. | Treatment | Result |
|---|---|---|---|---|---|
| 63-17 | 100 | 10 | $ZrH_{0.10}$ | Hom.[a] 100°C, 21 hr | $\alpha + \delta +$ tr $\gamma'$ |
| 63-16 | 125 | 10 | $ZrH_{0.15}$ | Hom. 125°C, 20.5 hr | $\alpha + \delta +$ tr $\gamma'$ |
| 63-15 | 150 | 12 | $ZrH_{0.246}$ | Hom. 150°C, 20 hr | $\alpha + \delta +$ tr $\gamma'$ |
| 63-9 | 150 | 45 | $ZrH_{0.48}$ | Hom. 150°C, 20 hr | $\alpha + \delta +$ s.a. $\gamma'$ |
| 65-11 | 150 | 81 | $ZrH_{0.52}$ | Hom. 250°C, 19 hr | $\alpha + \delta +$ tr $\gamma'$ |
| 65-12 | 250 | — | $ZrH_{0.52}$ | Prep. from $\epsilon$-phase | $\alpha + \delta +$ s.a. $\gamma'$ |
| 65-15 | 150 | 48 | $ZrH_{0.53}$ | Direct, no hom. | $\alpha + \delta +$ s.a. $\gamma'$ |
| 63-10 | 200 | 13 | $ZrH_{0.55}$ | Hom. 200°C, 20 hr | $\alpha + \delta +$ tr $\gamma'$ |
| 63-14 | 225 | 8 | $ZrH_{0.705}$ | Hom. 225°C, 20 hr | $\alpha + \delta +$ tr $\gamma'$ |
| 63-13 | 225 | 15 | $ZrH_{0.84}$ | Hom. 225°C, 20.3 hr | $\alpha + \delta +$ tr $\gamma'$ |
| 63-6 | 175 | 165 | $ZrH_{1.105}$ | Hom. 175°C, 15.5 hr | $\alpha + \delta +$ s.a. $\gamma'$ |
| 63-12 | 225 | 38 | $ZrH_{1.33}$ | Hom. 225°C, 20.5 hr | $\alpha + \delta +$ tr $\gamma'$ |
| 64-45 | 225 | 51 | $ZrH_{1.44}$ | Hom. 325°C, 18 hr | $\delta +$ tr $\gamma'$ |
| 64-41 | 225 | 65 | $ZrH_{1.44}$ | Hom. 225°C, 19 hr | $\delta +$ tr $\gamma'$ |
| 64-17 | 230 | 1 | $ZrH_{1.51}$ | Heated to 500°C, hom. 200°C, 63 hr | $\delta$ |
| 64-46 | 250 | 27 | $ZrH_{1.54}$ | Heated to 375°C, hom. 325°C, 19 hr | $\delta$ |
| 64-47 | 250 | 29 | $ZrH_{1.56}$ | Prep. from $\epsilon$-phase (fast) | $\delta +$ tr $\epsilon$ |
| 64-34 | 250 | 48 | $ZrH_{1.60}$ | Prep. from $\epsilon$-phase (fast) | $\delta + \epsilon$ |
| 64-35 | 270 | 51 | $ZrH_{1.64}$ | Hom. 250°C, 18 hr | $\epsilon$ |
| 63-18 | 275 | 23 | $ZrH_{1.64}$ | $H_2$ quenched | $\epsilon +$ tr $\delta$ |
| 63-11 | 225 | 57 | $ZrH_{1.647}$ | Hom. 225°C, 19.5 hr | $\delta$[b] |
| 63-21 | 225 | 82 | $ZrH_{1.77}$ | Hom. 225°C, 19 hr | $\epsilon$ |
| 62-52 | 150 | 5580 | $ZrH_{1.84}$ | $H_2$ cooled | $\epsilon$ |
| 63-4 | 200 | 300 | $ZrH_{1.87}$ | Hom. 175°C, 15 hr | $\epsilon$ |
| 63-2 | 225 | 180 | $ZrH_{1.965}$ | Hom. 200°C, 19 hr | $\epsilon$ |

[a] Homogenized.
[b] Not in agreement with other observations.
tr—Trace.
s.a.—Small amount.

Fig. 5 shows a summary of the decomposition pressures at 500°C on a logarithmic scale, together with room temperature crystal structure studies of the phases. These studies will be discussed later. Fig. 5 suggests the following conclusions at 500°C. (*A*) The $\epsilon$-phase has a range of homogeneity extending from $ZrH_{1.965}$ to a composition near $ZrH_{1.64}$. (*B*) The $\delta$-phase has a range of homogeneity from about $ZrH_{1.4}$ to $ZrH_{1.56}$. (*C*) A two-phase region $\epsilon + \delta$ may exist between $ZrH_{1.56}$ and $ZrH_{1.64}$ although this has not been proved. (*D*) A two-phase region consisting of $\alpha$- and $\delta$-phases was found to exist between $ZrH_{0.04}$ to $ZrH_{1.40}$. (*E*) Below a composition of $ZrH_{0.04}$ a single phase region of $\alpha$-Zr with hydrogen in solid solution was found to exist.

### *Crystal Structure Studies*

A summary of the results are shown in Table III and in a graphical form in Fig. 5. Thermodynamic studies at 500°C are in essential agreement with crystal structure studies made on specimens prepared at temperatures of 300°C and lower. One exception is to be noted. This is the presence in the crystal structure studies of a minor transitional phase. The existence of this phase now designated as the $\gamma'$-phase in the zirconium–hydrogen system was first recognized by Jack (19) in a preliminary x-ray study of our specimens. It was also suggested by Jack (19) that this phase is a transition phase between the hexagonal $\alpha$-Zr phase and Hägg's face-centered cubic $\delta$-phase. It is present only in small or trace amounts together with the $\alpha$- and $\delta$-phases.

The evidence for the existence of the $\gamma'$-phase is rather strong, as can be noted in Table III, since lines associated with this phase were found on many samples both etched and unetched. No evidence was found for this phase from the decomposition pressure studies at higher temperatures.

Fig. 6 shows a microphotometer trace of an x-ray diffraction pattern of a $ZrH_{0.52}$ composition prepared from $\epsilon$-phase by heating in vacuo. Three definite extra reflections are noted in the pattern. Calculations show these reflections fit a face-centered tetragonal cell with lattice parameters given in

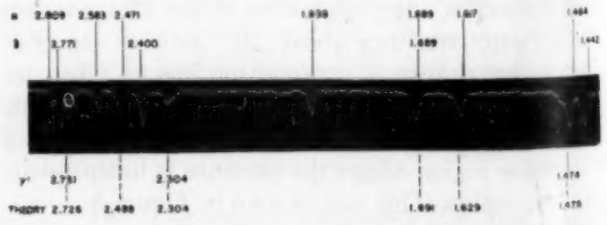


FIG. 6. Evidence for $\gamma'$ phase

TABLE IV. *Comparison lattice parameters zirconium hydride phases*

| Phase | Composition | Structure | Lattice parameters | |
|---|---|---|---|---|
| | | | Present work | Hägg |
| $\epsilon$ | $ZrH_{1.965} - ZrH_{1.64}$ | Face-centered tetragonal | $a = 4.97 \pm 0.01$ Å<br>$c = 4.48 \pm 0.01$ Å<br>$a/c = 1.11 \pm 0.01$ | $a = 4.974$ Å<br>$c = 4.440$ Å<br>$a/c = 1.118$ |
| $\delta$ | $ZrH_{1.44} - ZrH_{1.56}$ | Face-centered cubic | $a = 4.78 \pm 0.01$ Å | $a = 4.778$ Å |
| $\gamma'$ | $ZrH_x$ | Face-centered tetragonal | $a = 4.61 \pm 0.01$ Å<br>$c = 4.975 \pm 0.01$ Å<br>$a/c = 0.926 \pm 0.003$ | |

TABLE V. *Calculated patterns*

| $\gamma'$ Phase | | $\alpha$-Zr phase | | $\delta$-Phase | |
|---|---|---|---|---|---|
| hk | $d_{hkl}$ (Å) | hkil | $d_{hkil}$ (Å) | hkl | $d_{hkl}$ (Å) |
| | | $1\bar{1}01$ | 5.140 | | |
| 111 | 2.726 | $10\bar{1}0$ | 2.795 | 111 | 2.75 |
| 002 | 2.488 | $1\bar{1}02$ | 2.570 | 200 | 2.384 |
| 200 | 2.304 | $10\bar{1}1$ | 2.455 | 220 | 1.687 |
| 202 | 1.691 | $10\bar{1}2$ | 1.892 | 311 | 1.438 |
| 220 | 1.629 | $1\bar{1}03$ | 1.715 | 222 | 1.376 |
| 113 | 1.478 | $11\bar{2}0$ | 1.616 | 400 | 1.192 |
| 311 | 1.398 | $11\bar{2}1$ | 1.541 | 331 | 1.094 |
| 222 | 1.363 | $10\bar{1}3$ | 1.461 | 420 | 1.066 |
| 004 | 1.244 | $20\bar{2}0$ | 1.398 | 422 | .973 |
| 400 | 1.152 | $11\bar{2}2$ | 1.368 | {333, 511} | .921 |
| {313, 204} | 1.095 | $20\bar{2}1$ | 1.349 | | |
| 331 | 1.061 | $1\bar{1}04$ | 1.286 | | |
| 402 | 1.046 | $20\bar{2}2$ | 1.229 | | |
| 420 | 1.031 | $11\bar{2}3$ | 1.176 | | |
| f.c.t.<br>$a = 4.61$ Å<br>$a/c = 0.926$ | | h.c.p.<br>$a = 3.229$ Å<br>$c = 5.141$ | | f.c.c.<br>$a = 4.78$ Å | |

Table IV. The theoretical pattern based on this structure is shown in Table V and compared with the calculated patterns for the $\alpha$-Zr and $\delta$-phases. With the exception of the three observed reflections, the other lines are masked by lines from the $\alpha$- and $\delta$-phases.

Thermal properties of this new phase have not been investigated. It appears to form by direct preparation in the $\alpha + \delta$ region of composition or by removal of hydrogen from the $\epsilon$-phase. The composition of this phase has not been determined. However, a plot of the volume of the several hydride phases in Fig. 7 suggests a composition near $ZrH_{0.5}$ or the same composition as Hägg's hexagonal $\gamma$-phase which we have not observed in this study.

Table IV shows a summary of crystal structure data on the several phases formed in the zirconium–hydrogen system with the alloys being formed at low temperatures. Averaged lattice parameters are also given in Table IV. The $\delta$-phase was studied by direct hydriding to the given composition and also by removal of hydrogen from $\epsilon$-phase preparations until the proper composition was achieved. Results were in complete agreement with one possible exception noted in Table III.

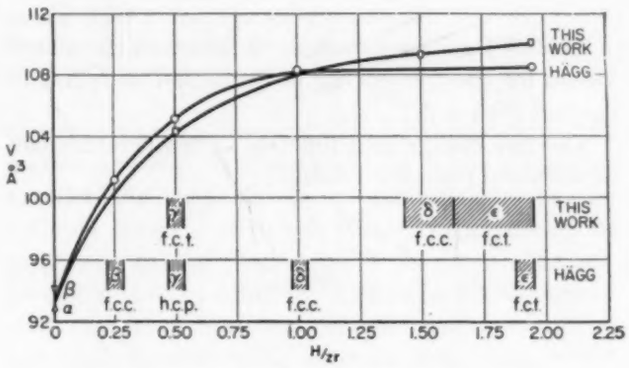


FIG. 7. Volume Zr and $ZrH_x$ structures

*Free Energy of Formation of the Delta Phase*

The decomposition pressure of the $\delta$-phase in Fig. 5 at 500°C was found to be dependent upon composition. However, in the two-phase region, the decomposition pressure of the $\delta$-phase is the same as that for the $\alpha$-phase saturated with hydrogen. Therefore, over the composition range of $ZrH_{0.04}$ to $ZrH_{1.40}$ a constant pressure is observed at 500°C. It is, therefore, of interest to determine the free energy equation for the $\delta$-phase in contact with the $\alpha$-phase saturated with hydrogen. For purposes of calculation a composition of $ZrH_{1.5}$ for the $\delta$-phase is taken.

Consider the equation

$$Zr(s) + 3/4H_2(g) \rightleftarrows ZrH_{1.5}(s) \qquad (I)$$

The equilibrium constant $K$ is given by

$$K = p_{H_2}^{-3/4} \qquad (II)$$

The standard free energy of formation $\Delta F^0$ is given by

$$\Delta F^0 = +3/4RT \ln p_{H_2} \qquad (III)$$

Here, $R$ is the gas constant, $T$ the temperature, and $p$ the pressure in atmospheres.

TABLE VI. *Decomposition pressure* $ZrH_{1.5}$ *(in contact with* $\alpha$-Zr)

| $t$ | $T$ | ln $P$ | $-\Delta F^0$ avg |
|---|---|---|---|
| 400 | 673.1 | −15.84 | 15,820 |
| 425 | 698.1 | −14.05 | 14,600 |
| 450 | 723.1 | −12.90 | 13,820 |
| 475 | 748.1 | −11.84 | 13,300 |
| 500 | 773.1 | −10.80 | 12,600 |
| 525 | 798.1 | −9.87 | 11,750 |
| 550 | 823.1 | −9.18 | 11,230 |
| 575 | 848.1 | −8.35 | 10,520 |

Table VI gives a summary of data and calculated values for the free energy of formation of $ZrH_{1.5}$ in contact with $\alpha$-Zr.

The free energy as a function of temperature can be obtained from the relation:

$$\frac{\partial \frac{\Delta F^0}{T}}{\partial T} = -\frac{\Delta H^0}{T^2} \qquad \text{(IV)}$$

where

$$\Delta H^0 = \Delta H_0^0 + \int_0^T \Delta C_p \, dT \qquad \text{(V)}$$

Here, $\Delta H^0$ is the standard heat of reaction at temperature $T$, $\Delta H_0^0$ is the standard heat of reaction at 0°K, $\Delta C_p$ is the difference in heat capacities of products and reactants.

Unfortunately, heat capacity data are not available on $ZrH_{1.5}$ and only a semi-empirical equation can be derived. Kubaschewski and Evans (18) suggest the use of an approximate value for $\Delta Cp$ for reactions of this type of $\Delta C_p = 2.25$. Substituting in equations (IV) and (V) and integrating

$$\Delta F^0 = \Delta H_0^0 - 2.25\ T \ln T + IT \qquad \text{(VII)}$$

Here, $I$ is the conventional integration constant and $\Delta H_0^0$ is determined from a conventional thermodynamic plot of $\Sigma$ against $1/T$. Here,

$$\Sigma = \frac{\Delta H_0^0}{T} + I \qquad \text{(VIII)}$$

$\Delta H_0^0$ is found equal to −34,930 cal/mole while the averaged value for $I = 43.88$.

The final semi-empirical equation for reaction (I) is

$$\Delta F^0 = -34{,}930 - 2.25\ T \ln T + 43.88\ T \qquad \text{(IX)}$$

ACKNOWLEDGMENT

The authors are indebted to Dr. K. H. Jack for pointing out the existence of the $\gamma'$ phase and for his helpful suggestions in the early stages of this work.

Any discussion of this paper will appear in a Discussion Section to be published in the June 1955 issue of the JOURNAL.

REFERENCES

1. D. P. SMITH, "Hydrogen in Metals," The University of Chicago Press, Chicago (1948).
2. E. A. GULBRANSEN, To be published.
3. W. T. MUDGE, JR., "Zirconium and Zirconium Alloys," p. 730, American Society for Metals, Cleveland (1953).
4. A. WINKLER, *Ber.*, **23**, 2642 (1890).
5. A. WINKLER, *ibid.*, **24**, 873 (1891).
6. E. WEDEKIND, *Liebigs Ann. Chem.*, **395**, 149 (1913).
7. R. SCHWARZ AND E. KONRAD, *Ber.*, **54**, 2122 (1921).
8. L. WEISS AND C. NEUMANN, *Z. anorg. Chem.*, **65**, 248 (1910).
9. E. WEDEKIND, *Liebigs Ann. Chem.*, **371**, 378 (1910).
10. A. SIEVERTS AND E. ROELL, *Z. anorg. u. allgem. Chem.*, **153**, 289 (1926).
11. M. N. A. HALL, S. L. H. MARTIN, AND A. L. G. REES, *Trans. Faraday Soc.*, **41**, 306 (1945).
12. G. HÄGG, *Z. physik. Chem.*, **11**, 439 (1930).
13. A. E. VAN ARKEL, "Reine Metalle," J. Springer, Berlin (1939).
14. N. F. M. HENRY, H. LIPSON, AND W. A. WOOSTER, "The Interpretation of X-ray Diffraction Photographs," Macmillan & Co., Ltd., London (1951).
15. J. FITZWILLIAM, A. KAUFMAN, AND C. SQUIRE, *J. Chem. Phys.*, **9**, 678 (1941).
16. "Advances in Catalysis," p. 133, vol. V, Academic Press, Inc., New York (1953).
17. E. A. GULBRANSEN AND K. F. ANDREW, *Ind. Eng. Chem.*, **41**, 2762 (1949).
18. O. KUBASCHEWSKI AND E. L. L. EVANS, "Metallurgical Thermochemistry," p. 174, Butterworth-Springer, Ltd., London (1951).
19. K. H. JACK, To be published.

# Determination of Barrier Layer Thickness of Anodic Oxide Coatings[1]

M. S. Hunter and P. Fowle

*Aluminum Research Laboratories, Aluminum Company of America, New Kensington, Pennsylvania*

ABSTRACT

A novel method is described for measuring the thickness of a barrier type anodic oxide coating or the barrier layer portion of a porous type anodic oxide coating. This method is used to follow the evolution of the barrier layer during the early stages of the formation of a porous type coating on aluminum and to establish certain dimensions of the fundamental oxide cells which comprise this type of coating.

## Introduction

The virtues of the durable, protective anodic oxide coatings applied to aluminum have long been known and appreciated, but only recently have the submicroscopic features and dimensions of these coatings been established (1). Anodic coatings may be either porous or nonporous, depending on the electrolyte in which they are formed, but all have one feature in common, a zone of nonporous oxide or "barrier layer" adjacent to the metal. This paper describes a method for measuring the thickness of this barrier oxide layer, and demonstrates the manner in which this method may be applied to the investigation of the characteristics of oxide coatings on aluminum.

## Barrier Layer

The barrier layer and forces that govern its formation and determine its behavior have been the subject of extensive research by many investigators. The primary forces governing formation of the coatings are believed to be ionic in nature, as indicated by Mott (2), Haring (3), Charlesby (4), and others. These investigators have stated that the barrier layer represents the distance through which a metal ion can penetrate a layer of its oxide under the influence of an applied potential. As such, the thickness of this layer is a function of the applied voltage, which is the driving force behind the metal ion. In the case of aluminum, Hass (5) has shown that barrier layer coatings form to a thickness of 14 Å per volt of applied potential.

When aluminum is made the anode in an electrolyte that can furnish oxygen-containing ions, combination between aluminum and oxygen occurs to form on the metal a continuous film composed principally of aluminum oxide. The nature of this film is such that it opposes the movement of ions and electrons which is necessary for continued oxide formation and coating growth as long as the aluminum remains the anode. If the aluminum is made the cathode, however, the oxide film offers practically no resistance to the movement of electrons, and appreciable current can flow. This behavior is responsible for the rectifying action characteristic of anodically-formed oxide films on aluminum.

In the absence of solvent action by the electrolyte, the oxide layer formed anodically reaches a limiting thickness, at which point it becomes an effective barrier to further movement of ions and electrons, and current flow substantially ceases. The thickness of film required to block current flow effectively is a linear function of the applied voltage and, once the barrier layer has been completely formed, increases in thickness can be effected only by increasing the applied voltage. In this case, the entire coating constitutes the barrier layer (Fig. 1), and the thickness of the barrier layer in Angstrom units is 14 times the applied voltage. When the barrier layer has reached its limiting thickness, only a very low leakage current persists. This leakage current is substantially current flow through regions in the metal that contain constituent particles on which a complete barrier type of coating does not form and, consequently, differs for various alloy compositions.

In electrolytes that have the ability to dissolve the oxide, the effect of solvent action is superimposed on the oxide formation process, with the result that a somewhat different situation exists. The electrolytic cell continues to form oxide as long as the barrier layer corresponding to the applied voltage is not complete. Solvent action, however, prevents the barrier layer from reaching its limiting thickness. Under these conditions, current continues to flow, a porous oxide structure is created, and relatively thick oxide coatings are formed. As oxide continues to form, there remains between the metal and the base of the pores a thin layer of barrier oxide which restricts, but does not block, current flow. Although

[1] Manuscript received April 26, 1954. This paper was prepared for delivery before the Chicago Meeting, May 2 to 6, 1954.

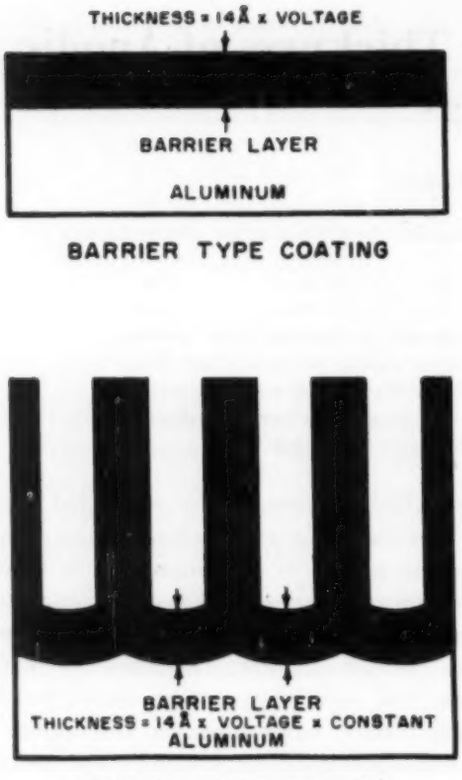


FIG. 1. Barrier layer of anodic oxide coatings

all the oxide formed was at one time in the barrier layer, this thin layer of oxide at the base of the pores is considered to be the barrier layer portion of the porous type of oxide coating (Fig. 1). The thickness of this layer in Angstrom units is 14 times the applied voltage times a factor having a value less than one. The actual value of this factor is determined by the electrolyte.

### BARRIER LAYER DETERMINATION

The thickness of barrier layer coatings and the barrier layer portion of porous oxide coatings is highly significant in terms of the characteristics and behavior of the coatings. In the case of barrier type coatings, where the entire coating constitutes the barrier layer, a fairly good approximation of coating thickness can be made from the interference colors, if the coating is greater than about 300 Å in thickness, or by microscopic examination if the coating is thicker than about 2000 Å. With the porous type of coating, which has a layer of porous oxide above the barrier layer and has only a very thin barrier layer because of the relatively low voltages used, these methods are not practical. The electron microscope has indicated the presence of the barrier layer portion of porous coatings (6), but present replica methods are not adequate for precise measurement.

A method has been developed by which the thickness of a barrier layer coating or the barrier portion of a porous type of coating can be determined with substantial accuracy. This method is based on oxide forming characteristics in electrolytes that do not dissolve the oxide. Here, oxide forms anodically to the 14 Å/v value, and thickness can be increased only by increasing voltage. By the same token, if any anodic voltage less than the formation voltage is applied, only leakage current will flow. If gradually increasing voltage is applied to this nonporous barrier type of coating in an electrolyte which does not exert significant solvent action, values up to and including the forming voltage will produce only leakage current. Any value above the formation voltage will produce current flow greater than the leakage value, as the coating tends to form to the thickness corresponding to the higher voltage.

The same principles hold with the barrier layer portion of the porous type of oxide coating. With this type of coating, however, the barrier layer forms to a thickness of some value less than 14 Å/v as indicated by the fact that current greater than leakage continues to flow. As a result, current higher than the leakage value will flow at some voltage below the formation voltage. The voltage at which current flow equals the leakage value is a measure of the thickness of the barrier layer portion of the coating.

An approximation of barrier layer thickness on an oxide coated sample may be made by observing current flow with increasing voltage in an electrolyte that forms a barrier type of coating. As voltage is increased, the leakage current rises very slowly until the voltage corresponding to the thickness of the barrier is approached. Once appreciable current starts to flow, small voltage increments produce large increases in current. The approximate thickness in Angstrom units of the barrier layer is 14 times the highest voltage that does not produce a pronounced rise in current flow. With reasonable care, it is possible to determine this voltage for coatings formed on high purity aluminum to within less than 1 v, which corresponds to a barrier thickness of about ± 14 Å. The value determined in this manner is always low, however, because the leakage current for the particular material has not been considered.

A more accurate value for the thickness of the barrier layer may be determined by taking into account the leakage current for the material under investigation. First, the approximate barrier voltage is determined as closely as possible in the manner described above. Then, the leakage current for the material under investigation is determined at this approximate voltage. This determination is made by applying the particular voltage to a freshly cleaned sample of the material and observing the final, steady leakage current after the barrier type of coating is completely formed. Finally, the voltage re-

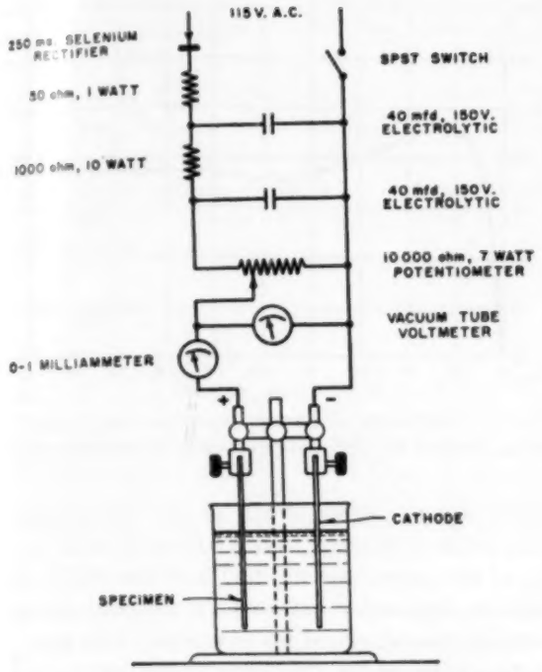


FIG. 2. Electrical arrangement for determining barrier layer thickness.

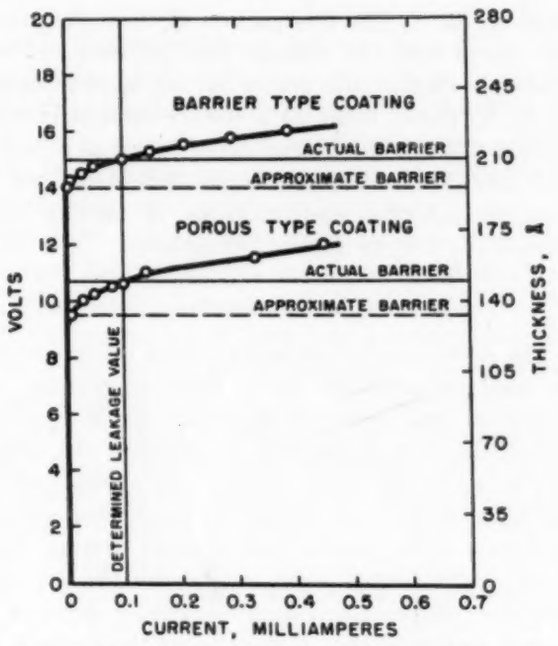


FIG. 3. Determination of barrier layer thickness

quired to produce this current flow with the unknown barrier layer is determined. This permits determination of the actual barrier layer voltage to within ± 0.1 v for coatings formed on high purity aluminum, which means that the barrier layer thickness can be found within about 3 Å.

In the case of coatings formed on high purity aluminum, leakage current varies only slightly over a rather wide range of voltages so that further measurements of leakage current and barrier layer voltage are not necessary. In the case of aluminum alloys that have higher leakage current and show greater variations in leakage with changing voltage, such additional measurements are frequently justified.

Excellent results can be obtained with this method using the simplest of equipment. All that is required is a variable direct current source, an accurate voltmeter, and a sensitive milliammeter. The arrangement used to make the barrier measurements discussed in this paper is shown by Fig. 2. To determine the barrier layer thickness, the specimen is made anode in an electrolyte that does not exert significant solvent action on the oxide. A freshly cleaned cathode of the same material is used to avoid potential differences between the two electrodes. Current readings are then made at increasing voltages and plotted as described above. In the work described in this paper, the electrolyte used was a 3% tartaric acid solution adjusted with ammonium hydroxide to a *p*H of 5.5, although any other electrolyte having similar characteristics should be satisfactory. The electrolyte was maintained at 75°F (24°C) during the measurement.

The manner in which barrier layer thickness values are obtained is illustrated in Fig. 3. Here, the current values for increasing voltage are plotted for two 15-v anodic coatings applied to 1 in.² (0.065 dm²) samples of high purity aluminum. One of these is a barrier type of coating formed in the ammonium tartrate electrolyte, and the other is a porous type of coating formed in a 15% sulfuric acid electrolyte at 70°F (21°C). Also, the steady current value representing leakage for these aluminum samples in the neighborhood of 15 volts is indicated.

In the case of the 15-v barrier type coating, the lowest voltage value to produce significant current flow was 14.0 v which gives an approximate barrier thickness value of 196 Å. The steady leakage current measured for the high purity aluminum sheet specimens of the particular area used was 0.1 ma in the range of 10 to 15 v. The intersection of the voltage-current curve with the line representing this current value occurs at exactly 15 v. This was the voltage used to form the coating and represents a barrier layer thickness of 210 Å, which is the maximum thickness of barrier coating that can be formed on aluminum by 15 v of applied potential.

With the porous type of coating, the barrier layer thickness must be less than the 14 Å/v value as discussed earlier. In the case of the coating formed in 15% sulfuric acid at 70°F (21°C) (Fig. 3), the approximate barrier layer thickness, as indicated by the voltage required to produce appreciable current

flow, is 133 Å. The intersection of the voltage-current curve with the leakage line occurs at 10.7 v, which shows that the actual barrier layer thickness is 150 Å. Thus, in the 15% sulfuric acid electrolyte at 70°F (21°C), the barrier layer forms at a rate of 10.0 Å/v. The term "unit barrier thickness" will be used to describe the thickness of barrier layer formed per volt of applied potential.

## Applications

The determination of barrier layer thickness may be used to establish many facts concerning the formation and behavior of anodic oxide coatings. For instance, it is possible to establish changes in barrier layer thickness which accompany current fluctuations observed during the initial stages of the formation of the porous type of oxide coating. Inasmuch as the barrier layer constitutes the principal resistance across the voltage source, a decrease in current indicates that barrier layer thickness is increasing and, conversely, an increase in current indicates a decrease in barrier layer thickness. In electrolytes that do not dissolve the oxide appreciably, current is initially high but decreases rapidly as barrier layer thickness increases. In a relatively short time, current reaches a low, steady leakage value, at which point the barrier layer has attained its limiting thickness of 14 Å/v.

In the case of electrolytes that dissolve the oxide, solvent action combined with coating formation produces a more complex situation. As in the case of the barrier type of coating, current flow is initially high and decreases with time as barrier layer thickness increases. With the porous type of coating, however, decrease in current is not as rapid because of solvent action which tends to reduce the thickness of the barrier layer. After a short time, current flow reaches a minimum value and then starts to rise as solvent action, which is increasing, first equals and then exceeds coating formation. Current flow becomes steady when formation and solution of oxide reach a balance, at which point barrier layer thickness becomes constant.

As an illustration of the evolution of the barrier layer portion of a porous type of oxide coating, changes in barrier layer thickness that occurred during the formation of a coating in a 15% sulfuric acid electrolyte at 70°F (21°C) using a potential of 15 v are presented. As shown by Fig. 4, the thickness of the barrier layer increased rapidly at first but as solvent action began to have an effect, the rate of increase of the barrier layer diminished. After about 5 sec, solvent action began to exceed the rate of oxide formation and barrier layer thickness decreased. After about 18 sec, oxide formation again exceeded solvent action and barrier layer thickness increased

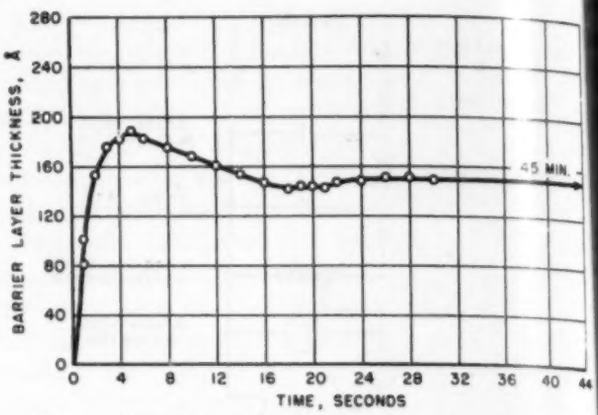


Fig. 4. Evolution of barrier layer portion of a 15-volt coating formed in 15% sulfuric acid electrolyte at 70°F.

slightly. Finally, after about 25 sec, the balance between oxide formation and solution of oxide at the base of the pores was reached and the barrier layer thickness became constant. No further change in thickness was observed up to a time of 45 min. The rapidity with which the initial fluctuations in current occur and the time required to reach equilibrium thickness are a function of the current capabilities of the voltage source. As a result, transient barrier layer thickness values shown apply only under the particular conditions of this experiment.

The method was also applied to sulfuric acid coatings sealed in boiling water to determine whether the hydrated oxide formed within the pores during sealing would interfere with the measurement of barrier voltage. If this hydrated oxide did interfere with the measurements, an apparent increase in barrier layer thickness with sealing would be noted. Measurements indicated, however, that the barrier layer thickness decreased with sealing time. Thus, the hydrated oxide produced during sealing does not interfere with this measurement. Therefore, the method can be applied to water-sealed as well as unsealed oxide coatings.

This decrease in barrier layer thickness observed on sealing in boiling water was investigated further to determine the actual effect of such sealing. It was found that barrier layer thickness was reduced by about 4 Å for each ten minutes of sealing, which indicates that prolonged sealing treatments in boiling water may be detrimental.

Determinations of unit barrier layer thickness have been made in four electrolytes used to make porous type anodic coatings inasmuch as barrier layer thickness is one of the important dimensions of the oxide cell. Electrolytes selected were those used in previous work on the dimensions of anodic oxide coatings. Unit barrier thickness was found to be practically independent of forming voltage but varied appreciably among the four electrolytes, as was the case with cell wall thickness. Also, variations in unit

barrier thickness and unit wall thickness were in the same order in the four electrolytes, although the unit barrier thickness was greater by a factor of about 1.2. The unit barrier thickness values from this work and the unit wall thickness and pore diameter values from previous work (1) are given in Table I. These values along with forming voltage establish the dimensions of oxide cells of coatings formed in these electrolytes.

TABLE I. *Basic dimensions of oxide cells*

| Electrolyte | Barrier Å/volt | Wall Å/volt | Pore diameter, Å |
|---|---|---|---|
| 4% Phosphoric acid, 75°F (24°C) | 11.9 | 10.0 | 330 |
| 2% Oxalic acid, 75°F (24°C) | 11.8 | 9.7 | 170 |
| 3% Chromic acid, 100°F (38°C) | 12.5 | 10.9 | 240 |
| 15% Sulfuric acid, 50°F (10°C) | 10.0 | 8.0 | 120 |

Barrier layer thickness determinations, in combination with determinations of oxide cell size by electron microscopic examinations of cell base patterns, may be used to obtain an approximation of the formation voltage of an unknown anodic coating made in any of these four electrolytes and the particular electrolyte in which it was formed. From previous work (1)

$$C = 2WE + P \qquad \text{(I)}$$

where $C$ is the size of the individual oxide cells, $W$ is unit wall thickness (the thickness of oxide in the cell wall per volt of forming potential), $E$ is forming voltage, and $P$ is pore diameter. Also,

$$T = BE \qquad \text{(II)}$$

where $T$ is total barrier thickness, $B$ is unit barrier thickness, and $E$ is forming voltage. Inasmuch as unit barrier thickness is approximately 1.2 times unit wall thickness, equation (II) may be written as

$$T = 1.2\,WE \qquad \text{(III)}$$

Combining equations (I) and (III) gives equation (IV) which defines pore diameter in terms of cell size and total barrier thickness.

$$P = C - 1.67\,T \qquad \text{(IV)}$$

$C$ can be determined from measurements of the cell base pattern of the unknown coating, and $T$ can be found from barrier layer thickness determinations. As a result, pore diameter can be calculated and, if the electrolyte was one of the group which has been investigated, the particular electrolyte can be established. Unit barrier thickness and unit wall thickness are then known and either equation (I) or (II) may be solved to establish forming voltage.

The examples which have been presented are but a few of the many ways in which the determination of barrier layer thickness may be applied to the investigation of anodic oxide coatings. These measurements have revealed many interesting and unusual facts relating to the formation of these coatings and have been useful in establishing the electrolyte type and forming conditions used to produce coatings having certain desirable characteristics. Determination of the barrier layer thickness may be used to establish the effect of various treatments or environments on anodically formed oxide, to investigate the nature and characteristics of the natural oxide film on aluminum, and to explore other phases of anodic coating formation and behavior, the scope of which is limited only by the imagination of the investigator.

## Acknowledgment

The authors wish to express their appreciation to F. Keller, under whose direction this work was conducted.

Any discussion of this paper will appear in a Discussion Section to be published in the June 1955 issue of the Journal.

## References

1. M. S. Hunter and D. L. Robinson, *This Journal*, **100**, 411 (1953).
2. N. F. Mott, *Trans. Faraday Soc.*, **43**, 429 (1947).
3. H. E. Haring, *This Journal*, **99**, 30 (1952).
4. A. Charlesby, *Proc. Phys. Soc.*, **B66**, 317 (1953).
5. G. Hass, *J. Opt. Soc. Amer.*, **39**, 532 (1949).
6. J. D. Edwards and F. Keller, *Trans. Amer. Inst. Mining Met. Engrs.*, **156**, 288 (1944).

# Officers of Local Sections of the Society

*Chicago*

B. F. Freeberg, Chairman
E. L. Koehler, Vice-Chairman
R. D. Misch, Treasurer
J. E. Draley, Secretary
Argonne National Laboratory
P. O. Box 299
Lemont, Ill.

*Cleveland*

Ernest B. Yeager, Chairman
W. H. Stoll, Vice-Chairman
Merle E. Sibert, Treasurer
Karl S. Willson, Secretary
General Dry Batteries Co.
13000 Athens Ave.
Cleveland, Ohio

*Detroit*

Wright Wilson, Chairman
Andrew Liger, 1st Vice-Chairman
Gerald V. Kingsley, 2nd Vice-Chairman
Manny Shaw, Sec.-Treas.
19411 Winthrop Ave.
Detroit, Mich.

*Midland*

F. N. Alquist, Chairman
M. P. Neipert, Vice-Chairman
P. R. Juckniess, Sec.-Treas.
The Dow Chemical Company
Midland, Mich.

Representatives on Council of Local Sections:

F. W. Koerker (1 year)
H. A. Robinson (2 years)

*New York Metropolitan*

M. F. Quaely, Chairman
M. B. Diggin, Vice-Chairman
Kenneth B. McCain, Sec.-Treas.
Wilbur B. Driver Company
150 Riverside Ave.
Newark, N. J.

Representatives on Council of Local Sections:

A. C. Loonam (1 year)
Herbert Bandes (2 years)

*Niagara Falls*

Harry R. Oswald, Chairman
Warren D. Sherrow, Vice-Chairman
John E. Currey, Sec.-Treas.
Hooker Electrochemical Company
Niagara Falls, N. Y.

*Pacific Northwest*

Joseph B. Heitman, Chairman
G. H. Kissin, Vice-Chairman
Kenneth L. Sanborn, Sec.-Treas.
General Electric Company
2005 Pullen
Richland, Wash.

*Philadelphia*

J. Fred Hazel, Chairman
Edgar L. Eckfeldt, Vice-Chairman
G. Franklin Temple, Treasurer
George W. Bodamer, Secretary
Rohm & Haas Company
Philadelphia, Pa.

Representatives on Council of Local Sections:

John F. Gall (1 year)
Edgar L. Eckfeldt (2 years)

*Pittsburgh*

M. T. Simnad, Chairman
R. D. Williams, Vice-Chairman
Robert A. Woofter, Sec.-Treas.
Jones & Laughlin Steel Corp.
Pittsburgh, Pa.

*Washington-Baltimore*

Fielding Ogburn, Chairman
D. T. Ferrell, Jr., Vice-Chairman
Jeanne B. Burbank, Sec.-Treas.
Naval Research Laboratory
Washington, D. C.

Representatives on Council of Local Sections:

J. C. White (1 year)
D. T. Ferrell, Jr. (2 years)

*San Francisco*

R. F. Bechtold, Chairman
C. W. Tobias, Vice-Chairman
H. F. Myers, Sec.-Treas.
Columbia Steel Company
Pittsburg, Calif.

*Ontario-Quebec*

A. E. Westman, Honorary Chairman
John Convey, Chairman
P. J. Enzio, Vice-Chairman
R. R. Rogers, Vice-Chairman
John Sumner, Sec.-Treas.
637 Craig St. West
Montreal 3, Canada

Representative on Council of Local Sections:

P. J. Enzio

*India*

M. S. Thacker, Chairman
B. Narayan Das, Vice-Chairman
S. Ramaswamy, 2nd Vice-Chairman
S. Krishnamurthy, Sec.-Treas.
543/1, 17th Cross Rd.
Malleswaram P. O.
Bangalore, India

Representatives on Council of Local Sections:

L. Charat Ram
K. Rajagopal